National Defence / Défense nationale

SOME APPLICATIONS OF KALMAN FILTERING IN ADVANCED LAND FIRE CONTROL SYSTEMS (U)

by

J.S. Bird

DEFENCE RESEARCH ESTABLISHMENT OTTAWA
REPORT NO. 1172

Canada

April 1993
Ottawa

National Defence / Défense nationale

SOME APPLICATIONS OF KALMAN FILTERING IN ADVANCED LAND FIRE CONTROL SYSTEMS (U)

by

J.S. Bird
Communications and Navigation Systems Section
Electronics Division

DEFENCE RESEARCH ESTABLISHMENT OTTAWA
REPORT NO. 1172

PCN
1410SC

April 1993
Ottawa

ABSTRACT

This report describes several potential applications of Kalman filters for advanced land fire control systems. Two areas that are especially important in the moving-target / moving-platform scenario are addressed in some detail: the tracking and trajectory prediction of multiple maneuvering targets and the prediction of gun pointing angles in the instant before firing. This is particularly important in the design of a dynamic muzzle reference system. The equations for the filters are developed, simulations are described, and some real data is processed through the muzzle angle prediction filter. An architecture for a complete advanced land fire control system is proposed.

RÉSUMÉ

Ce rapport décrit plusieurs applications potentielles de filtres Kalman pour les systèmes avancés de contrôle d'artillerie au sol. Deux secteurs qui sont spécialement importants dans le sénario plate-forme mobile/cible mobile sont abordés dans certains détails: la prédiction de la capture et de la trajectoire de cibles manoeuvrées multiples et la prédiction de l'angle de visée du canon au moment précédant le feu. Ceci est particulièrement important dans la conception d'un système de référence dynamique de goulot. Les équations des filtres sont développées, des simulations sont décrites, et des données réelles sont traitées par le filtre de prédiction de l'angle du canon. Une architecture d'un système avancé complet de contrôle d'artillerie au sol y est proposée.

EXECUTIVE SUMMARY

The Defence Research Establishment Ottawa (DREO) was asked to look at potential applications of Kalman Filtering technology to various aspects of mobile land fire control systems, with particular emphasis on the reduction of errors in the moving-target, moving-platform scenario. Such errors are exacerbated by the high dynamic environment, for example, when targets are tracked manually and when shells are launched through a flexing gun barrel.

Today's direct-fire support vehicles (DFSV) have large guns that are inertially stabilized, day and night sighting systems, pulsed laser range finders, and digital fire control computers to calculate lead angles that correct for target range and crossing velocity, weather conditions, etc. However increasing requirements for high accuracy at extended ranges while firing on the move have meant that a new generation fire control system will be required to remove even more sources of error.

Improvements in sensor technology and the decreasing cost and size of high-speed computers has created opportunities for sophisticated signal processing algorithms aboard tomorrow's land vehicles. Many tasks that crews find extremely difficult can often be routinely done in a computer. For example, accurately tracking a moving target when one's own vehicle is bouncing wildly over rough terrain is nearly impossible for the gunner but is a fairly simple exercise in target tracking for an image processing computer. As well, present ballistic computers use relatively simple look-up tables because of the limitations of on-board processing power. Modern computers can compute and effect much more accurate gun laying angles that take into account more up-to-the-millisecond gun barrel sensor information. However, at present, few land vehicles exist with such capabilities.

Kalman filtering is a signal processing technique that has tremendous potential for next generation fire control. It can address most of the remaining error sources, provided that they can be mathematically modelled and that sensitive sensors are installed to measure such errors. Its predictive nature makes it ideally suited to estimate where the target is going to be when the shell arrives, for example, or when the gun barrel is going to be pointed in the correct direction.

This report will first summarize the fundamentals of the Kalman filter algorithm and give some simple examples of how it is used in common military systems. Next, a series of problem areas in mobile fire control systems that can benefit from the application of the filter will be described. Two areas that were studied in some detail, namely target tracking and dynamic muzzle referencing will be the focus of subsequent chapters. The equations used to design the filters will be developed; a software simulator that implements the filter is described; simulations of tracking performance are demonstrated; and real barrel flex data is processed through a candidate pointing angle filter for a predictive muzzle reference system. Broadening the scope somewhat, the next chapter outlines a potential architecture for an Advanced Development Model (ADM) that encompasses these subsystems as well as those related to image processing, vehicle dynamics, human interaction, etc.

TABLE OF CONTENTS

LIST OF FIGURES

LIST OF ACRONYMS

2D	2-Dimensional
3D	3-Dimensional
ADM	Advanced Development Model
DCM	Direction Cosine Matrix
DFSV	Direct Fire Support Vehicle
DLAEEM	Directorate of Land Armament and Electronics Engineering and Maintenance
DMRS	Dynamic Muzzle Referencing System
DRE	Defence Research Establishment
ECA(r)	Exponentially Correlated Acceleration (rectangular)
ECA(s)	Exponentially Correlated Acceleration (spherical)
ECV(r)	Exponentially Correlated Velocity (rectangular)
ECV(s)	Exponentially Correlated Velocity (spherical)
EKF	Extended Kalman Filter
GPS	Global Positioning System
IEWA	Inter-Establishment Working Arrangement
INS	Inertial Navigation System
KF	Kalman Filter
KTA	Key Technical Area
MBT	Main Battle Tank
MRS	Muzzle Referencing System
PSD	Power Spectral Density
RMS	Root Mean Square
RWA(r)	Random Walk Acceleration (rectangular)
RWA(s)	Random Walk Acceleration (spherical)
RWV(r)	Random Walk Velocity (rectangular)
RWV(s)	Random Walk Velocity (spherical)
TTCP	The Technical Cooperation Panel
WAG	TTCP Subgroup W, Action Group 10

1.0 INTRODUCTION TO ADVANCED LAND FIRE CONTROL

1.1 BACKGROUND OF THE RESEARCH PROJECT

As part of DLAEEM Task 139 - "Kalman Filter Design for Tank Fire Control Systems," the Defence Research Establishment Ottawa (DREO) was asked to look at potential applications of Kalman filtering technology in various aspects of mobile land fire control systems, with particular emphasis on the reduction of errors in the moving-target, moving-platform scenario. Such errors are exacerbated by the high dynamic environment, for example, when targets are tracked manually and when shells are launched through a flexing gun barrel.

The task description sheet specified the following general aim: "To conduct a design and feasibility study for an MBT (Main Battle Tank) positioning and target tracking system." Among the work items were the following:

- develop dynamical models for tank/target motion and robust algorithms for Kalman filter tracking, prediction, error estimation, motion compensation, sensor integration;
- develop a software simulation test-bed to evaluate the algorithms against real or simulated data in a variety of motion scenarios;
- analyze the simulations and identify the effects of the algorithms on tracking performance; and
- recommend hardware and software configurations for possible advanced development model construction.

The original tasking was very broad by intent and it was expected that research directions would shift as it became apparent which were the primary error sources that might be solved by these filtering techniques. For example, the extent of terrain-induced muzzle motion was underestimated until discussions were held with several tank gun experts. Characterization, analysis and methods for compensation of these motions subsequently became one of the largest areas of study. On the other hand, battlefield navigation, as specifically mentioned in the aim of the task description sheet, took on a lower priority since it did not affect fire control accuracy *per se*, though it is an area where the application of a Kalman filter-based, integrated land navigation system would enhance the overall survivability of the platform on the battlefield.

In fact, the project directions became so broad that other establishments and several contractors became involved. During the course of this task, an Inter-Establishment Working Arrangement (IEWA) was initiated to bring together researchers from DREO, DREV (Defence Research Establishment Valcartier), DRES (Suffield), and DCIEM (the Defence and Civil Institute for Environmental Medicine) that were working in various aspects of land vehicles and fire control. As well, a major development program (D6374) was initiated to carry on the work and deliver a field-testable model of an advanced fire control system that could demonstrate the

techniques of this report and those of the other investigators.

The work summarized in this report was carried out from May 1988 to December 1990 under project no. PCN 0318E.

1.2 BUILDING ON MODERN DAY FIRE CONTROL SYSTEMS

Today's direct-fire support vehicles (DFSV) generally have good fire control systems, especially when compared to their forerunners of World War II. Gone are the days when the drivers of turretless tanks stopped to face each other on the battlefield and fired volleys of hand-aimed shells. Modern DFSV's have large guns that are stabilized in azimuth and elevation (to allow a reasonably steady aimpoint when the vehicle is moving), long-range (out to several kilometres) stabilized day and night vision sighting systems, and pulsed laser range finders to measure target range to within a few meters. Most have digital fire control computers to calculate lead angles and elevation offsets that correct for target range and crossing velocity, wind speed and direction, air pressure, ammunition type and temperature, sight parallax and even the static droop of the gun barrel as it warms. However, increasing requirements for high accuracy at extended ranges, while firing on the move, have meant that a new generation fire control system will be required to remove even more sources of error.

Given the level of sophistication of the equipment in a modern armoured vehicle, one can ask the fair question: is there any more that can be done? The answer of course, is yes; several countries are rigorously pursuing mobile land fire control research and several NATO and TTCP panels and action groups have been initiated to investigate outstanding problem areas and identify sources of errors that are presently limiting fire control performance. TTCP Panel W, Action Group 10 (WAG-10) visited several US, UK and Canadian organizations pursuing such issues (and more as their mandate referred to tank gun accuracy in general). The final report, (TTCP-WAG10 (1989)), summarized the primary error sources and recommended the creation of two Key Technical Areas, KTA 5-17 "Advanced Integrated Tank Fire Control," and KTA 2-11 "Sabot Separation," to further investigate them.

Among the findings of WAG-10 was that among the major sources of error in a typical state-of-the-art main battle tank engaging a moving target, while itself moving cross country, was 1) the inability of the gun to remain pointed in the proper direction, and 2) the inability of the gunner to maintain a sufficiently accurate aimpoint on a maneuvering target. Though the magnitudes of the errors are fairly small, on the order of 1 milliradian or so (or about 1/20 of a degree or 3 arc minutes), in the context of the modern battlefield, errors of even these magnitudes can be disastrous, especially if the adversary has a comparable system. Modern high-intensity battles are fought at ranges from a few hundred meters out to a few kilometers. Even at a nominal battle range of 1200 meters, a 1 mrad pointing error means a miss distance (from the desired aimpoint) of 1.2 meters ($1200 \times \tan 0.001$). This may mean the difference between disabling the target and missing it entirely (typical practice targets are 2.3 m wide).

Improvements in sensor technology and the decreasing cost and size of high-speed computers have created opportunities for sophisticated signal processing algorithms aboard tomorrow's land vehicles. Many tasks that crews find extremely difficult can often be routinely done in a computer. For example, accurately tracking a moving target when one's own vehicle is bouncing wildly over rough terrain is nearly impossible for the gunner but is a fairly simple exercise in target tracking for an image processing computer. As well, present ballistic computers use relatively simple look-up tables because of the limitations of on-board processing power. Modern computers can compute and effect much more accurate gun laying angles that take into account more up-to-the-millisecond gun barrel sensor information. However, at present, few land vehicles exist with such capabilities. It should be mentioned, on the other hand, that there are some tasks that are relatively simple for humans but exceedingly difficult for computers - target recognition, for example. Research into such algorithms is progressing, however, and may one day be feasible in fire control systems.

Kalman filtering is a signal processing technique that has tremendous potential for next generation fire control. It can address most of the remaining error sources, provided that they can be mathematically modelled and that sensitive sensors are installed to measure such errors. Its predictive nature makes it ideally suited to estimate where the target is going to be when the shell arrives, for example, or when the gun barrel is going to be pointed in the correct direction. The filter, named after Rudy Kalman who developed it in the early 1960's, is a method of estimating the true state of an imprecisely known dynamical system from noisy measurements. Since this describes almost every system that one has to deal with in practice, it is not surprising that the Kalman filter has seen tremendous application in many fields; everything from target tracking to navigation to communications to economics. A very good collection of both theoretical and applications papers is available in Sorenson (1985). The filter can be relatively computationally intensive and, until recent generations of microprocessors, its real-time applications have often required approximations or other ad-hoc modifications. Now however, large size filters are routinely implemented in real-time.

1.3 THE SCOPE OF THIS REPORT

This report will first summarize the fundamentals of the Kalman filter algorithm and give some simple examples of how it is used in common military systems. Next, a series of problem areas in mobile fire control systems that can benefit from the application of the filter will be described. Two areas that were studied in some detail, namely target tracking and dynamic muzzle referencing will be the focus of the next chapters. The equations used to design the filters will be developed; a software simulator that implements the filter is described; simulations of tracking performance are demonstrated; and real barrel flex data is processed through a candidate pointing angle filter for a predictive muzzle reference system. Broadening the scope somewhat, the next chapter outlines a potential architecture for an Advanced Development Model (ADM) that encompasses these subsystems as well as those related to image processing, vehicle dynamics, human interaction, etc.

2.0 KALMAN FILTERING FUNDAMENTALS

2.1 CONCEPTS

A Kalman filter is a minimum variance estimator that can be used to estimate, predict and/or smooth the true state of an imprecisely known dynamical system from noisy measurements. It is usually implemented in software as a digital filtering algorithm but in the past, steady-state Kalman filter approximations were often implemented in analog hardware.

It is fairly straightforward to describe the operation of the filter in words. First, a mathematical model is derived that describes the state of the system to be estimated. This is often in the form of a set of differential equations. The filter also allows for a noise process to enter the state equations, which models the random or uncertain nature of their evolution. Another set of equations that relates the sensor measurements to the system states is derived and knowledge of the type of noise that the sensors generate is also required. Finally, the filter must be given a rough initial estimate of the true state and a guess of the accuracy, in the form of an initial error covariance matrix, of that initial state estimate.

The filter operates in a recursive mode. With its initial estimate of the state, and the differential equations describing the evolution of the state, the filter algorithm can propagate the state estimate forward to any point in time. However, given the noise and uncertainty inherent in the system model, the estimate will start to diverge from the true state. When sensor data is available, the filter removes as much noise from it as possible by extracting the maximum amount of information. It then uses this information to correct its estimate of the state. At this point, the error in the state estimate will have been reduced substantially. The filter then propagates its new state estimate forward in time until more sensor data is available.

2.2 SOME POSSIBLE APPLICATIONS IN FIRE CONTROL

Kalman filters appear in many military systems in various forms. Often they are only simple approximations to the full filter (because of the number of computations that must be performed at each time step) but they still perform fairly well. A common example of such an approximation is the α-β or α-β-γ target tracker. Modern battlefield computers now have the capacity to routinely implement the full set of filter equations at a very high rate enabling the particular system to achieve better accuracy and reliability.

There are many systems aboard mobile land vehicles that can benefit from the integration of a Kalman filter into the fire control system. Two areas that have seen the near universal application of the filter are multi-sensor integrated navigation systems and advanced target tracking systems. In fact, the filter was developed for navigation systems in the 1960's and nearly all integrated navigation systems in service today have a Kalman filter at the heart of their processing algorithms. Tracking systems are ideally suited to the algorithm because of the inherent filtering and prediction operations that are necessary for accurate tracking without loss of lock during target maneuvers or obscurations. The tracking application of the filter will be

expanded upon in a later chapter. Dynamic muzzle referencing is a relatively new idea that is also an excellent candidate for the Kalman filter algorithm. These potential applications are briefly described in the following paragraphs.

a) *Navigation* - Accurate positioning on the battlefield at night, in adverse weather or on featureless terrain has proven to be a tremendous advantage in modern warfare. The advent of GPS (the Global Positioning System) has allowed individual vehicles to obtain very accurate position and velocity information (at discrete times) very inexpensively. The integration (via a Kalman filter) of GPS and an inexpensive inertial navigation system (INS) greatly improves the accuracy and reliability of the system because the filter uses the GPS data to help remove the errors from the INS and the INS provides continuous position, velocity and attitude information and can navigate through outages or obscurations of the GPS satellites. A simplified INS/GPS system is used as an example later in this chapter to demonstrate the idea behind Kalman filter based sensor integration.

b) *Target Tracking* - Manual tracking of a distant target through a high-power optical sight is not easy. Even though the mirrors in the sight are often inertially stabilized, providing a reasonably steady image of the target and the background, the sight's eyepiece and the gunner's head, for that matter, are not. One can imagine trying to look through the eyepiece and make minute adjustments with the hand controls to keep the target in the center of the sight while being jostled about by the vehicle as it is moving at high speed over rough, uneven terrain. Trying to keep one's head steady and to keep one's hands from transmitting motions into the controls is exceedingly difficult. An image processing system attached to the sight offers many possibilities to improve performance. Automatic tracking algorithms can lock onto the target and keep it in the center of the field of view. Alleviating the gunner of this intensive task can free him for other functions. The tracking algorithm can be a Kalman filter, or perhaps a simplified variation of one, that uses a mathematical model of the dynamics of the target along with azimuth and elevation measurements of the target from the image processing system, to determine its most probable position at the next time step. This can be fed back to the image processing algorithm to aid it in determining what portion of the field of view should be concentrated on to locate the target in the next frame, especially if the target has briefly disappeared behind an obscuration.

c) *Target State Estimation / Trajectory Prediction* - Most current fire control systems assume very simplistic target dynamics when computing lead angles. For example, the target is often assumed to be travelling at a constant horizontal velocity with no vertical velocity. This simplifies the lead angle computations, since horizontal lead will be a function of the angular rate of the turret (caused by the gunner rotating the sight to keep the target centered) and the range to the target, while the vertical lead is only a function of the range (plus the usual shell flight compensation terms, etc.). A trajectory prediction filter, similar to, but somewhat more complicated than, a filter used in the tracker in an image processing system, can be designed to predict with much more accuracy, the location of the target at the expected time of impact of the shell. Such a filter can estimate target acceleration, as well as velocity, in all three directions - range, cross range, and vertical. This would greatly enhance the accuracy

of the fire control system against highly maneuverable targets such as high-speed evasive ground targets and, especially, helicopters.

d) *Stabilization System Error Compensation* - The gun and turret stabilization systems on current land vehicles are good, but they are not perfect. Under static conditions, a modern electric drive, or even a later-generation hydraulic drive, can position the gun to within a fraction of a milliradian of the desired position. However, under dynamic conditions the gun control system will be unable to remove all of the motion disturbances. Current DFSV's often use a simple "fire inhibit" scheme that prevents firing until the gun is sufficiently aligned to the target. If these motions can be reasonably well modelled, a Kalman filter based compensation system could be designed to predict when the stabilization system will have the gun pointing in the proper direction.

e) *Dynamic Muzzle Referencing* - The terrain-induced flexing of the gun barrel will result in the muzzle of the barrel pointing in a different direction than the gun control system assumes it is. These motions can be reasonably well modelled and hence can be used in a Kalman filter based compensation system to predict when the muzzle will be pointing in the desired direction. This is the subject of Chapter 6. The ignition of the charge can be delayed for a few milliseconds so that the shot exit time coincides with a barrel flex zero-crossing time.

2.3 KALMAN FILTER EQUATIONS

The Kalman filter equations can be given in several forms, since they have been developed for both continuous and discrete time, linear and nonlinear, and time-varying or time-invariant systems. Here we will show the case of the linear, discrete, time-invariant form. The reader is referred to *e.g.* Gelb (1974) for other variations and more complete derivations.

Let $\boldsymbol{x}_k$ denote a vector (generally, bold face will denote vectors and capitals will denote matrices, E(•) denotes expected value and := denotes a definition) of dimension n representing the true state of a linear, discrete-time system at time index k:

$$\boldsymbol{x}_{k+1} = \Phi_k \boldsymbol{x}_k + \boldsymbol{w}_k \tag{2-1}$$

where Φ_k is a known $n \times n$ matrix governing the transition of the state from time t_k to t_{k+1} and $\boldsymbol{w}_k$ is an n-dimensional, zero mean, Gaussian random vector with covariance Q_k that enters the system at t_k and perturbs the state in a random manner. This type of model is often assumed to have arisen from a continuous time system of the form

$$\dot{\boldsymbol{x}}_c(t) = F\boldsymbol{x}_c(t) + \boldsymbol{w}_c(t) \tag{2-2}$$

where $\dot{x}_c(t) = dx_c/dt$ denotes the time derivative of the continuous time signal, $x_c(t)$. Here, $w_c(t)$ is a continuous time, zero mean, uncorrelated Gaussian stochastic process vector with power spectral density matrix $Q_c(t)$,

$$E\{w_c(t)w_c(\tau)^T\} = Q_c(t)\delta(t-\tau)$$

where $\delta(t)$ is the Dirac delta functional. Equation (2-2) can be discretized to obtain the difference equation (2-1) via:

$$\begin{aligned}
\Phi_k &= e^{F(t_{k+1}-t_k)} \\
w_k &= \int_{t_k}^{t_{k+1}} e^{F(t_{k+1}-\tau)} w_c(\tau)d\tau \\
Q_k &= \int_{t_k}^{t_{k+1}} e^{F(t_{k+1}-\tau)} Q_c(\tau) e^{F^T(t_{k+1}-\tau)} d\tau
\end{aligned} \tag{2-3}$$

It is assumed that the sensors of the system provide information about elements of the state vector at time t_k but that this may be corrupted by noise. This is represented by

$$z_k = H_k x_k + v_k \tag{2-4}$$

where z_k is an m-dimensional vector of measurements, H_k is a known $m \times n$ matrix relating these measurements to the system states, and v_k is an m-dimensional random noise sequence that corrupts the sensor data.

Certain simplifying assumptions are usually made about the noise sequences, though they are not all necessary in the most general Kalman filter formulations and can often be relaxed. The measurement noise is assumed to be a zero-mean, Gaussian sequence with covariance R_k, and is uncorrelated with the initial state, the state noise, w_k, and previous values of itself:

$$\begin{aligned}
E(v_k) &= 0, \qquad E(v_k v_j^T) = R_k \delta_{kj} \\
E(v_k w_j^T) &= 0, \qquad E(v_k x_0^T) = 0
\end{aligned} \tag{2-5}$$

where δ_{kj} is the Kronecker delta function defined as

$$\delta_{kj} := \begin{cases} 1, & j=k \\ 0, & j \neq k \end{cases}$$

The state noise is assumed to have a similar form:

$$
\begin{aligned}
E(w_k) &= 0 \\
E(w_k w_j^T) &= Q_k \delta_{kj} \\
E(w_k x_0^T) &= 0
\end{aligned}
\tag{2-6}
$$

In order to start the Kalman filter, an initial estimate of the state and its covariance, P, must be given. Often, the designer has some knowledge of the statistics of the initial state vector so the initial state estimate is set to the expected value of the true state:

$$
\begin{aligned}
\hat{x}_0 &= E(x_0) \\
P_0 &= E\{(x_0 - \hat{x}_0)(x_0 - \hat{x}_0)^T\}
\end{aligned}
\tag{2-7}
$$

(In practice, though, the first few measurements are often used to estimate the initial states.)

Given all these assumptions, the Kalman filter will produce the optimal linear estimate of the true state at time k, given all available measurements. Optimal, here, is defined as the unbiased linear estimator which has the *minimum variance* or *minimum mean square error*. That is, the state estimate is chosen from the set of all possible $\hat{x}$ vectors to satisfy

$$
\begin{aligned}
& E\{x - \hat{x}\} = 0 \\
\text{and,} \quad & \min_{\hat{x}} E\{(x-\hat{x})^T(x-\hat{x})\}
\end{aligned}
\tag{2-8}
$$

Let Z_k denote the set of all measurements up to and including time k:

$$
Z_k = \{z_0, z_1, \ldots, z_k\} \tag{2-9}
$$

One can show that the value of $\hat{x}$ that satisfies (2-8) is given by the conditional expectation of x given all the measurements up to t_k. This will be denoted by $\hat{x}_{k|k}$:

$$
\hat{x}_{k|k} := E(x_k | Z_k)
$$

The covariance matrix of the estimation error at time t_k given measurements up to that time will be denoted by $P_{k|k}$:

$$
P_{k|k} := E\{[x_k - \hat{x}_{k|k}][x_k - \hat{x}_{k|k}]^T\}
$$

Similarly, the optimal estimate of x given only the measurements up to t_{k-1} is

$$\hat{x}_{k|k-1} := E(x_k|Z_{k-1})$$

and the corresponding error covariance matrix is

$$P_{k|k-1} := E\{[x_k - \hat{x}_{k|k-1}][x_k - \hat{x}_{k|k-1}]^T\}$$

The Kalman iteration proceeds with an *update*, followed by a *propagate*. A block diagram of a general Kalman filter is shown in Fig. 2-1. For the update, assume that estimates of the state vector and its covariance matrix are available at t_k that make use of all measurements up to t_{k-1}, *i.e.*, $\hat{x}_{k|k-1}$ and $P_{k|k-1}$. When a new measurement, z_k, arrives, the Kalman filter *updates* its estimate of the state with the following:

$$\hat{x}_{k|k} = \hat{x}_{k|k-1} + K_k [z_k - H_k \hat{x}_{k|k-1}] \qquad (2\text{-}10)$$

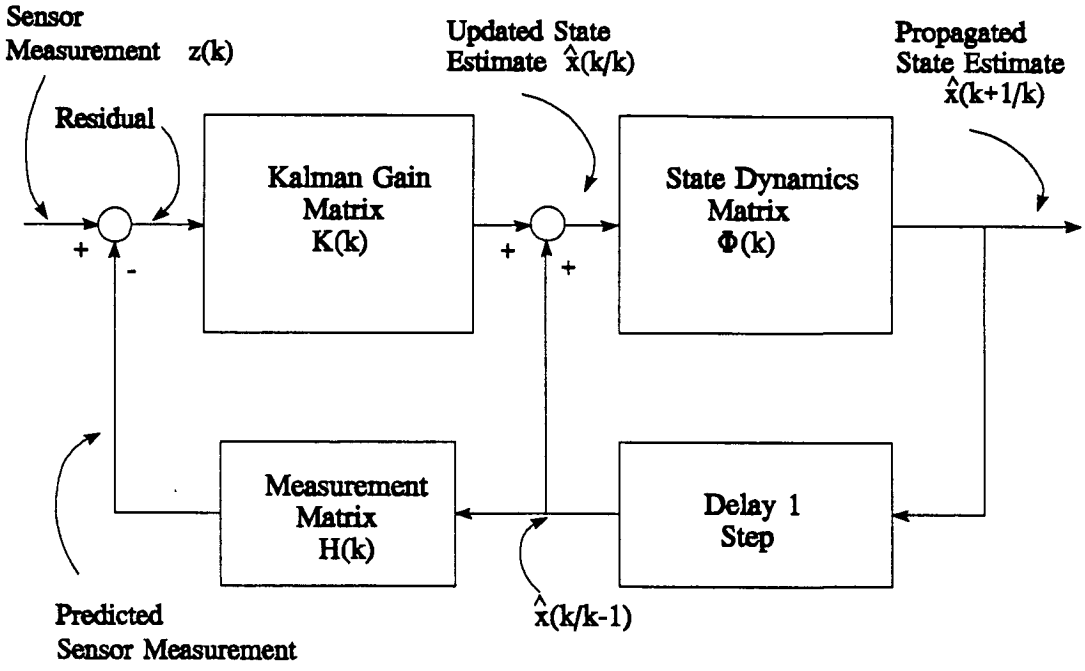

Fig. 2-1: The General Kalman Filter Algorithm

A closer look at this update equation shows that the filter improves its estimate of the state by adding a correction term to its previous estimate. This correction is formed by taking the *residual* (the difference between the sensor measurement, z_k, and the estimate of what the measurement should be, $H_k\hat{x}_{k|k-1}$) and then multiplying this by the *Kalman gain matrix*, K_k. The gain matrix is chosen to satisfy (2-8) and can be shown to be given by

$$K_k = P_{k|k-1}H_k^T [H_k P_{k|k-1} H_k^T + R_k]^{-1} \tag{2-11}$$

The filter also updates its estimate of the error covariance matrix at this time via

$$P_{k|k} = P_{k|k-1} - K_k H_k P_{k|k-1} \tag{2-12}$$

From this equation, it is reasonable to see (and, in fact, can be shown) that the error covariance matrix will become smaller, since a term is being subtracted from its previous value. Thus the Kalman filter has reduced the uncertainty in its error estimate when it has been updated with a new measurement.

The purpose of the other stage of the filter, the *propagate* stage, is to advance the current estimates of the state and the error covariance ahead in time until the next measurement becomes available at t_{k+1}. This step is relatively simple as it merely uses the transition matrix (or *dynamics* matrix, as in Fig. 2-1) that is assumed to describe the system in (2-1):

$$\begin{aligned} \hat{x}_{k+1|k} &= \Phi_k \hat{x}_{k|k} \\ P_{k+1|k} &= \Phi_k P_{k|k} \Phi_k^T + Q_k \end{aligned} \tag{2-13}$$

Equations (2-10) to (2-13), together with the assumptions (2-5) and (2-6) and initial conditions (2-7) form the basic Kalman filter algorithm.

2.4 EXTENDED KALMAN FILTER

As was mentioned before, there are many variations of the basic filter. A version of the *Extended Kalman Filter (EKF)*, will be outlined in this section.

Consider the case when the measurements are *nonlinear* functions of the state vector:

$$z_k = h_k(x_k) + v_k \tag{2-14}$$

where $h_k(\cdot)$ can be a general nonlinear vector function of x_k. Such a system description is very common in target tracking systems. For example, since the target is often modelled in an x-y-z Cartesian coordinate frame and the sensor is often a range-angle-angle measuring radar, a nonlinear coordinate transformation is required between the state and measurement equations.

It can be shown that a very close approximation to the optimal Kalman filter can be obtained when this non-linear function, $h_k(\cdot)$, is linearized around the current value of the state estimate; that is, the matrix $H_k(\hat{x}_{k|k-1})$ is computed by differentiating $h_k(x)$ with respect to the vector x and evaluating the result at the current value of $\hat{x}_{k|k-1}$:

$$H_k(\hat{x}_{k|k-1}) := \frac{\partial h_k(x)}{\partial x}\Big|_{\hat{x}_{k|k-1}} \tag{2-15}$$

where differentiation of one vector with respect to another is defined in the standard way as

$$\left[\frac{\partial f(x)}{\partial x}\right]_{ij} := \frac{\partial f_i}{\partial x_j}$$

where the subscripts here denote the corresponding vector and matrix elements. This adds only a small amount of extra computation to the filter and is fairly simple to implement. The Kalman filter update equations change slightly: Equations (2-10) to (2-12) become:

$$\hat{x}_{k|k} = \hat{x}_{k|k-1} + K_k\,[z_k - h_k(\hat{x}_{k|k-1})] \tag{2-16}$$

$$K_k = P_{k|k-1}H_k^T(\hat{x}_{k|k-1})\,[H_k(\hat{x}_{k|k-1})P_{k|k-1}H_k^T(\hat{x}_{k|k-1}) + R_k]^{-1} \tag{2-17}$$

$$P_{k|k} = P_{k|k-1} - K_kH_k(\hat{x}_{k|k-1})P_{k|k-1} \tag{2-18}$$

The propagate stage, (2-13), remains unchanged for the Extended Kalman filter:

$$\hat{x}_{k+1|k} = \Phi_k \hat{x}_{k|k}$$
$$P_{k+1|k} = \Phi_k P_{k|k} \Phi_k^T + Q_k \qquad (2\text{-}19)$$

2.5 AN EXAMPLE: A SINGLE AXIS INTEGRATED NAVIGATION SYSTEM

A simplified, one-dimensional navigation example will be described here to show the principles of designing a Kalman filter for a multi-sensor integrated system that provides a more accurate and reliable solution than if the sensors were used individually. Modern navigation systems often consist of several independent sensors, all giving measurements related to position, velocity or heading that the navigator must assemble into a reasonable estimate of his true situation. The Kalman filter has been successfully applied to automate this process. A large system may have one or more inertial navigation systems (INS's), a Global Positioning System (GPS) receiver, other receivers for land-based radio wave systems such as Loran-C and Omega, a velocity sensor (water speed log, air speed data, doppler velocity, or odometer for example), heading sensors (magnetic compass, gyrocompass), height sensor (barometric altimeter, radar altimeter), or a number of others. (See McMillan (1987) for details of such a navigation system as applied to arctic land vehicles.) A full Kalman filter is quite complex, often estimating as many as 50 or 60 state variables from 10 to 20 measurements.

Consider the much simplified problem of integrating two sensors (an INS and a GPS set) to estimate position p in one direction, say latitude (similar to Example 4.2-4 of Gelb (1974)). In most navigation applications, the filter does not estimate the position, *per se*, but rather the *error* in the position as reported by the INS. This is because these errors can be very accurately modelled in terms of linear stochastic processes, whereas the position itself is dominated by non-random control input (from the vehicle operator) which cannot be so accurately modelled. Also, if the aiding sensor becomes unavailable, the filter will still be providing corrected INS position outputs, even though the filter estimates of the errors will slowly degrade (a fail-operational system).

Our simple model of the single axis INS will be an accelerometer with an output $a(t)$, that is integrated to give speed $s(t)$, and then again to give position $p(t)$:

$$p(t) = \int_0^t s(\tau)d\tau$$
$$s(t) = \int_0^t a(\tau)d\tau$$

However, the accelerometer has an unknown but constant bias error, b, that is being twice integrated so that the indicated position has an error that is growing as t^2. The Kalman filter will try to estimate this error so that it can be removed. The INS error states modelled in the filter are INS position error δp, INS speed error δs, and INS accelerometer error δa. The relations between the states are

$$\frac{d}{dt}\delta p(t) = \delta\dot{p}(t) = \delta s(t)$$
$$\frac{d}{dt}\delta s(t) = \delta\dot{s}(t) = \delta a(t) \quad (= b, \text{ the unknown bias})$$
$$\frac{d}{dt}\delta a(t) = \delta\dot{a}(t) = 0$$

which can be written in matrix form as

$$\begin{bmatrix}\delta\dot{p}(t)\\ \delta\dot{s}(t)\\ \delta\dot{a}(t)\end{bmatrix} = \begin{bmatrix}0 & 1 & 0\\ 0 & 0 & 1\\ 0 & 0 & 0\end{bmatrix}\begin{bmatrix}\delta p(t)\\ \delta s(t)\\ \delta a(t)\end{bmatrix}$$

Note that this is in the form of the continuous time system of Eq. (2-2) with $w_c = 0$. This system can be discretized, at a sampling interval of $\Delta T = t_{k+1}-t_k$, via (2-3) to get the state transition matrix Φ_k. If we define F as

$$F := \begin{bmatrix}0 & 1 & 0\\ 0 & 0 & 1\\ 0 & 0 & 0\end{bmatrix}$$

then

$$\Phi_k = e^{F\Delta T} = I + F\Delta T + \frac{F^2\Delta T^2}{2!} + \frac{F^3\Delta T^3}{3!} + \ldots$$
$$= \begin{bmatrix}1 & \Delta T & \frac{\Delta T^2}{2}\\ 0 & 1 & \Delta T\\ 0 & 0 & 1\end{bmatrix}$$

so the discrete system corresponding to (2-1) is

$$\begin{bmatrix} \delta p \\ \delta s \\ \delta a \end{bmatrix}_{k+1} = \begin{bmatrix} 1 & \Delta T & \frac{\Delta T^2}{2} \\ 0 & 1 & \Delta T \\ 0 & 0 & 1 \end{bmatrix} \begin{bmatrix} \delta p \\ \delta s \\ \delta a \end{bmatrix}_k + 0 \tag{2-20}$$

or, by making the appropriate association of notation,

$$x_{k+1} = \Phi_k x_k + 0$$

The measurement for this example will be the difference between the indicated positions of the GPS set and the INS:

$$z_k = p_k(GPS) - p_k(INS) \tag{2-21}$$

The measurement from the INS consists of the true position plus the INS position error:

$$p_k(INS) = p_k + \delta p_k$$

and the measurement from the GPS will modelled as the true position plus the GPS position error, which we call v_k:

$$p_k(GPS) = p_k + v_k$$

Thus the measurement equation (2-21) becomes

$$\begin{aligned} z_k &= v_k - \delta p_k \\ &= [-1\ 0\ 0] \begin{bmatrix} \delta p \\ \delta s \\ \delta a \end{bmatrix}_k + v_k \\ &= Hx_k + v_k \end{aligned}$$

which is in the form required in (2-4) with $H := [-1\ 0\ 0]$. The GPS positioning error will be modelled as an uncorrelated Gaussian random noise sequence that satisfies (2-5) with covariance σ^2_{GPS}:

$$E\{v_k v_k\} = R_k = \sigma^2_{GPS}$$

All that remains in the filter design is to specify the initial conditions on the state vector, $\hat{x}_{0|-1}$, and the state covariance matrix, $P_{0|-1}$. As is usual, the initial state estimate is set to zero, and the initial covariance estimate is chosen as some physically reasonable estimate of the error variance:

$$\hat{x}_{0|-1} = \begin{bmatrix} 0 \\ 0 \\ 0 \end{bmatrix}$$

$$P_{0|-1} = \begin{bmatrix} \delta\hat{p}_0^2 & 0 & 0 \\ 0 & \delta\hat{s}_0^2 & 0 \\ 0 & 0 & \delta\hat{a}_0^2 \end{bmatrix}$$

The specification of the Kalman filter matrices for this simplified system is complete. Just to complete the design, some numerical values such as those shown below can be specified:

$$\sigma_{GPS}^2 = (100\ m)^2$$
$$\delta\hat{p}_0^2 = (1000\ m)^2$$
$$\delta\hat{s}_0^2 = (10\ m/s)^2$$
$$\delta\hat{a}_0^2 = (1\ m/s^2)^2$$

That is the essence of the procedure involved in Kalman filter design. There are many complications to this in most real systems. For example, the state process noise, w_c, is seldom assumed to be zero as this can cause the filter gains to go to zero and the filter essentially stops operating. The numerical values of the noise parameters are chosen after careful analysis, simulation and testing on real data to achieve satisfactory performance. The state dynamics and measurement matrices (Φ_k, H) are generally much more complex and various precautions must be taken to ensure numerical stability and to safeguard against invalid measurements. The sequence of operations can also be more complex since all aiding measurements are seldom available in such a synchronous fashion.

3.0 TRACKING AND TRAJECTORY PREDICTION

3.1 INTRODUCTION

This chapter summarizes the design of a simulation system that was used to evaluate various Kalman tracking filter configurations that could enable land platforms to track and engage multiple maneuvering targets, either passively or actively. Typically a direct-fire support vehicle (DFSV) acquires and must track multiple targets with a passive, 2-dimensional imaging sensor such as a TV or infrared camera. When a particular target is chosen to be engaged, an active sensor, such as a laser range finder, radar, or laser radar, would be used to obtain range and possibly range-rate information. In most current generation vehicles, a laser range finder is used to obtain one range measurement just prior to firing that is used to calculate the elevation and azimuth lead angles using two decoupled, second-order, constant angular rate filters. Target trajectory prediction can be improved substantially if a fully coupled 3-dimensional Kalman filter tracking algorithm is used especially if range is measured for even a few scans.

3.2 TARGET MODELLING

This section looks at some of the typical coordinate frames, the transformations between them and the structure of some target dynamics models that can be used.

3.2.1 Coordinate Frames and Transformations

A point in three dimensional space can be specified in a variety of ways but usually in either rectangular or spherical coordinates. As was mentioned Section 2.4, the sensor of a tracking system is usually most naturally represented in a spherical frame but the target knows nothing about the sensor frame and is more naturally modelled in rectangular coordinates, since it is more likely to travel in a straight line than it is to move along the surface of a sphere.

Consider the coordinate frames shown in Fig. 3-1. The principle rectangular frame is defined by the X_G-Y_G-Z_G axes which are aligned with the local geographic North, East and Down directions with the origin at the sensor location. The target at point $\boldsymbol{p}$ can be described in rectangular coordinates at the point $(p_{X_G}, p_{Y_G}, p_{Z_G})$ or in spherical coordinates at (r,b,e) where b is the bearing angle from X_G (North), e is the elevation angle above the horizon, and r is the distance or range from the sensor location at the origin. The other rectangular frame shown as X_L-Y_L-Z_L is called the *line-of-sight-to-target* frame and is obtained by rotating the geographic frame, first about the Z_G axis through an angle b and then elevating it (rotating about the new Y_G axis) by the angle e. It has the same origin as the geographic frame, although it is shown separated to reduce the clutter on the diagram. The line-of-sight frame is called such because the x-axis of the frame always points directly to the target.

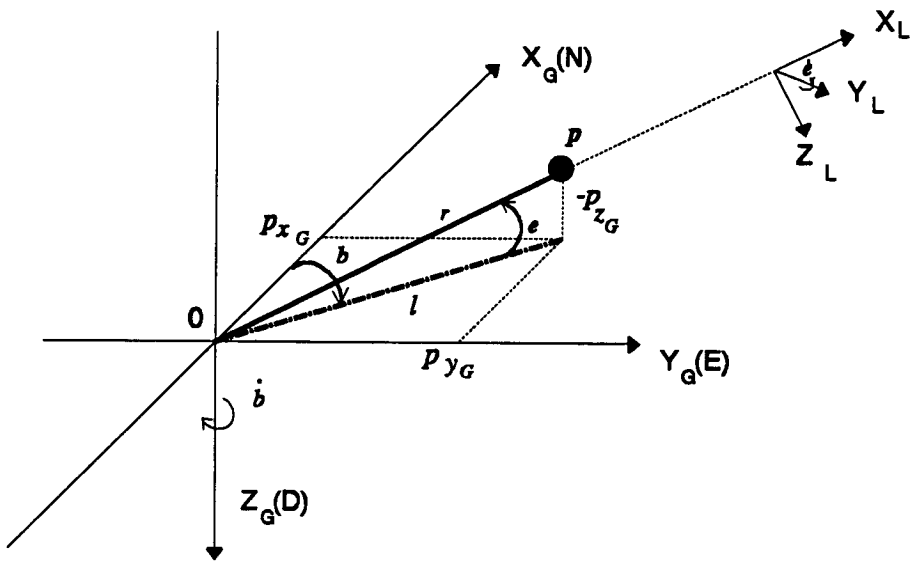

Fig. 3-1: Target Coordinate Frames

Vectors in the geographic frame can be expressed in the line-of-sight frame by

$$\begin{bmatrix} p_{X_L} \\ p_{Y_L} \\ p_{Z_L} \end{bmatrix} = \begin{bmatrix} \cos e \cos b & \cos e \sin b & -\sin e \\ -\sin b & \cos b & 0 \\ \sin e \cos b & \sin e \sin b & \cos e \end{bmatrix} \begin{bmatrix} p_{X_G} \\ p_{Y_G} \\ p_{Z_G} \end{bmatrix} =: C_G^L \begin{bmatrix} p_{X_G} \\ p_{Y_G} \\ p_{Z_G} \end{bmatrix} \tag{3-1}$$

where C_G^L is the *Direction Cosine Matrix* (DCM) that converts a vector expressed in G coordinates to one expressed in L coordinates. Similarly the inverse transformation is

$$\begin{bmatrix} p_{X_G} \\ p_{Y_G} \\ p_{Z_G} \end{bmatrix} = \begin{bmatrix} \cos e \cos b & -\sin b & \sin e \cos b \\ \cos e \sin b & \cos b & \sin e \sin b \\ -\sin e & 0 & \cos e \end{bmatrix} \begin{bmatrix} p_{X_L} \\ p_{Y_L} \\ p_{Z_L} \end{bmatrix} =: C_L^G \begin{bmatrix} p_{X_L} \\ p_{Y_L} \\ p_{Z_L} \end{bmatrix} \tag{3-2}$$

To simplify notation slightly, let $\boldsymbol{p}^{(G)}$ denote an arbitrary 3-dimensional vector that is expressed in G coordinates. Then we simply write

$$\begin{aligned} \boldsymbol{p}^{(G)} &= C_L^G \, \boldsymbol{p}^{(L)} \\ \boldsymbol{p}^{(L)} &= C_G^L \, \boldsymbol{p}^{(G)} \end{aligned}$$

The bearing and elevation angles can be expressed in terms of the geographic coordinates as

$$\begin{aligned} r &= \sqrt{p_{X_G}^2 + p_{Y_G}^2 + p_{Z_G}^2} \\ b &= \tan^{-1}(p_{X_G}/p_{Y_G}) \\ e &= \sin^{-1}(-p_{Z_G}/r) \end{aligned} \tag{3-3}$$

and similarly the reverse is

$$\begin{aligned} p_{X_G} &= r \cos e \cos b \\ p_{Y_G} &= r \cos e \sin b \\ p_{Z_G} &= -r \sin e \end{aligned} \tag{3-4}$$

Since the target is moving relative to the sensor, the line-of-sight frame is rotating with respect to the geographic frame. The rate of rotation of the L frame with respect to the G frame will be denoted as $\omega_{L/G}$ and can be written in L frame coordinates as

$$\begin{aligned} \omega_{L/G}^{(L)} &= \dot{b} \, \boldsymbol{u}_{Z_G}^{(G)} + \dot{e} \, \boldsymbol{u}_{Y_L}^{(L)} \\ &= \dot{b} \, (\boldsymbol{u}_{Z_L}^{(L)} \cos e - \boldsymbol{u}_{X_L}^{(L)} \sin e) + \dot{e} \, \boldsymbol{u}_{Y_L}^{(L)} \\ &= \begin{bmatrix} -\dot{b} \sin e \\ \dot{e} \\ \dot{b} \cos e \end{bmatrix}^{(L)} \end{aligned} \tag{3-5}$$

where $\boldsymbol{u}_v$ denotes a unit vector in the direction v, $\dot{b}$ is the bearing slewing rate and $\dot{e}$ is the elevation slew rate. The Coriolus equation can be used to transform velocities in a rotating frame to a non-rotating frame: the rate of change of a vector $\boldsymbol{p}$ in the rotating frame as seen from the

nonrotating frame is known to be (*e.g.* Goldstein (1950) p. 133)

$$\left(\frac{d\boldsymbol{p}}{dt}\right)_G = \left(\frac{d\boldsymbol{p}}{dt}\right)_L + \omega_{L/G} \times \boldsymbol{p} \tag{3-6}$$

where the notation $(.)_G$ denotes the coordinate frame from which the vector is being viewed. Expressing all vectors of (3-6) in the same, say L, coordinates and defining velocity as

$$\boldsymbol{v} := \left(\frac{d\boldsymbol{p}}{dt}\right)_G \tag{3-7}$$

yields

$$\begin{pmatrix} v_{X_L} \\ v_{Y_L} \\ v_{Z_L} \end{pmatrix}^{(L)} = \left(\frac{d\boldsymbol{p}}{dt}\right)_G^{(L)} = \left(\frac{d\boldsymbol{p}}{dt}\right)_L^{(L)} + \omega_{L/G}^{(L)} \times \boldsymbol{p}^{(L)}$$

Now, since the L frame is aligned with its X axis towards $\boldsymbol{p}$ which is a distance r away, the target position and velocity in L coordinates are simply

$$\boldsymbol{p}^{(L)} = \begin{bmatrix} r \\ 0 \\ 0 \end{bmatrix}^{(L)}, \qquad \left(\frac{d\boldsymbol{p}}{dt}\right)_L^{(L)} = \begin{bmatrix} \dot{r} \\ 0 \\ 0 \end{bmatrix}^{(L)}$$

so that by substituting these in the Coriolus equation, we get the velocity vector of $\boldsymbol{p}$ as seen from the non-rotating G frame (though it is still coordinatized in L coordinates):

$$\begin{aligned} \begin{bmatrix} v_{X_L} \\ v_{Y_L} \\ v_{Z_L} \end{bmatrix}_G^{(L)} &= \begin{bmatrix} \dot{r} \\ 0 \\ 0 \end{bmatrix}_L^{(L)} + \begin{bmatrix} -\dot{b}\,\sin e \\ \dot{e} \\ \dot{b}\,\cos e \end{bmatrix}^{(L)} \times \begin{bmatrix} r \\ 0 \\ 0 \end{bmatrix}^{(L)} \\ &= \begin{bmatrix} \dot{r} \\ r\,\dot{b}\,\cos e \\ -r\,\dot{e} \end{bmatrix}^{(L)} \end{aligned} \tag{3-8}$$

The appropriate DCM can be used to convert these velocities as seen in the G frame from L to G coordinates via

$$\begin{bmatrix} v_{X_G} \\ v_{Y_G} \\ v_{Z_G} \end{bmatrix}^{(G)} = \left[C_L^G\right] \begin{bmatrix} v_{X_L} \\ v_{Y_L} \\ v_{Z_L} \end{bmatrix}^{(L)}$$

Equation (3-8) can be inverted so that the angular rates are obtained from the velocities:

$$\begin{bmatrix} \dot{r} \\ \dot{b} \\ \dot{e} \end{bmatrix} = \begin{bmatrix} v_{X_L} \\ v_{Y_L}/(r\cos e) \\ -v_{Z_L}/r \end{bmatrix} \tag{3-9}$$

Similarly the Coriolus equation can be used to derive accelerations as seen in rotating coordinate frames:

$$\left(\frac{d^2\boldsymbol{p}}{dt^2}\right)_G = \frac{d}{dt}\left[\left(\frac{d\boldsymbol{p}}{dt}\right)_G\right]_G$$

$$= \frac{d}{dt}\left[\left(\frac{d\boldsymbol{p}}{dt}\right)_L + \omega_{L/G}\times\boldsymbol{p}\right]_G$$

$$= \frac{d}{dt}\left[\left(\frac{d\boldsymbol{p}}{dt}\right)_L\right]_G + \frac{d}{dt}\left(\omega_{L/G}\times\boldsymbol{p}\right)_G$$

$$= \frac{d}{dt}\left[\left(\frac{d\boldsymbol{p}}{dt}\right)_L\right]_L + \omega_{L/G}\times\left(\frac{d\boldsymbol{p}}{dt}\right)_L + \left(\frac{d\omega_{L/G}}{dt}\right)_G\times\boldsymbol{p} + \omega_{L/G}\times\left(\frac{d\boldsymbol{p}}{dt}\right)_G$$

$$= \left(\frac{d^2\boldsymbol{p}}{dt^2}\right)_L + \omega_{L/G}\times\left(\frac{d\boldsymbol{p}}{dt}\right)_L + \left(\frac{d\omega_{L/G}}{dt}\right)_G\times\boldsymbol{p} + \omega_{L/G}\times\left[\left(\frac{d\boldsymbol{p}}{dt}\right)_L + \omega_{L/G}\times\boldsymbol{p}\right]$$

$$= \left(\frac{d^2\boldsymbol{p}}{dt^2}\right)_L + 2\omega_{L/G}\times\left(\frac{d\boldsymbol{p}}{dt}\right)_L + \left(\frac{d\omega_{L/G}}{dt}\right)_G\times\boldsymbol{p} + \omega_{L/G}\times(\omega_{L/G}\times\boldsymbol{p})$$

and then choosing the L frame to coordinitize all vectors and defining acceleration as

$$\boldsymbol{a} := \left(\frac{d\boldsymbol{p}^2}{dt^2}\right)_G \tag{3-10}$$

yields

$$\begin{bmatrix} a_{X_L} \\ a_{Y_L} \\ a_{Z_L} \end{bmatrix}^{(L)} = \left(\frac{d^2\boldsymbol{p}}{dt^2}\right)_G^{(L)} = \left(\frac{d^2\boldsymbol{p}}{dt^2}\right)_L^{(L)} + 2\omega_{L/G}^{(L)} \times \left(\frac{d\boldsymbol{p}}{dt}\right)_L^{(L)} + \left(\frac{d\omega_{L/G}}{dt}\right)_G^{(L)} \times \boldsymbol{p}^{(L)} + \omega_{L/G}^{(L)} \times (\omega_{L/G}^{(L)} \times \boldsymbol{p}^{(L)}) \tag{3-11}$$

The angular acceleration of the rotating coordinate frame can be found by

$$\left(\frac{d\omega_{L/G}}{dt}\right)^{(L)} = \frac{d}{dt}\begin{bmatrix} -\dot{b}\sin e \\ \dot{e} \\ \dot{b}\cos e \end{bmatrix}^{(L)} = \begin{bmatrix} -\ddot{b}\sin e - \dot{b}\dot{e}\cos e \\ \ddot{e} \\ \ddot{b}\cos e - \dot{b}\dot{e}\sin e \end{bmatrix}^{(L)}$$

so substituting the individual L frame components of this into (3-11) yields

$$\begin{pmatrix} a_{X_L} \\ a_{Y_L} \\ a_{Z_L} \end{pmatrix}^{(L)} = \begin{pmatrix} \ddot{r} \\ 0 \\ 0 \end{pmatrix} + 2\begin{pmatrix} -\dot{b}\sin e \\ \dot{e} \\ \dot{b}\cos e \end{pmatrix} \times \begin{pmatrix} \dot{r} \\ 0 \\ 0 \end{pmatrix} + \begin{pmatrix} -\ddot{b}\sin e - \dot{b}\dot{e}\cos e \\ \ddot{e} \\ \ddot{b}\cos e - \dot{b}\dot{e}\sin e \end{pmatrix} \times \begin{pmatrix} r \\ 0 \\ 0 \end{pmatrix} + \begin{pmatrix} -\dot{b}\sin e \\ \dot{e} \\ \dot{b}\cos e \end{pmatrix} \times \left[\begin{pmatrix} -\dot{b}\sin e \\ \dot{e} \\ \dot{b}\cos e \end{pmatrix} \times \begin{pmatrix} r \\ 0 \\ 0 \end{pmatrix}\right] \tag{3-12}$$

$$= \begin{pmatrix} \ddot{r} - r\dot{e}^2 - r\dot{b}^2\cos^2 e \\ 2\dot{r}\dot{b}\cos e + r\ddot{b}\cos e - 2r\dot{b}\dot{e}\sin e \\ -2\dot{r}\dot{e} - r\ddot{e} - r\dot{b}^2\cos e\sin e \end{pmatrix}^{(L)}$$

and finally, the DCM can be used to convert the accelerations as viewed from the G frame to coordinates in that frame:

$$\begin{bmatrix} a_{X_G} \\ a_{Y_G} \\ a_{Z_G} \end{bmatrix}^{(G)} = \left[C_L^G\right] \begin{bmatrix} a_{X_L} \\ a_{Y_L} \\ a_{Z_L} \end{bmatrix}^{(L)}$$

Again, Eq. (3-12) can be inverted to find the accelerations as seen by the tracking system:

$$\begin{pmatrix} \ddot{r} \\ \ddot{b} \\ \ddot{e} \end{pmatrix} = \begin{pmatrix} a_{X_L} + r\dot{e}^2 + r\dot{b}^2\cos^2 e \\ \dfrac{a_{Y_L}}{r\cos e} - 2\dfrac{\dot{r}}{r}\dot{b} + 2\dot{b}\dot{e}\tan e \\ \dfrac{-a_{Z_L}}{r} - 2\dfrac{\dot{r}}{r}\dot{e} - \dot{b}^2\cos e\sin e \end{pmatrix} \tag{3-13}$$

3.2.2 Target Dynamical Models

The mathematical model used to describe the motion of the target is of course dependent on the type of target. Tracking an evasive target through frequent obscurations requires a much different model than that used for a cooperative one. A good selection of common target models is summarized in Bogler (1990), Chapter 9. There are roughly 4 main categories of generic models that are used. Following the nomenclature of Fitzgerald (1981) these are:

1. Random Walk Velocity (RWV)
2. Exponentially Correlated Velocity (ECV)
3. Random Walk Acceleration (RWA)
4. Exponentially Correlated Acceleration (ECV)

Each of these models could be used in either rectangular or spherical coordinates. Listed below are the full state dynamics equations that can be used for each of these models in each coordinate frame (r - rectangular, s - spherical).

R1. Random Walk Velocity: rectangular (RWV(r)):

$$\frac{d}{dt}\begin{bmatrix} p_{X_G} \\ p_{Y_G} \\ p_{Z_G} \\ v_{X_G} \\ v_{Y_G} \\ v_{Z_G} \end{bmatrix} = \begin{bmatrix} v_{X_G} \\ v_{Y_G} \\ v_{Z_G} \\ a_{X_G} \\ a_{Y_G} \\ a_{Z_G} \end{bmatrix} = \begin{bmatrix} 0 & 0 & 0 & 1 & 0 & 0 \\ 0 & 0 & 0 & 0 & 1 & 0 \\ 0 & 0 & 0 & 0 & 0 & 1 \\ 0 & 0 & 0 & 0 & 0 & 0 \\ 0 & 0 & 0 & 0 & 0 & 0 \\ 0 & 0 & 0 & 0 & 0 & 0 \end{bmatrix} \begin{bmatrix} p_{X_G} \\ p_{Y_G} \\ p_{Z_G} \\ v_{X_G} \\ v_{Y_G} \\ v_{Z_G} \end{bmatrix} + \begin{bmatrix} 0 \\ 0 \\ 0 \\ w_{a_{XG}} \\ w_{a_{YG}} \\ w_{a_{ZG}} \end{bmatrix} \tag{3-14}$$

where w are the uncorrelated white noise processes representing the acceleration components.

R2. Exponentially Correlated Velocity: rectangular (ECV(r)):

$$\frac{d}{dt}\begin{bmatrix} p_{X_G} \\ p_{Y_G} \\ p_{Z_G} \\ v_{X_G} \\ v_{Y_G} \\ v_{Z_G} \end{bmatrix} = \begin{bmatrix} v_{X_G} \\ v_{Y_G} \\ v_{Z_G} \\ a_{X_G} \\ a_{Y_G} \\ a_{Z_G} \end{bmatrix} = \begin{bmatrix} 0 & 0 & 0 & 1 & 0 & 0 \\ 0 & 0 & 0 & 0 & 1 & 0 \\ 0 & 0 & 0 & 0 & 0 & 1 \\ 0 & 0 & 0 & -\beta_{vx} & 0 & 0 \\ 0 & 0 & 0 & 0 & -\beta_{vy} & 0 \\ 0 & 0 & 0 & 0 & 0 & -\beta_{vz} \end{bmatrix} \begin{bmatrix} p_{X_G} \\ p_{Y_G} \\ p_{Z_G} \\ v_{X_G} \\ v_{Y_G} \\ v_{Z_G} \end{bmatrix} + \begin{bmatrix} 0 \\ 0 \\ 0 \\ w_{a_{XG}} \\ w_{a_{YG}} \\ w_{a_{ZG}} \end{bmatrix} \tag{3-15}$$

where the β terms define the correlation times of the Markov processes (as described in Gelb (1974)) representing the acceleration components.

R3. Random Walk Acceleration: rectangular (RWA(r)):

$$\frac{d}{dt}\begin{bmatrix} p_{X_G} \\ p_{Y_G} \\ p_{Z_G} \\ v_{X_G} \\ v_{Y_G} \\ v_{Z_G} \\ a_{X_G} \\ a_{Y_G} \\ a_{Z_G} \end{bmatrix} = \begin{bmatrix} v_{X_G} \\ v_{Y_G} \\ v_{Z_G} \\ a_{X_G} \\ a_{Y_G} \\ a_{Z_G} \\ j_{X_G} \\ j_{Y_G} \\ j_{Z_G} \end{bmatrix} = \begin{bmatrix} 0 & 0 & 0 & 1 & 0 & 0 & 0 & 0 & 0 \\ 0 & 0 & 0 & 0 & 1 & 0 & 0 & 0 & 0 \\ 0 & 0 & 0 & 0 & 0 & 1 & 0 & 0 & 0 \\ 0 & 0 & 0 & 0 & 0 & 0 & 1 & 0 & 0 \\ 0 & 0 & 0 & 0 & 0 & 0 & 0 & 1 & 0 \\ 0 & 0 & 0 & 0 & 0 & 0 & 0 & 0 & 1 \\ 0 & 0 & 0 & 0 & 0 & 0 & 0 & 0 & 0 \\ 0 & 0 & 0 & 0 & 0 & 0 & 0 & 0 & 0 \\ 0 & 0 & 0 & 0 & 0 & 0 & 0 & 0 & 0 \end{bmatrix} \begin{bmatrix} p_{X_G} \\ p_{Y_G} \\ p_{Z_G} \\ v_{X_G} \\ v_{Y_G} \\ v_{Z_G} \\ a_{X_G} \\ a_{Y_G} \\ a_{Z_G} \end{bmatrix} + \begin{bmatrix} 0 \\ 0 \\ 0 \\ 0 \\ 0 \\ 0 \\ w_{j_{XG}} \\ w_{j_{YG}} \\ w_{j_{ZG}} \end{bmatrix} \tag{3-16}$$

where *j* denotes "jerk" or the rate of change of acceleration.

R4. Exponentially Correlated Acceleration: rectangular (ECA(r)):

$$\frac{d}{dt}\begin{bmatrix} p_{X_G} \\ p_{Y_G} \\ p_{Z_G} \\ v_{X_G} \\ v_{Y_G} \\ v_{Z_G} \\ a_{X_G} \\ a_{Y_G} \\ a_{Z_G} \end{bmatrix} = \begin{bmatrix} v_{X_G} \\ v_{Y_G} \\ v_{Z_G} \\ a_{X_G} \\ a_{Y_G} \\ a_{Z_G} \\ j_{X_G} \\ j_{Y_G} \\ j_{Z_G} \end{bmatrix} = \begin{bmatrix} 0 & 0 & 0 & 1 & 0 & 0 & 0 & 0 & 0 \\ 0 & 0 & 0 & 0 & 1 & 0 & 0 & 0 & 0 \\ 0 & 0 & 0 & 0 & 0 & 1 & 0 & 0 & 0 \\ 0 & 0 & 0 & 0 & 0 & 0 & 1 & 0 & 0 \\ 0 & 0 & 0 & 0 & 0 & 0 & 0 & 1 & 0 \\ 0 & 0 & 0 & 0 & 0 & 0 & 0 & 0 & 1 \\ 0 & 0 & 0 & 0 & 0 & 0 & -\beta_{ax} & 0 & 0 \\ 0 & 0 & 0 & 0 & 0 & 0 & 0 & -\beta_{ay} & 0 \\ 0 & 0 & 0 & 0 & 0 & 0 & 0 & 0 & -\beta_{az} \end{bmatrix} \begin{bmatrix} p_{X_G} \\ p_{Y_G} \\ p_{Z_G} \\ v_{X_G} \\ v_{Y_G} \\ v_{Z_G} \\ a_{X_G} \\ a_{Y_G} \\ a_{Z_G} \end{bmatrix} + \begin{bmatrix} 0 \\ 0 \\ 0 \\ 0 \\ 0 \\ 0 \\ w_{j_{XG}} \\ w_{j_{YG}} \\ w_{j_{ZG}} \end{bmatrix} \tag{3-17}$$

S1. Random Walk Velocity: spherical (RWV(s)):

$$\frac{d}{dt}\begin{bmatrix} b \\ e \\ r \\ \dot{b} \\ \dot{e} \\ \dot{r} \end{bmatrix} = \begin{bmatrix} 0 & 0 & 0 & 1 & 0 & 0 \\ 0 & 0 & 0 & 0 & 1 & 0 \\ 0 & 0 & 0 & 0 & 0 & 1 \\ 0 & 0 & 0 & 0 & 0 & 0 \\ 0 & 0 & 0 & 0 & 0 & 0 \\ 0 & 0 & 0 & 0 & 0 & 0 \end{bmatrix} \begin{bmatrix} b \\ e \\ r \\ \dot{b} \\ \dot{e} \\ \dot{r} \end{bmatrix} + \begin{bmatrix} 0 \\ 0 \\ 0 \\ w_{a_b} \\ w_{a_e} \\ w_{a_r} \end{bmatrix} \tag{3-18}$$

S2. Exponentially Correlated Velocity: spherical (ECV(s)):

$$\frac{d}{dt}\begin{bmatrix} b \\ e \\ r \\ \dot{b} \\ \dot{e} \\ \dot{r} \end{bmatrix} = \begin{bmatrix} 0 & 0 & 0 & 1 & 0 & 0 \\ 0 & 0 & 0 & 0 & 1 & 0 \\ 0 & 0 & 0 & 0 & 0 & 1 \\ 0 & 0 & 0 & -\beta_{vb} & 0 & 0 \\ 0 & 0 & 0 & 0 & -\beta_{ve} & 0 \\ 0 & 0 & 0 & 0 & 0 & -\beta_{vr} \end{bmatrix} \begin{bmatrix} b \\ e \\ r \\ \dot{b} \\ \dot{e} \\ \dot{r} \end{bmatrix} + \begin{bmatrix} 0 \\ 0 \\ 0 \\ w_{a_b} \\ w_{a_e} \\ w_{a_r} \end{bmatrix} \tag{3-19}$$

S3. Random Walk Acceleration: spherical (RWA(s)):

$$\frac{d}{dt}\begin{bmatrix} b \\ e \\ r \\ \dot{b} \\ \dot{e} \\ \dot{r} \\ \ddot{b} \\ \ddot{e} \\ \ddot{r} \end{bmatrix} = \begin{bmatrix} 0 & 0 & 0 & 1 & 0 & 0 & 0 & 0 & 0 \\ 0 & 0 & 0 & 0 & 1 & 0 & 0 & 0 & 0 \\ 0 & 0 & 0 & 0 & 0 & 1 & 0 & 0 & 0 \\ 0 & 0 & 0 & 0 & 0 & 0 & 1 & 0 & 0 \\ 0 & 0 & 0 & 0 & 0 & 0 & 0 & 1 & 0 \\ 0 & 0 & 0 & 0 & 0 & 0 & 0 & 0 & 1 \\ 0 & 0 & 0 & 0 & 0 & 0 & 0 & 0 & 0 \\ 0 & 0 & 0 & 0 & 0 & 0 & 0 & 0 & 0 \\ 0 & 0 & 0 & 0 & 0 & 0 & 0 & 0 & 0 \end{bmatrix} \begin{bmatrix} b \\ e \\ r \\ \dot{b} \\ \dot{e} \\ \dot{r} \\ \ddot{b} \\ \ddot{e} \\ \ddot{r} \end{bmatrix} + \begin{bmatrix} 0 \\ 0 \\ 0 \\ 0 \\ 0 \\ 0 \\ w_{j_b} \\ w_{j_e} \\ w_{j_r} \end{bmatrix} \tag{3-20}$$

S4. Exponentially Correlated Acceleration: spherical (ECA(s)):

$$\frac{d}{dt}\begin{bmatrix} b \\ e \\ r \\ \dot{b} \\ \dot{e} \\ \dot{r} \\ \ddot{b} \\ \ddot{e} \\ \ddot{r} \end{bmatrix} = \begin{bmatrix} 0 & 0 & 0 & 1 & 0 & 0 & 0 & 0 & 0 \\ 0 & 0 & 0 & 0 & 1 & 0 & 0 & 0 & 0 \\ 0 & 0 & 0 & 0 & 0 & 1 & 0 & 0 & 0 \\ 0 & 0 & 0 & 0 & 0 & 0 & 1 & 0 & 0 \\ 0 & 0 & 0 & 0 & 0 & 0 & 0 & 1 & 0 \\ 0 & 0 & 0 & 0 & 0 & 0 & 0 & 0 & 1 \\ 0 & 0 & 0 & 0 & 0 & 0 & -\beta_{ab} & 0 & 0 \\ 0 & 0 & 0 & 0 & 0 & 0 & 0 & -\beta_{ae} & 0 \\ 0 & 0 & 0 & 0 & 0 & 0 & 0 & 0 & -\beta_{ar} \end{bmatrix} \begin{bmatrix} b \\ e \\ r \\ \dot{b} \\ \dot{e} \\ \dot{r} \\ \ddot{b} \\ \ddot{e} \\ \ddot{r} \end{bmatrix} + \begin{bmatrix} 0 \\ 0 \\ 0 \\ 0 \\ 0 \\ 0 \\ w_{j_b} \\ w_{j_e} \\ w_{j_r} \end{bmatrix} \tag{3-21}$$

3.3 MEASUREMENT MODELS

Target measurements are almost always given in spherical coordinates as bearing and elevation angles (relative to some known reference frame) and, if available, a range from the sensor to the target. We will denote the measurement vector as z:

$$z := \begin{bmatrix} z_b & z_e & z_r \end{bmatrix}^T$$

These measurements will be assumed to consist of the true values of the quantities being measured plus random white noise components, ν, consistent with the standard Kalman filter measurement model equation, (2-4):

$$\begin{bmatrix} z_b \\ z_e \\ z_r \end{bmatrix} = \begin{bmatrix} b \\ e \\ r \end{bmatrix} + \begin{bmatrix} \nu_b \\ \nu_e \\ \nu_e \end{bmatrix}$$

For a state vector in spherical coordinates, the map between the measurement and state is linear

$$\begin{bmatrix} z_b \\ z_e \\ z_r \end{bmatrix} = \begin{bmatrix} 1 & 0 & 0 & 0 & 0 & \dots \\ 0 & 1 & 0 & 0 & 0 & \dots \\ 0 & 0 & 1 & 0 & 0 & \dots \end{bmatrix} \begin{bmatrix} b \\ e \\ r \\ \dot{b} \\ \dot{e} \\ \vdots \end{bmatrix} + \begin{bmatrix} \nu_b \\ \nu_e \\ \nu_r \end{bmatrix} \tag{3-22}$$

but for a state vector in rectangular coordinates, the relationship is nonlinear:

$$\begin{bmatrix} z_b \\ z_e \\ z_r \end{bmatrix} = \begin{bmatrix} h_b(x) \\ h_e(x) \\ h_r(x) \end{bmatrix} + \begin{bmatrix} \nu_b \\ \nu_e \\ \nu_r \end{bmatrix} \tag{3-23}$$

where the nonlinear functions are as in (3-3):

$$\begin{aligned} h_b(x) &= \tan^{-1}\left(\frac{p_{X_G}}{p_{Y_G}}\right) \\ h_e(x) &= \sin^{-1}\left(\frac{-p_{Z_G}}{\sqrt{p_{X_G}^2 + p_{Y_G}^2 + p_{Z_G}^2}}\right) \\ h_r(x) &= \sqrt{p_{X_G}^2 + p_{Y_G}^2 + p_{Z_G}^2} \end{aligned} \tag{3-24}$$

For use in an Extended Kalman filter, this nonlinear measurement vector will be linearized about the state vector estimate $\hat{x} = [\hat{p}_{X_G}\ \hat{p}_{Y_G}\ \hat{p}_{Z_G}\ \dots]^T$ according to (2-15):

$$H(\hat{x}) = \frac{\partial \boldsymbol{h}(\hat{x})}{\partial \hat{x}} = \left[\frac{\partial h_i}{\partial \hat{x}_j}\right]_{ij} = \begin{bmatrix} \partial h_b/\partial \hat{p}_{X_G} & \partial h_b/\partial \hat{p}_{Y_G} & \partial h_b/\partial \hat{p}_{Z_G} & \dots & \dots \\ \partial h_e/\partial \hat{p}_{X_G} & \partial h_e/\partial \hat{p}_{Y_G} & \partial h_e/\partial \hat{p}_{Z_G} & \dots & \dots \\ \partial h_r/\partial \hat{p}_{X_G} & \partial h_r//\partial \hat{p}_{Y_G} & \partial h_r/\partial \hat{p}_{Z_G} & \dots & \dots \end{bmatrix}$$

which, after one has taken the derivatives, becomes

$$H(\hat{x}) = \begin{bmatrix} \dfrac{\hat{p}_{Y_G}}{\hat{l}^2} & -\dfrac{\hat{p}_{X_G}}{\hat{l}^2} & 0 & 0 & \dots & 0 \\ -\dfrac{\hat{p}_{X_G}\,\hat{p}_{Z_G}}{\hat{l}\hat{\rho}^2} & -\dfrac{\hat{p}_{Y_G}\,\hat{p}_{Z_G}}{\hat{l}\hat{\rho}^2} & \dfrac{\hat{l}}{\hat{\rho}^2} & 0 & \dots & 0 \\ \dfrac{\hat{p}_{X_G}}{\hat{\rho}} & \dfrac{\hat{p}_{Y_G}}{\hat{\rho}} & \dfrac{\hat{p}_{Z_G}}{\hat{\rho}} & 0 & \dots & 0 \end{bmatrix} \tag{3-25}$$

where

$$\hat{\rho} := \sqrt{\hat{p}_{X_G}^{\,2} + \hat{p}_{Y_G}^{\,2} + \hat{p}_{Z_G}^{\,2}}$$
$$\hat{l} := \sqrt{\hat{p}_{X_G}^{\,2} + \hat{p}_{Y_G}^{\,2}} \tag{3-26}$$

3.4 CHOICE OF TARGET MODEL

There has been a tremendous amount of literature arguing the various merits and shortcomings of each of these models. Countless variations, combinations and extensions have been proposed, studied, simulated, tested and implemented. A number of adaptive schemes that switch between models or combine outputs of parallel models also exist. Relatively recent survey papers include Woolfson (1985), Chang and Tabaczynski (1984) and the texts of Blackman (1986), Farina and Studer (1985) and others are all invaluable sources. One early reference, Burke *et al.* (1976), used random walk acceleration models to track a maneuvering tank in both geographic and line-of-sight coordinates. New refinements, such as Rouhi and Farooq (1989), appear continuously.

The choice of target model can best be done when the specific scenario is known and some real data is available to evaluate the various models. A good tracking simulator will allow different models to be tested and evaluated so that a suitable one (or more) is chosen for the purpose at hand. The next two chapters describe a simulator that was developed for potential fire

control systems. It can implement any of the above models and it has some interesting features that may be particularly useful for land fire control. Developing a flexible simulation package, rather than extensive model evaluation, was the primary goal of the effort.

There are a few rules of thumb that assist in the choice of a model. In general, the inclusion of acceleration states makes a filter more able to track sudden maneuvers but at the expense of a noisier estimate when the target is not accelerating. On the other hand, the exclusion of acceleration states will make the filter estimate more accurate when the target is not maneuvering but a sudden target acceleration may cause the filter to loose the target. The amount of noise, w, that is assumed to enter the state model can have a similar effect: the larger its covariance, Q_k, the noisier but more responsive the filter; the smaller the Q_k, the quieter but more sluggish the filter. In general, one often sees high Q uncorrelated acceleration filters for tracking highly maneuverable targets such as fighter aircraft, and low Q correlated velocity filters for tracking ships and submarines. Land combat vehicles would fall somewhere in between. For this study, moderate Q values were used with both velocity and acceleration models.

4.0 TRACKING FILTER SIMULATIONS

This chapter presents some results from the simulation program that was developed to test the various Kalman filter based tracking algorithms presented in the previous chapter. The software was written in "C" and is very generic. The initial Kalman filter matrices and parameters are read in from files as is the simulated sensor data. Only a few routines exploit certain features or ordering of the state vector elements and these were grouped together to remind the developer which routines might have to be modified if a different state vector formulation was used.

4.1 DATA GENERATION

4.1.1 Truth Data Generation

A pre-existing program (TGen) was used to generate the truth data for the target trajectories. Through a plain language input text file, the user specifies the target's initial position, velocity and heading and changes to these values at any subsequent point in time. The program computes the deterministic position, velocity, acceleration, attitude and attitude rates of the target and saves these in a data file.

4.1.2 Sensor Data Generation

A simple program called SensData was developed that would take the data files representing the true target trajectories and produce simulated bearing, elevation and, if requested, range measurements as might be produced by a generic imaging sensor system. The program allows pseudorandom noise to be added to the true bearing, elevation and ranges, permits the turning on and off of ranging information to simulate passive to active mode switching, and can simulate target obscuration by removing sensor data for arbitrary intervals. If there is more than one target, it will merge the sensor data associated with all targets into one file and sort by time stamp. It can also simulate clutter by generating false targets at any specified probability of false alarm.

Shown in Fig. 4-1 below (and in x-y form as Target 1 in Fig. 5-1) is a simulated trajectory of a land target moving at a constant speed of 15.0 m/s (= 54.0 km/hr) at a range of initially 1500m. It recedes from the sensor for 8 seconds, makes a 90 degree right-hand turn (at t=8s, duration 5 seconds), travels across the sensor field of view for another 4 seconds, then makes another right hand turn (at t=17s, duration 5s) and travels toward the sensor for the final 3 seconds. The figure shows the true range, bearing and elevation to the target as well as the noisy measurements of these quantities made by the sensor at 0.1s intervals. The measurements are

$$\begin{bmatrix} z_b(k) \\ z_e(k) \\ z_r(k) \end{bmatrix} = \begin{bmatrix} b(k) \\ e(k) \\ r(k) \end{bmatrix} + \begin{bmatrix} v_b(k) \\ v_e(k) \\ v_r(k) \end{bmatrix} \tag{4-1}$$

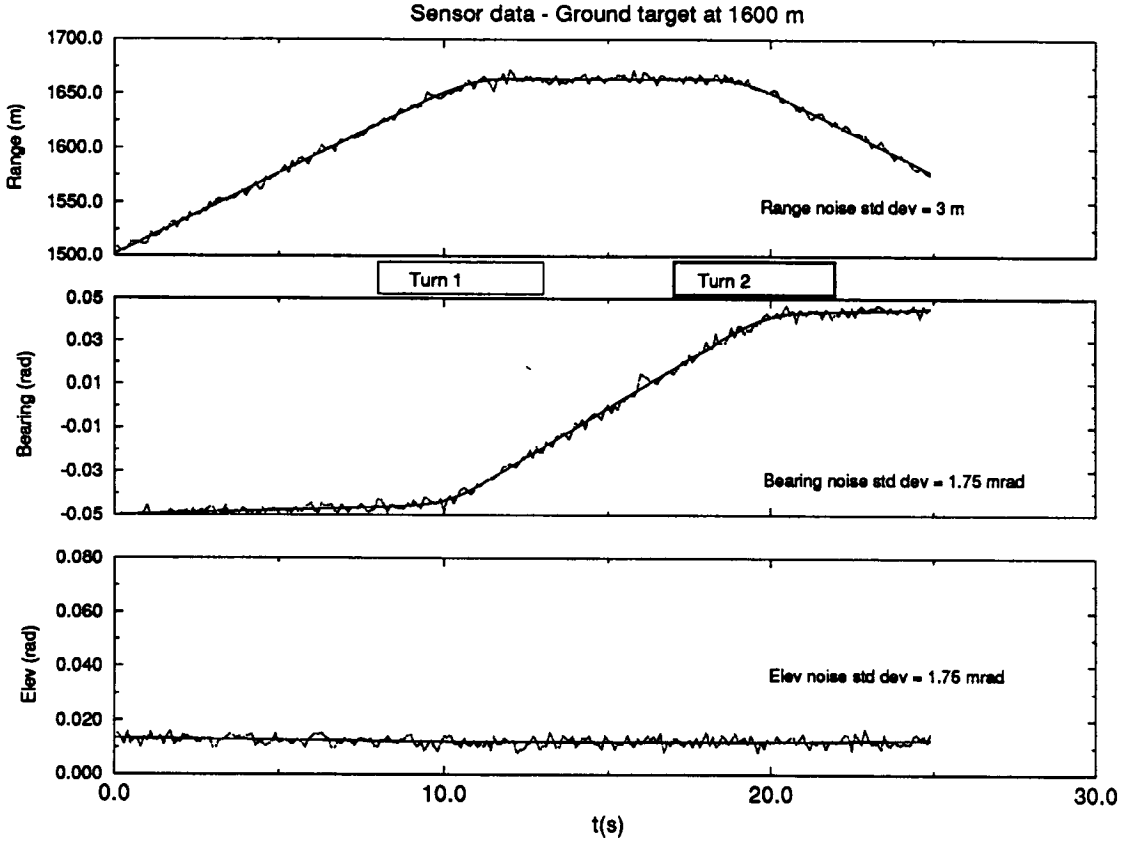

Fig. 4-1: Simulated sensor data for a ground target at 1600m, first receeding, then crossing, then closing on sensor location. Both truth and noisy data are shown.

where the covariance values of the measurement noises are

$$R(k) = \mathrm{E}\begin{bmatrix} v_b(k) \\ v_e(k) \\ v_r(k) \end{bmatrix}\begin{bmatrix} v_b(k) & v_e(k) & v_r(k) \end{bmatrix}^T = \begin{bmatrix} (0.00175 \text{ rad})^2 & 0 & 0 \\ 0 & (0.00175 \text{ rad})^2 & 0 \\ 0 & 0 & (3 \text{ m})^2 \end{bmatrix}$$

4.2 TRACKING FILTER RESULTS

This section shows some representative results of typical simulations. The purpose is not necessarily to show the best tracking filter for the simulated trajectory but rather to show some

of the features that are available in the simulator. Again the choice of the "best" filter depends on the application. In this chapter we assume that the range information is either available for the entire trajectory, or unavailable for the entire trajectory. The next chapter describes a method to handle the case when range data is intermittently available and presents some simulated results of such a situation.

The Kalman filter program, called "tracker", was written in C. It accepts a configuration file with various control parameters, as well as the continuous time state dynamics matrix, F, and power spectral density matrix, Q_c. It also reads in the assumed level of measurement noise, i.e., the R matrix and the names of the sensor data file and the truth data file. It produces output files for the values of the states, the state errors, and residuals, as well as the square roots of the corresponding diagonals of the covariance matrix. The program first does a discretization of the continuous time matrices, and thereafter operates as a discrete EKF.

4.2.1 Random Walk Velocity (RWV(r)) Model - Range Available

In this case, range information is available and the RWV(r) model, Eq. (3-14), is used. This is a 3 dimensional rectangular coordinate frame model. The measurement equation is the nonlinear form of (3-23) so the extended Kalman filter formulation is used. The power spectral density matrix of the state process noise required for the discretization equations (2-3) is estimated in Appendix A where it is shown to be

$$Q_c(t) = \begin{bmatrix} 0 & 0 & 0 & 0 & 0 & 0 \\ 0 & 0 & 0 & 0 & 0 & 0 \\ 0 & 0 & 0 & 0 & 0 & 0 \\ 0 & 0 & 0 & 3.0 & 0 & 0 \\ 0 & 0 & 0 & 0 & 3.0 & 0 \\ 0 & 0 & 0 & 0 & 0 & 0.03 \end{bmatrix} \text{m}^2/\text{s}^3$$

Shown in Fig. 4-2 below are the errors in the state estimates of each cartesian position coordinate as well as the filter estimates of the square root of the covariance of that estimate, i.e., $\tilde{x}_i(k/k) = x_i(k) - \hat{x}_i(k/k)$ and $\sqrt{P_{ii}(k/k)}$ where the subscript refers to an individual element. As well, the velocity state estimation errors and covariance elements are shown in Fig. 4-3. The measurement residuals, $\nu_i(k/k) = z_i(k) - h_i(\hat{x}(k/k))$ as well as the square root of the filter estimated residual covariance, $\{[H(k)P(k/k)H(k)^T]_{ii} + R_{ii}(k)\}^{1/2}$, are shown in Fig. 4-4.

The state estimate errors for the most part lie within their expected standard deviation, indicating a reasonably well-tuned filter. The target right hand turns during t=8 to t=13 and t=17 to t=22 cause larger state errors to occur during the maneuvers and they disappear after the maneuver is completed. The smaller Q value for the vertical velocity state shows up in the figures as smaller state estimation errors and covariances for both the vertical position and

velocity. This shows the type of tradeoff one expects as Q varies.

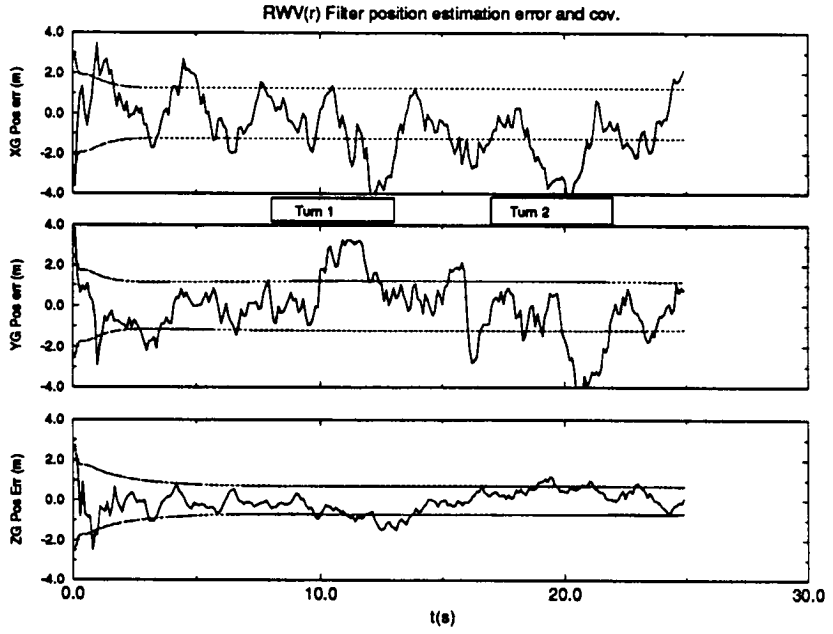

Fig. 4-2: RWV(r) model. Position state estimation errors and covariance matrix elements.

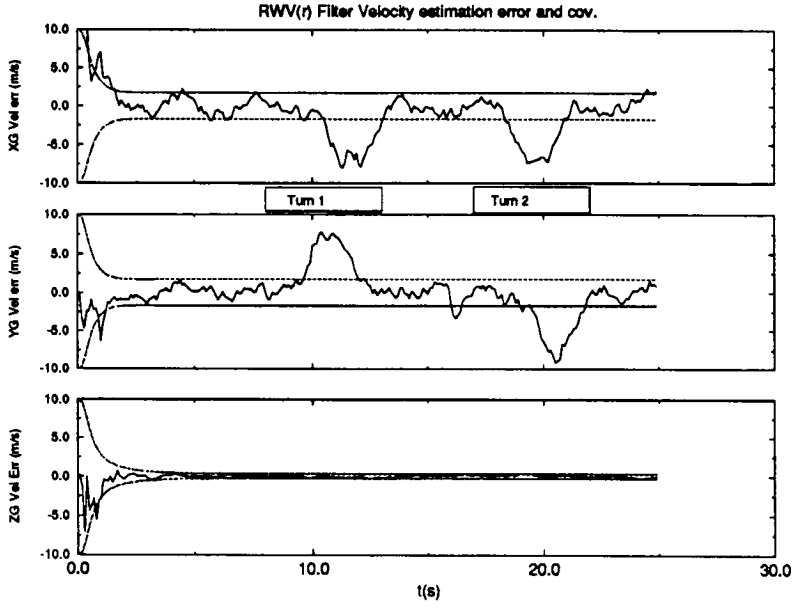

Fig. 4-3: RWV(r) model. Velocity state estimation errors and covariance matrix elements.

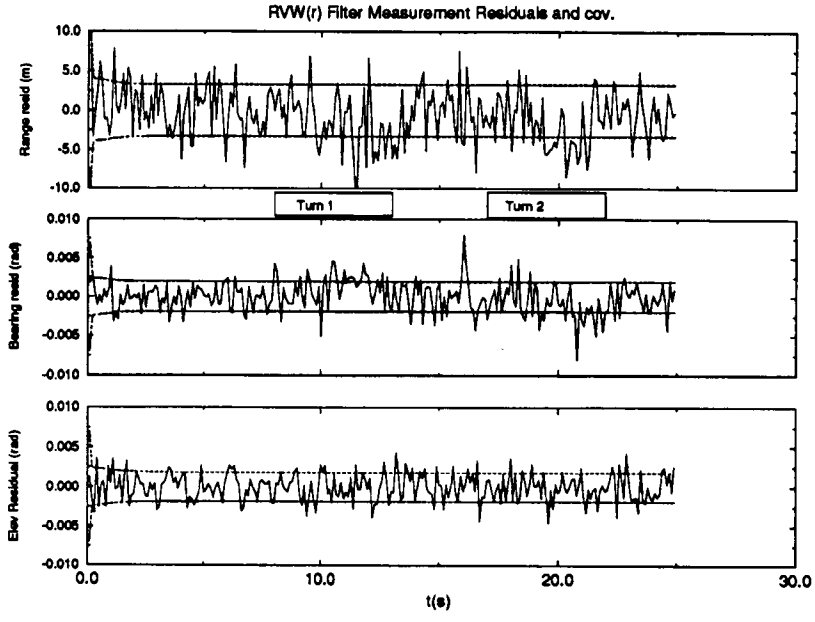

Fig. 4-4: RWV(r) model. Measurement residuals and covariance matrix elements.

4.2.2 Random Walk Velocity (RWV(s)) Model - Range Unavailable

When range information is unavailable a spherical coordinate velocity model similar to Eq. (3-18) is used. The range states are deleted so we are left with the 4 state filter:

$$\frac{d}{dt}\begin{bmatrix} b \\ e \\ \dot{b} \\ \dot{e} \end{bmatrix} = \begin{bmatrix} 0 & 0 & 1 & 0 \\ 0 & 0 & 0 & 1 \\ 0 & 0 & 0 & 0 \\ 0 & 0 & 0 & 0 \end{bmatrix}\begin{bmatrix} b \\ e \\ \dot{b} \\ \dot{e} \end{bmatrix} + \begin{bmatrix} 0 \\ 0 \\ w_{a_b} \\ w_{a_e} \end{bmatrix} \tag{4-2}$$

The measurement equation is now a linear function of the states so an extended Kalman filter formulation is not required. The power spectral density matrix of the state process noise required for the discretization equations (2-3) is taken as (again, see Appendix A)

$$Q_c(t) = \begin{bmatrix} 0 & 0 & 0 & 0 \\ 0 & 0 & 0 & 0 \\ 0 & 0 & 6.25\times10^{-7} & 0 \\ 0 & 0 & 0 & 6.25\times10^{-9} \end{bmatrix} (\text{rad}^2/\text{s}^3)$$

The results of this "angle only" filter are shown in the following figures. First the angular position state errors and their estimated covariances are in Fig. 4-5, and the angular velocity state errors and associated estimated covariances are shown in Fig. 4-6. For completeness the measurement residuals are shown in Fig. 4-7.

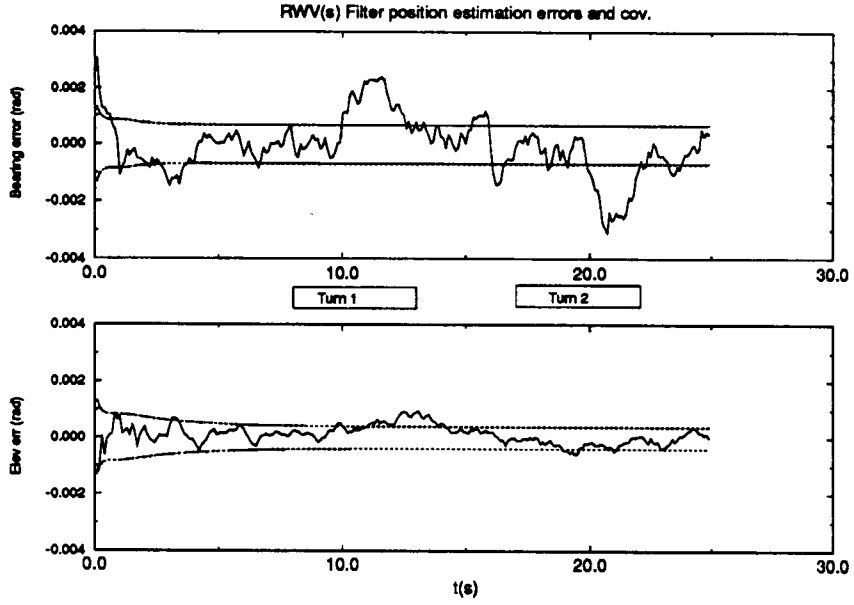

Fig. 4-5: RWV(s) model. Angle state estimation errors and covariance matrix elements.

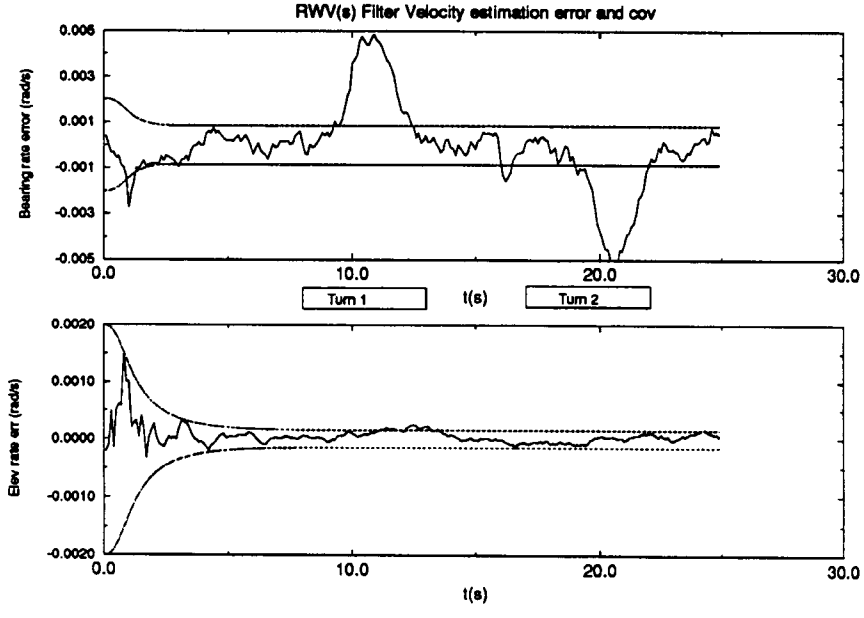

Fig. 4-6: RWV(s) model. Angular rate state estimation errors and covariances.

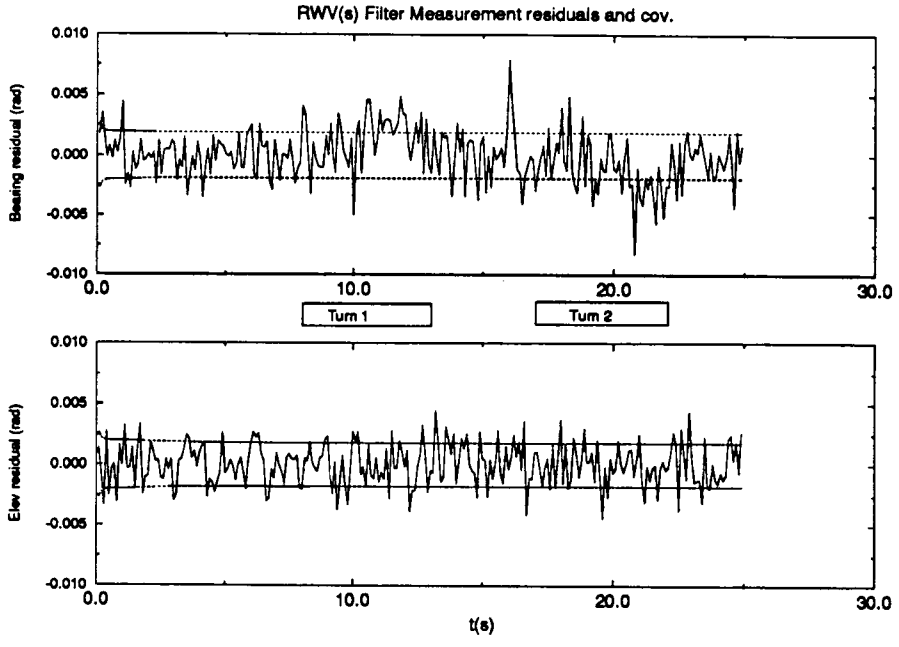

Fig. 4-7: RWV(s) model. Measurement residuals and covariance matrix elements.

With the relatively large noise (1.75 mrad) that was superimposed on the bearing and elevation measurements, the filters are performing about as well as could be expected. Again the target maneuvers starting at t=8 and t=17 produce brief biases in the errors of estimates of both the bearing and bearing rate states. Any number of maneuver detectors (e.g. Woolfson (1985)) are available for this problem but none are included in the simulations to date. A look at the bearing residual Fig. 4-7 shows very little effect of the maneuvers because of the high measurement noise used in these examples.

4.3 DISCUSSION

The simulation results presented here should be taken only as examples of scenarios that may or may not be particularly realistic. With the simulation tools as they exist now, it is easy to rapidly prototype various filter configurations and evaluate their performance against real target measurement data from specific imaging sensors. What is satisfactory for one type of sensor may not be so for another. For example, a maneuver detector based on filter residuals may work well for a relatively low noise sensor, but may not if the sensor generates position data as noisy as was used in the previous section. Also, the next chapter outlines a multi-target algorithm that uses filter residuals to determine which measurement to associate with which track. In that case, most maneuver detectors based on residuals will not work particularly well.

5.0 TRACKING FILTER ENHANCEMENTS

This chapter outlines a few enhancements that were made to the tracking algorithms of the previous chapter that may make them more applicable to direct-fire support applications. These include a swapping algorithm that allows the filter to swap from an angle-only filter to a full 3 dimensional cartesian coordinate filter when an active range-finding sensor is activated; and a simple but practical multiple target tracking algorithm that allows the fire control system to maintain lock on several targets in the field of view while another target is being engaged.

5.1 MULTIPLE TARGET TRACKING

When a target is to be tracked in a cluttered environment (*i.e.* one with potential false targets) or when more than one target must be tracked simultaneously, there must be a method in the algorithm to determine which track a particular measurement belongs to, or if it is a false target. There are many such algorithms available in the literature and include the *nearest neighbour* method, the *probabilistic data association* method, the *multiple hypothesis tracking* method, among others, all of which are summarized in Roy (1990) or McMillan and Lim (1990) or described in more detail in texts such as Blackman (1986) or Farina and Studer (1985). The simplest of these, but arguably the least satisfactory for very closely spaced targets, is the nearest neighbour method. Nonetheless, this method was implemented and found to perform quite well given its simplicity. The method and some simulation results are described in this chapter.

5.1.1 Nearest Neighbour Method

The nearest neighbour algorithm first finds all current tracks that are reasonably close to the measurement by a process known as "gating", described below. If there are none, then the data is either a new target or a piece of clutter. In either case, a tentative track filter is initiated for the measurement which becomes valid only if there are subsequent measurements associated with it. If, on the other hand, there are one or more tracks that are close, then simply the track that is the closest is updated with that measurement.

To make the notion of gating more precise, define a normalized "distance", d, from the location of the measurement at time k, $z(k)$, to the tracking filter's prediction of the measurement, $\boldsymbol{h}(\hat{\boldsymbol{x}}(k|k-1))$, for each track:

$$d^2(k|k-1) := [z(k) - \boldsymbol{h}(\hat{\boldsymbol{x}}(k|k-1))]^T [H(\hat{\boldsymbol{x}}(k|k-1))P(k|k-1)H^T(\hat{\boldsymbol{x}}(k|k-1)) + R]^{-1} [z(k) - \boldsymbol{h}(\hat{\boldsymbol{x}}(k|k-1))] \quad (5\text{-}1)$$

(The notation here is the same as that of Chapter 2.) Note that this "distance" is essentially the length of the residual vector, normalized by its estimated covariance. A *gate threshold* must be

specified, to which d is compared to see if the measurement is close to the filter. This threshold is typically around 5. The nearest neighbour algorithm can be summarized as:

1. Obtain the new measurement, $z(k)$.
2. Propagate all current tracks to the new time (*i.e.*, compute $\hat{x}(k|k-1)$, $P(k|k-1)$).
3. Compute d as in (5-1) for each track.
4. If d of all tracks > gate threshold then initiate a new tentative track filter.
5. Otherwise update the track having the minimum d with the measurement.

Tracks can be deleted if they are not updated with a new sensor measurement after a certain period of time or a certain number of scans.

5.2 FILTER SWAPPING ALGORITHMS

Typically the fire control system searches for targets in a passive mode with an optical or infrared imaging sensor and tracks these targets with angle-only filters. When a target is to be engaged, an active ranging sensor is turned on and information from the third spatial dimension becomes available to the tracking filters. It would be preferred, then, to use one of the cartesian coordinate target models since target motions are more naturally described in cartesian coordinates. If for some reason the target is disengaged but still is to be tracked, the filters will have to revert to a passive, angle-only tracking mode. This section describes a method that can be used to swap a 2 (spatial) dimensional passive, angle-only tracking filter to a 3 dimensional active, cartesian one when range information becomes available and vice versa when it ceases.

5.2.1 Passive to Active Filter Swap

In essence, the filter swapping technique uses the current state estimate and covariance matrix to initialize another Kalman filter that uses the new set of dynamical equations. To swap from an angular filter (with current state vector $[\ \hat{b}\ \hat{e}\ \dot{\hat{b}}\ \dot{\hat{e}}\ \ddot{\hat{b}}\ \ddot{\hat{e}}\ ]^T$) to a rectangular one (with a new state vector $[\ \hat{p}_{X_G}\ \hat{p}_{Y_G}\ \hat{p}_{Z_G}\ \hat{v}_{X_G}\ \hat{v}_{Y_G}\ \hat{v}_{Z_G}\ \hat{a}_{X_G}\ \hat{a}_{Y_G}\ \hat{a}_{Z_G}\ ]^T$) when a valid piece of range, range rate or range acceleration (z_r, $z_{\dot{r}}$, or $z_{\ddot{r}}$) data becomes available, the following steps can be initiated:

1. Compute the Line-of-sight to Geographic DCM, $\hat{C}_L^G$, using the current best estimate of bearing and elevation available from the filter:

$$\hat{C}_L^G := \begin{bmatrix} \cos\hat{e}\cos\hat{b} & -\sin\hat{b} & \sin\hat{e}\cos\hat{b} \\ \cos\hat{e}\sin\hat{b} & \cos\hat{b} & \sin\hat{e}\sin\hat{b} \\ -\sin\hat{e} & 0 & \cos\hat{e} \end{bmatrix}$$

2. Estimate the geographic relative position vector from the measured range and filtered bearing and elevation:

$$\hat{\boldsymbol{p}}^{(G)} = \hat{C}_L^G \, \hat{\boldsymbol{p}}^{(L)}$$

$$\Rightarrow \begin{bmatrix} \hat{p}_{X_G} \\ \hat{p}_{Y_G} \\ \hat{p}_{Z_G} \end{bmatrix}^{(G)} = \hat{C}_L^G \begin{bmatrix} \hat{p}_{X_L} \\ \hat{p}_{Y_L} \\ \hat{p}_{Z_L} \end{bmatrix}^{(L)} = \hat{C}_L^G \begin{bmatrix} z_r \\ 0 \\ 0 \end{bmatrix}^{(L)}$$

$$= \begin{bmatrix} z_r \cos\hat{e}\cos\hat{b} \\ z_r \cos\hat{e}\sin\hat{b} \\ -z_r \sin\hat{e} \end{bmatrix}^{(G)}$$

3. Estimate the line-of-sight relative velocities from the estimated angular rates and the measured range and range rates (if range rate not available, use $z_{\dot{r}} = 0$):

$$\hat{\boldsymbol{v}}^{(L)} := \begin{bmatrix} \hat{v}_{X_L} \\ \hat{v}_{Y_L} \\ \hat{v}_{Z_L} \end{bmatrix}^{(L)} = \begin{bmatrix} z_{\dot{r}} \\ z_r \, \hat{\dot{b}} \cos\hat{e} \\ -z_r \, \hat{\dot{e}} \end{bmatrix}^{(L)}$$

4. Convert the line-of-sight velocities to geographic velocities:

$$\hat{v}^{(G)} := \begin{bmatrix} \hat{v}_{X_G} \\ \hat{v}_{Y_G} \\ \hat{v}_{Z_G} \end{bmatrix}^{(G)} = \hat{C}_L^G \begin{bmatrix} \hat{v}_{X_L} \\ \hat{v}_{Y_L} \\ \hat{v}_{Z_L} \end{bmatrix}^{(L)}$$

5. Estimate the line-of-sight accelerations from the estimated angular accelerations and the measured range and range rates (if range acceleration not available, use $z_{\ddot{r}} = 0$):

$$\hat{a}^{(L)} := \begin{bmatrix} \hat{a}_{X_L} \\ \hat{a}_{Y_L} \\ \hat{a}_{Z_L} \end{bmatrix}^{(L)} = \begin{bmatrix} z_{\ddot{r}} - z_r \hat{\dot{e}}^2 - z_r \hat{\dot{b}}^2 \cos^2 \hat{e} \\ 2z_{\dot{r}} \hat{\dot{b}} \cos \hat{e} + z_r \hat{\ddot{b}} \cos \hat{e} - 2z_r \hat{\dot{b}}\, \hat{\dot{e}} \sin \hat{e} \\ -2z_{\dot{r}} \hat{\dot{e}} - z_r \hat{\ddot{e}} - z_r \hat{\dot{b}}^2 \cos \hat{e} \sin \hat{e} \end{bmatrix}^{(L)}$$

6. Convert the line-of-sight accelerations to geographic accelerations:

$$\hat{a}^{(G)} := \begin{bmatrix} \hat{a}_{X_G} \\ \hat{a}_{Y_G} \\ \hat{a}_{Z_G} \end{bmatrix}^{(G)} = \hat{C}_L^G \begin{bmatrix} \hat{a}_{X_L} \\ \hat{a}_{Y_L} \\ \hat{a}_{Z_L} \end{bmatrix}^{(L)}$$

The corresponding swapping of exact covariance matrix information would be very complex (due to the nonlinearity of the coordinate transformations) and of minimal value since the covariance matrix quickly converges to its steady state values. The following is an approximation that will initialize a new diagonal covariance matrix from the diagonals of the old and which should result in relatively modest covariance element transients following a filter swap:

1. Extract the square roots of the diagonals of the existing covariance matrix:

$$\text{For position states:} \quad \begin{bmatrix} \sigma_r \\ \sigma_b \\ \sigma_e \end{bmatrix} := \begin{bmatrix} \sqrt{P_{rr}} \\ \sqrt{P_{bb}} \\ \sqrt{P_{ee}} \end{bmatrix}$$

$$\text{For velocity states:} \quad \begin{bmatrix} \sigma_{\dot{r}} \\ \sigma_{\dot{b}} \\ \sigma_{\dot{e}} \end{bmatrix} := \begin{bmatrix} \sqrt{P_{\dot{r}\dot{r}}} \\ \sqrt{P_{\dot{b}\dot{b}}} \\ \sqrt{P_{\dot{e}\dot{e}}} \end{bmatrix}$$

$$\text{For acceleration states:} \quad \begin{bmatrix} \sigma_{\ddot{r}} \\ \sigma_{\ddot{b}} \\ \sigma_{\ddot{e}} \end{bmatrix} := \begin{bmatrix} \sqrt{P_{\ddot{r}\ddot{r}}} \\ \sqrt{P_{\ddot{b}\ddot{b}}} \\ \sqrt{P_{\ddot{e}\ddot{e}}} \end{bmatrix}$$

It should be noted that a passive filter may not have range states and consequently no corresponding covariance elements (P_{rr}, $P_{\dot{r}\dot{r}}$, $P_{\ddot{r}\ddot{r}}$). The filter obtains estimates for these parameters from a configuration file.

2. Approximate the corresponding L frame standard deviations via:

$$\text{For position states:} \quad \begin{bmatrix} \sigma_{p_{XL}} \\ \sigma_{p_{YL}} \\ \sigma_{p_{ZL}} \end{bmatrix}^{(L)} \approx \begin{bmatrix} \sigma_r \\ z_r \ \sigma_b \ |\cos \hat{e}| \\ z_r \ \sigma_e \end{bmatrix}$$

$$\text{For velocity states:} \quad \begin{bmatrix} \sigma_{v_{XL}} \\ \sigma_{v_{YL}} \\ \sigma_{v_{ZL}} \end{bmatrix}^{(L)} \approx \begin{bmatrix} \sigma_{\dot{r}} \\ z_r \ \sigma_{\dot{b}} \ |\cos \hat{e}| \\ z_r \ \sigma_{\dot{e}} \end{bmatrix}$$

$$\text{For acceleration states:} \quad \begin{bmatrix} \sigma_{a_{XL}} \\ \sigma_{a_{YL}} \\ \sigma_{a_{ZL}} \end{bmatrix}^{(L)} \approx \begin{bmatrix} \sigma_{\ddot{r}} \\ z_r \ \sigma_{\ddot{b}} \ |\cos \hat{e}| \\ z_r \ \sigma_{\ddot{e}} \end{bmatrix}$$

(Compare these transformations with Eqn. (3-8) which related the bearing, elevation and range rates to the velocites in L coordinates. Such a transformation takes the components of the covariance matrix representing the uncertainty in, say, the angular position estimate (σ_r, σ_b, σ_e) and uses the measured range and elevation to convert these to rectangular coordinates. The uncertainty in range, σ_r, transforms directly to σ_{PXL}, since the X_L axis points along the range. The uncertainty in elevation, σ_e, multiplied by the range gives the uncertainty in the vertical cartesian direction Z_L. Similarly for the bearing and the Y_L direction. The same transformation is applied to the angular velocity and acceleration uncertainties.)

3. Convert these to G frame coordinates with the current DCM:

$$\text{For position states:} \quad \begin{bmatrix} \sigma_{p_{XG}} \\ \sigma_{p_{YG}} \\ \sigma_{p_{ZG}} \end{bmatrix}^{(G)} = \hat{C}_L^G \begin{bmatrix} \sigma_{p_{XL}} \\ \sigma_{p_{YL}} \\ \sigma_{p_{ZL}} \end{bmatrix}^{(L)}$$

$$\text{For velocity states:} \quad \begin{bmatrix} \sigma_{v_{XG}} \\ \sigma_{v_{YG}} \\ \sigma_{v_{ZG}} \end{bmatrix}^{(G)} = \hat{C}_L^G \begin{bmatrix} \sigma_{v_{XL}} \\ \sigma_{v_{YL}} \\ \sigma_{v_{ZL}} \end{bmatrix}^{(L)}$$

$$\text{For acceleration states:} \quad \begin{bmatrix} \sigma_{a_{XG}} \\ \sigma_{a_{YG}} \\ \sigma_{a_{ZG}} \end{bmatrix}^{(G)} = \hat{C}_L^G \begin{bmatrix} \sigma_{a_{XL}} \\ \sigma_{a_{YL}} \\ \sigma_{a_{ZL}} \end{bmatrix}^{(L)}$$

4. Initiate the covariance matrix as:

$$P^{(G)} := \text{diag}\,[\sigma_{p_{XG}}{}^2, \sigma_{p_{YG}}{}^2, \sigma_{p_{ZG}}{}^2, \sigma_{v_{XG}}{}^2, \sigma_{v_{YG}}{}^2, \sigma_{v_{ZG}}{}^2, \sigma_{a_{XG}}{}^2, \sigma_{a_{YG}}{}^2, \sigma_{a_{ZG}}{}^2]$$

5.2.2 Active to Passive Filter Swap

When the system loses ranging information to the target, the filter will coast through a few updates using the predicted range measurement as new data. After a certain number of successive updates with no new range data, the filter will revert to a bearing and elevation angle tracker. The initial conditions for the new filter are derived from the last state and covariance matrix estimates from the cartesian filter in a manner similar to that above. To obtain the new state vector $[\ \hat{b}\ \hat{e}\ \dot{\hat{b}}\ \dot{\hat{e}}\ \ddot{\hat{b}}\ \ddot{\hat{e}}\ ]^T$ from the old $[\ \hat{p}_{X_G}\ \hat{p}_{Y_G}\ \hat{p}_{Z_G}\ \hat{v}_{X_G}\ \hat{v}_{Y_G}\ \hat{v}_{Z_G}\ \hat{a}_{X_G}\ \hat{a}_{Y_G}\ \hat{a}_{Z_G}\ ]^T$:

1. Compute the Geographic to Line-of-sight DCM, $\hat{C}_G^L$, using the current best estimate of bearing and elevation available from the filter:

$$\hat{r} := \sqrt{\hat{p}_{X_G}{}^2 + \hat{p}_{Y_G}{}^2 + \hat{p}_{Y_G}{}^2}$$

$$\hat{b} := \tan^{-1}\left(\hat{p}_{Y_G}/\hat{p}_{X_G}\right)$$

$$\hat{e} := \sin^{-1}\left(-\hat{p}_{Z_G}/\hat{r}\right)$$

$$\hat{C}_G^L := \begin{bmatrix} \cos\hat{e}\cos\hat{b} & \cos\hat{e}\sin\hat{b} & -\sin\hat{e} \\ -\sin\hat{b} & \cos\hat{b} & 0 \\ \sin\hat{e}\cos\hat{b} & \sin\hat{e}\sin\hat{b} & \cos\hat{e} \end{bmatrix}$$

2. Convert the geographic velocities to line-of-sight velocities:

$$\hat{v}^{(L)} := \begin{bmatrix} \hat{v}_{X_L} \\ \hat{v}_{Y_L} \\ \hat{v}_{Z_L} \end{bmatrix}^{(L)} = \hat{C}_G^L \begin{bmatrix} \hat{v}_{X_G} \\ \hat{v}_{Y_G} \\ \hat{v}_{Z_G} \end{bmatrix}^{(G)}$$

3. Estimate the angular rates from the line-of-sight velocities:

$$\begin{bmatrix} \dot{\hat{r}} \\ \dot{\hat{b}} \\ \dot{\hat{e}} \end{bmatrix} = \begin{bmatrix} \hat{v}_{X_L} \\ \hat{v}_{Y_L}/(\hat{r}\cos\hat{e}) \\ -\hat{v}_{Z_L}/\hat{r} \end{bmatrix}$$

4. Convert the geographic accelerations to line-of-sight accelerations:

$$\hat{a}^{(L)} := \begin{bmatrix} \hat{a}_{X_L} \\ \hat{a}_{Y_L} \\ \hat{a}_{Z_L} \end{bmatrix}^{(L)} = \hat{C}_G^L \begin{bmatrix} \hat{a}_{X_G} \\ \hat{a}_{Y_G} \\ \hat{a}_{Z_G} \end{bmatrix}^{(G)}$$

5. Estimate the angular accelerations from the line-of-sight accelerations:

$$\begin{bmatrix} \ddot{\hat{r}} \\ \ddot{\hat{b}} \\ \ddot{\hat{e}} \end{bmatrix} = \begin{bmatrix} \hat{a}_{X_L} + \hat{r}\,\dot{\hat{e}}^2 + \hat{r}\,\dot{\hat{b}}^2\cos^2\hat{e} \\ \hat{a}_{Y_L}/(\hat{r}\cos\hat{e}) - 2(\dot{\hat{r}}/\hat{r})\,\dot{\hat{b}} + 2\,\dot{\hat{b}}\,\dot{\hat{e}}\tan\hat{e} \\ -\hat{a}_{Z_L}/\hat{r} - 2(\dot{\hat{r}}/\hat{r})\,\dot{\hat{e}} - \dot{\hat{b}}^2\cos\hat{e}\sin\hat{e} \end{bmatrix}$$

The covariance matrix for the new filter can be initiated from:

1. Extract the square roots of the diagonals of the existing covariance matrix:

For position states:
$$\begin{bmatrix} \sigma_{p_{XG}} \\ \sigma_{p_{YG}} \\ \sigma_{p_{ZG}} \end{bmatrix} := \begin{bmatrix} \sqrt{P_{p_{XG}\,p_{XG}}} \\ \sqrt{P_{p_{YG}\,p_{YG}}} \\ \sqrt{P_{p_{ZG}\,p_{ZG}}} \end{bmatrix}$$

For velocity states:
$$\begin{bmatrix} \sigma_{v_{XG}} \\ \sigma_{v_{YG}} \\ \sigma_{v_{ZG}} \end{bmatrix} := \begin{bmatrix} \sqrt{P_{v_{XG}\,v_{XG}}} \\ \sqrt{P_{p_{YG}\,v_{YG}}} \\ \sqrt{P_{v_{ZG}\,v_{ZG}}} \end{bmatrix}$$

For acceleration states:
$$\begin{bmatrix} \sigma_{a_{XG}} \\ \sigma_{a_{YG}} \\ \sigma_{a_{ZG}} \end{bmatrix} := \begin{bmatrix} \sqrt{P_{a_{XG}\,a_{XG}}} \\ \sqrt{P_{a_{YG}\,a_{YG}}} \\ \sqrt{P_{a_{ZG}\,a_{ZG}}} \end{bmatrix}$$

2. Convert these to L frame coordinates with the current DCM:

$$\text{For position states:} \quad \begin{bmatrix} \sigma_{p_{XL}} \\ \sigma_{p_{YL}} \\ \sigma_{p_{ZL}} \end{bmatrix}^{(L)} = \hat{C}_G^L \begin{bmatrix} \sigma_{p_{XG}} \\ \sigma_{p_{YG}} \\ \sigma_{p_{ZG}} \end{bmatrix}^{(G)}$$

$$\text{For velocity states:} \quad \begin{bmatrix} \sigma_{v_{XL}} \\ \sigma_{v_{YL}} \\ \sigma_{v_{ZL}} \end{bmatrix}^{(L)} = \hat{C}_G^L \begin{bmatrix} \sigma_{v_{XG}} \\ \sigma_{v_{YG}} \\ \sigma_{v_{ZG}} \end{bmatrix}^{(G)}$$

$$\text{For acceleration states:} \quad \begin{bmatrix} \sigma_{a_{XL}} \\ \sigma_{a_{YL}} \\ \sigma_{a_{ZL}} \end{bmatrix}^{(L)} = \hat{C}_G^L \begin{bmatrix} \sigma_{a_{XG}} \\ \sigma_{a_{YG}} \\ \sigma_{a_{ZG}} \end{bmatrix}^{(G)}$$

3. Approximate the corresponding spherical frame standard deviations via:

$$\text{For position states:} \quad \begin{bmatrix} \sigma_b \\ \sigma_e \\ \sigma_r \end{bmatrix} \approx \begin{bmatrix} \sigma_{p_{YL}}/(\hat{r}\cos\hat{e}) \\ -\sigma_{p_{ZL}}/\hat{r} \\ \sigma_{p_{XG}} \end{bmatrix}$$

$$\text{For velocity states:} \quad \begin{bmatrix} \sigma_{\dot{b}} \\ \sigma_{\dot{e}} \\ \sigma_{\dot{r}} \end{bmatrix} \approx \begin{bmatrix} \sigma_{v_{YL}}/(\hat{r}\cos\hat{e}) \\ -\sigma_{v_{ZL}}/\hat{r} \\ \sigma_{v_{XG}} \end{bmatrix}$$

$$\text{For acceleration states:} \quad \begin{bmatrix} \sigma_{\ddot{b}} \\ \sigma_{\ddot{e}} \\ \sigma_{\ddot{r}} \end{bmatrix} \approx \begin{bmatrix} \sigma_{a_{YL}}/(\hat{r}\cos\hat{e}) \\ -\sigma_{a_{ZL}}/\hat{r} \\ \sigma_{a_{XG}} \end{bmatrix}$$

4. Initiate the covariance matrix as:

$$P := \text{diag}\,[\sigma_b^2,\ \sigma_e^2,\ \sigma_{\dot{b}}^2,\ \sigma_{\dot{e}}^2,\ \ldots]$$

5.3 SIMULATIONS OF ENHANCED TRACKER ALGORITHMS

This section shows some numerical results of the filter swapping algorithms described in the previous sections. Consider the trajectories of the two targets shown in Fig. 5-1. This represents two targets about 20 m apart and about 1600 m from the sensor moving at 54.0 km/hr. Initially they are travelling away from the sensor but then turn and head towards the sensor. Assume passive sensors are used except for the portions of the trajectories shown in the rectangles (from t=15 to t=20 for Target 1 and from t=17 to t=19 for Target 2) when a ranging sensor is turned on.

5.3.1 Simulations of Filter Swapping

To demonstrate the performance of the filter swapping algorithms, consider only a single target (Target 1 of Fig. 5-1, the same target in example of the previous chapter) which is tracked with a 4 state bearing-elevation angle filter for 15 seconds. At t=15 seconds, valid range measurements are available for the next 5 seconds and then cease for the final 5 seconds of the engagement. The Kalman filter matrices and parameters were the same as those used in the previous chapter. Shown in Fig. 5-2 below is the first element of the state vector. For the first 15 seconds and the final 5, it represents the filter estimate of the target bearing angle in radians. Between t=15 and t=20, it is the estimate of p_{XG}, the northerly distance to the target in meters. The truth data for these are shown in Fig. 5-3. Since the scales of the different portions of the graph are not compatible, the next two figures, Fig. 5-4 and Fig. 5-5, show the distinct regions of interest. The corresponding covariance estimates are also shown in Fig. 5-6 and Fig. 5-7. Again since the scales of the different segments of the plots are not compatible, two figures are used.

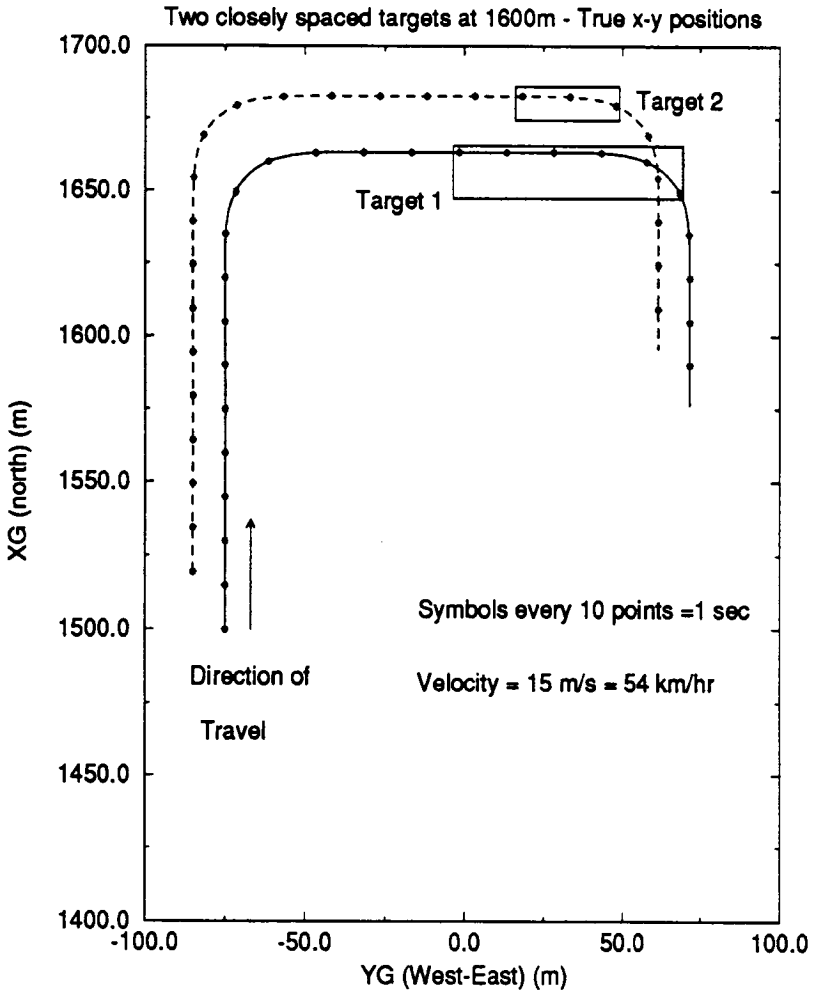

Fig. 5-1: True x-y trajectories of two targets. Ranging information is assumed to be available in the portions of the trajectories enclosed by rectangles.

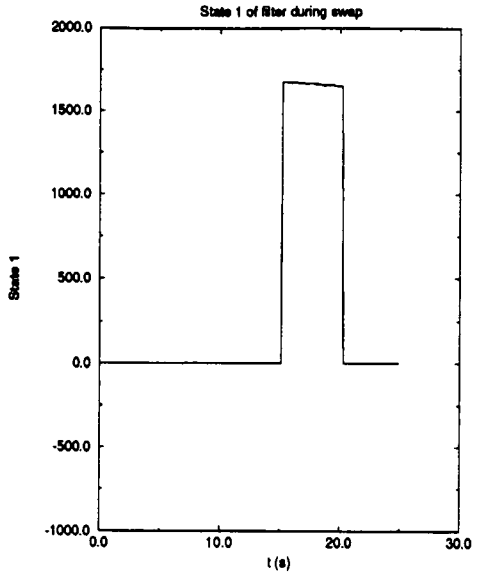

Fig. 5-2: First element of state vector as range becomes valid during t=15 to t=20.

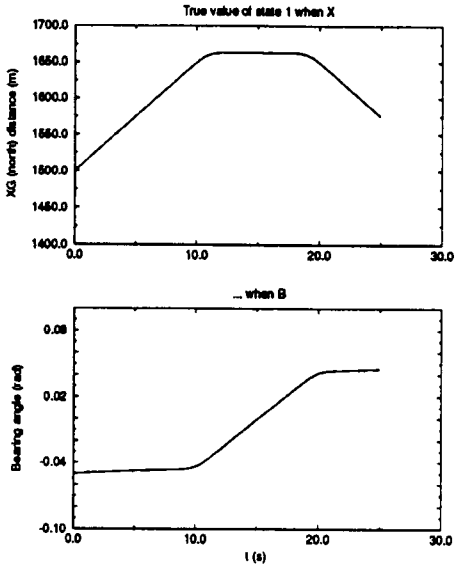

Fig. 5-3: True values of the XG (north position) and the bearing angle

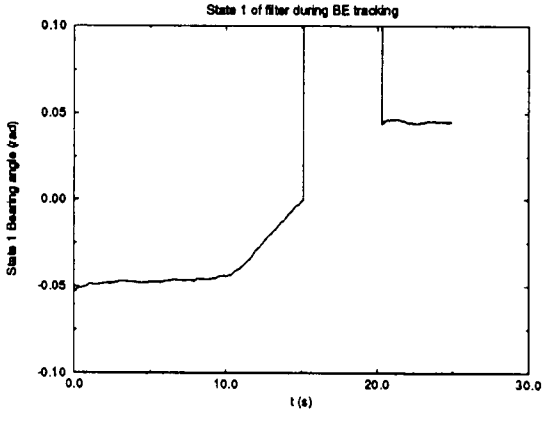

Fig. 5-4: State 1 when range invalid

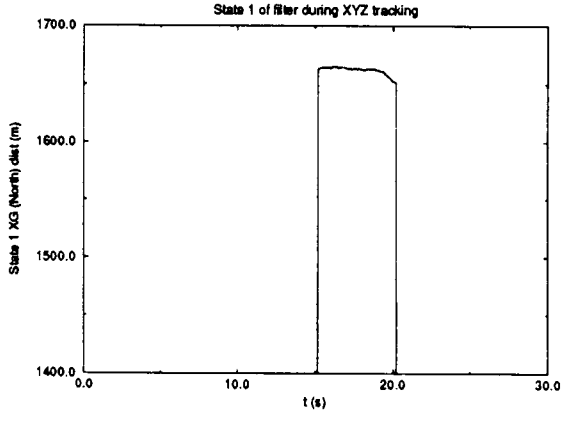

Fig. 5-5: State 1 when range valid

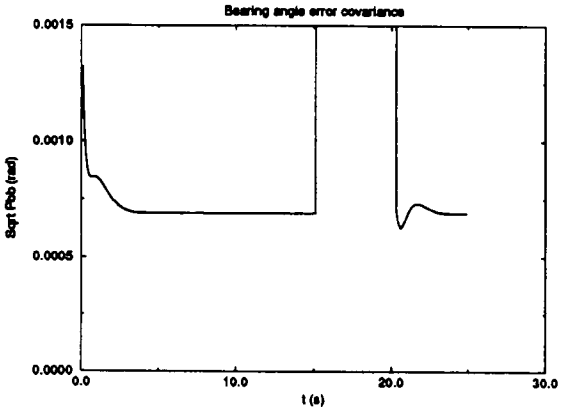

Fig. 5-6: Covariance of first state (bearing) when range is not available. Notice small transient after swap at t=20.

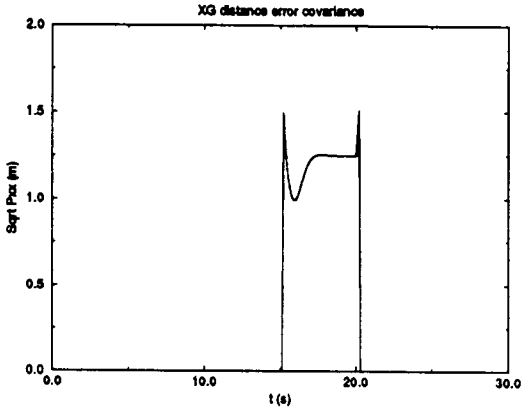

Fig. 5-7: Covariance of first state (X_G position) when range is available from t=15 to t=20.

The covariance of the p_{XG} state in Fig. 5-7 shows some initial transients after it was formed when range became available at t=15. When range information ceased at t=20, the cartesian filter tried to coast along for the next three updates (0.3s) with no range measurements and consequently the covariance estimates started to diverge rapidly at t=20. The filter was then swapped back to the bearing-elevation filter and the corresponding covariance element became that of the bearing state again, Fig. 5-6, after some brief transients after t=20.

5.3.2 Simulations of Multi-Target Nearest Neighbour Tracking With Filter Swapping

The simulation system previously described was modified to include the nearest neighbour multitarget algorithm. Sensor data files of closely spaced targets were generated and the files were merged and sorted by time stamp with no indication as to which target generated which return. The algorithm associates a new measurement to the closest existing track (if there is one within the gate threshold) or it spawns a new filter for a measurement lying outside all thresholds. When the filters were properly tuned, the algorithm would eventually settle on one filter for each target with only the occasional misassociation. Clutter points generated at random would also spawn new filters, but without subsequent measurements being associated with them, these filters would quickly die.

Fig. 5-8 below shows the true and measured bearings to the two targets of Fig. 5-1. Likewise Fig. 5-9 shows the true and measured elevations. The true and measured ranges shown in Fig. 5-10 require a bit of explanation: the measured range is negative in the portions of the trajectory when the ranging sensor is turned off. That is how the simulator distinguishes between a passive and an active sensor. The performance of the nearest neighbour algorithm is represented in the top chart of Fig. 5-11. A spike in the plot for Filter 1, for example, means that it was incorrectly updated with a measurement from target 2. Fig. 5-12 shows the second state variable from Filter 1 (which is the elevation state when it was a bearing-elevation angle filter, and is the east position state when it is swapped to a cartesian filter at t=15). The bottom portion of the same figure shows the corresponding state error and its covariance. The Kalman filter matrices and parameters remained same as in the previous example, and the "gate thresholds" were chosen as 6.0 for a cartesian filter and 4.5 for a bearing-elevation filter. Filter 1 is spawned immediately and takes all the measurements from both targets and associates them with the same filter for the first 2 seconds or so. Eventually the filter converges sufficiently to recognize there are two distinct targets and spawns a new filter for Target 2 at about t=2. From then on, the two targets are distinguished most of the time, with occasional misassociations occurring at the times of the spikes. The lower graph in Fig. 5-11 represents the times that the filters were swapped as the range information became available or ceased: Filter 1 was swapped from a BE (bearing-elevation) filter to an XYZ (cartesian) filter when the range information of Target 1 was valid from t=15 and reverted to the BE filter shortly after t=20. Likewise for Filter 2 when the range of Target 2 was available from t=17 to t=19.

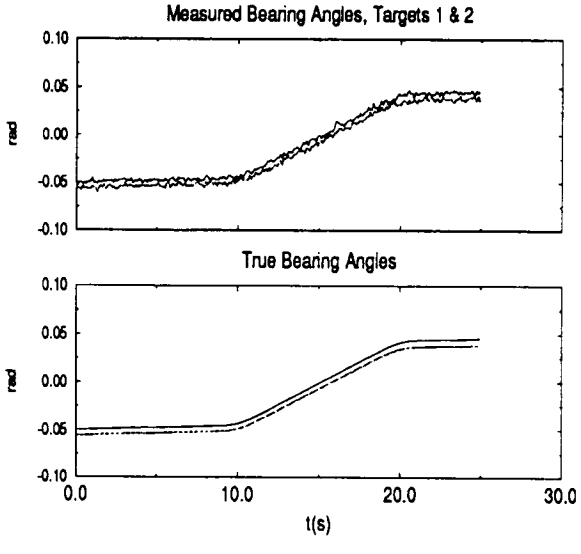

Fig. 5-8 Measured and true bearing angles, two closely spaced targets

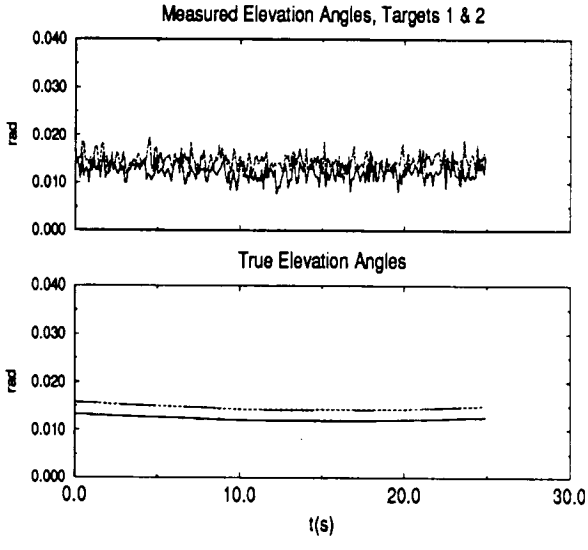

Fig. 5-9 Measured and true elevation angles, two targets

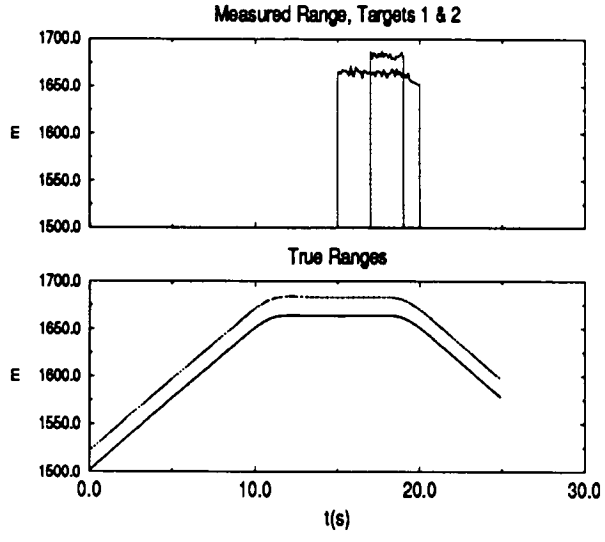

Fig. 5-10 Measured and true range, two targets. (Negative range indicates it is unavailable to the filter.)

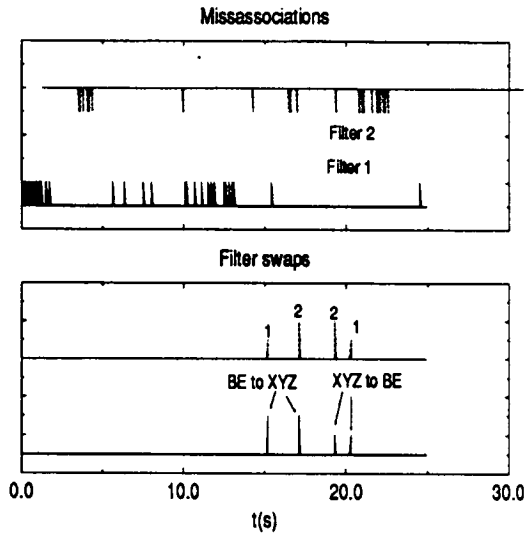

Fig. 5-11 Times of misassociations (top figure) and times of filter swaps (below).

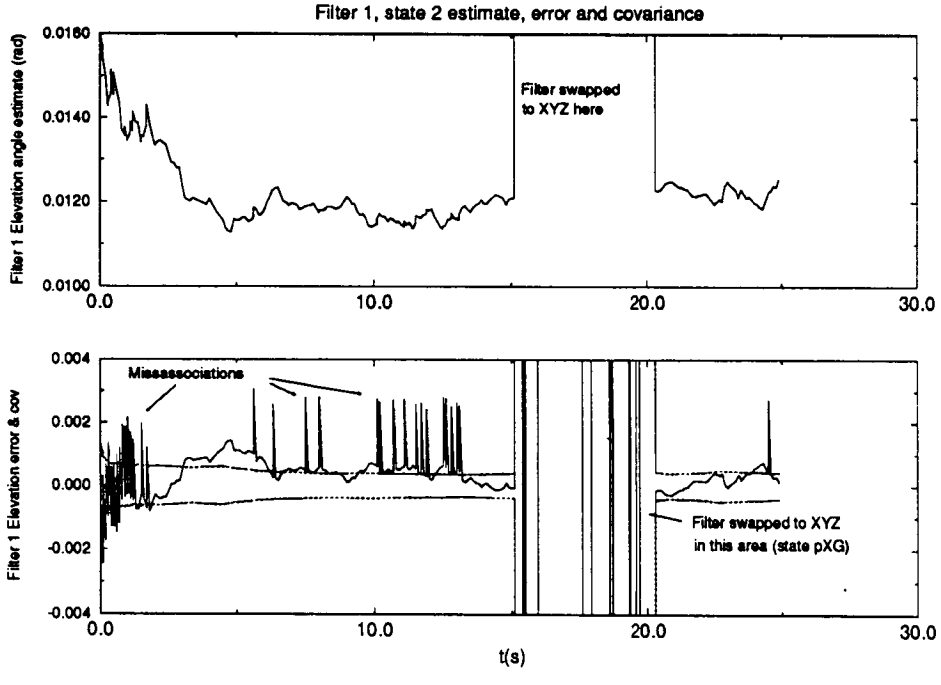

Fig. 5-12: Elevation state estimate from Filter 1, showing misassociations & swap

6.0 KALMAN FILTERS FOR MUZZLE REFERENCE SYSTEMS

6.1 INTRODUCTION

This chapter describes the modelling and simulation work that was done with the goal of applying Kalman filtering to a dynamic muzzle referencing system. The DMRS hardware consists of a small laser transceiver mounted on or near the mantlet of the gun. A small mirror is mounted on the muzzle to reflect the laser beam back to the receiver. As the barrel flexes due the motion of the vehicle over rough ground, the angle of the laser return will deviate proportionally. This angle can be detected, sampled and made available to the fire control system. Signal processing is then required to process these angles and predict when the barrel flex will be close enough to zero so that the shell can be launched through a barrel that is relatively straight. A preliminary Kalman filter design is presented in this chapter and is shown to perform this prediction quite well.

First, the gun barrel dynamics will be modelled by considering the first four modes of vibration of a long, flexible, hollow tube with the physical dimensions of a tank gun. Then, these equations are transformed to a series of state equations that can be used for simulations. The power spectrum of the simulated gun is compared with that obtained from actual field data. Finally, a Kalman filter is designed with a subset of these state equations and its ability to predict the muzzle pointing angle is tested on actual data.

There has been some ground work that used Kalman filters in dynamic muzzle referencing systems. In particular, Levin (1978) used a simple second order model for an analog Kalman filter and Baran *et al.* (1987) described an algorithm that first estimated the gun barrel model (by finding the coefficients of an auto-regressive, moving average process) with the first few seconds of barrel dynamics measurements and then used these coefficients in a Kalman filter to predict the muzzle angle 20 ms later. The encouraging results led them to demonstrate the system in real time on an M1A1 tank , as described in Brosseau *et al.* (1990). The methods described in this chapter offer another alternative to developing the gun barrel model for the predictive Kalman filter; that is, starting from the modal equations of a long, uniform, hollow tube that approximates the gun barrel.

6.2 TRANSVERSE VIBRATIONS OF LONG HOLLOW BEAMS

The theory of vibration of uniform beams is a well-studied area. In general, however a gun barrel is not uniform. It has several different cross sections along its length and is very often tapered at some points. Closed form solutions for the modal shapes and frequencies are not known in general and require extensive modelling and numerical simulation efforts to approximate. Such modelling work is done by gun designers and is presented in detail by Gast (1987), for example.

For the purposes of this report, however, we will assume the gun barrel can be modelled

as a uniform hollow tube that is free at the muzzle end and is either fixed or hinged (depending on the operation of the gun control system) at the mantlet end. The development in this chapter uses standard theory of free, undamped, transverse vibrations of linearly elastic beams, also known as Bernoulli-Euler beam theory (*e.g.* Craig (1991)). There are a number of assumptions in Bernoulli-Euler theory:

a) the longitudinal axis of the beam undergoes no extension or contraction;
b) transverse shear deformation is neglected;
c) the material is linearly elastic;
d) the beam has uniform cross-section; and
e) the slope of the beam remains small.

These assumptions are not unreasonable for an approximation of the gun barrel that is suitable for a short term predictive model for the Kalman filter.

Denote the displacement of the centerline of the beam from its at-rest centerline as $\eta(l,t)$. Note that η is a function of both the distance along the beam, l, and time, t. See Fig. 6-1 for a pictorial representation of the beam. Using standard Newtonian mechanics and the above assumptions, it can be shown that η satisfies

$$\frac{\partial^2}{\partial l^2}\left(EI\frac{\partial^2\eta(l,t)}{\partial l^2}\right) + \rho A\frac{\partial^2\eta(l,t)}{\partial t^2} = f(l,t) \tag{6-1}$$

where $f(l,t)$ is an external applied force, E is the elastic modulus of the material, ρ is its density, A is the cross-sectional area and I is the transverse moment of inertia of the beam.

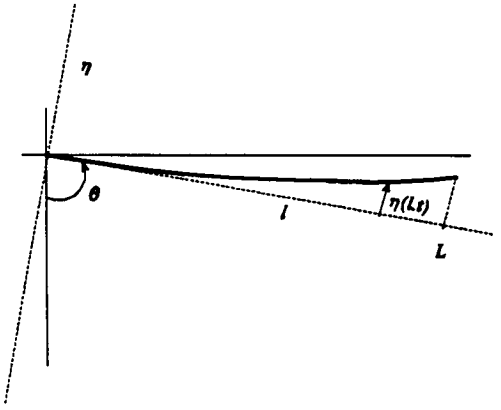

Fig. 6-1: Schematic of generic flexible beam

There are different boundary conditions for this differential equation depending on the physical constraints placed on the beam for fixed, free or hinged ends:

$$\text{Fixed end:} \quad \begin{cases} \eta(l_e,t) = 0 \\ \left.\dfrac{\partial \eta}{\partial l}\right]_{l=l_e} = 0 \end{cases} \tag{6-2}$$

$$\text{Free end:} \quad \begin{cases} \left.\dfrac{\partial^2 \eta}{\partial l^2}\right]_{l=l_e} = 0 \\ \left.\dfrac{\partial^3 \eta}{\partial l^3}\right]_{l=l_e} = 0 \end{cases} \tag{6-3}$$

$$\text{Hinged end:} \quad \begin{cases} \eta(l_e,t) = 0 \\ \left.\dfrac{\partial^2 \eta}{\partial l^2}\right]_{l=l_e} = 0 \end{cases} \tag{6-4}$$

Specifying the type of support at each end of the beam will provide 4 boundary conditions. To obtain a solution for the unforced ($f(l,t)$=0) part of (6-1), we must make an assumption on the form of the solution $\eta(l,t)$. It is assumed that the temporal and spatial portions of η can be separated as the product of a modal shape function, $\phi(l)$, (that depends only on the distance l) and a simple harmonic function, $h(t) = c_0 \cos(\omega t - \alpha)$, that depends only on time:

$$\eta(l,t) = \phi(l)\ h(t) = c_0\ \phi(l)\ \cos(\omega t - \alpha) \tag{6-5}$$

where c_0 is a constant. From this, we see that

$$\frac{\partial^2 \eta(l,t)}{\partial t^2} = -c_0\ \omega^2\ \phi(l)\ \cos(\omega t - \alpha)$$

and

$$\frac{\partial^4 \eta(l,t)}{\partial l^4} = \frac{d^4 \phi(l)}{dl^4} c_0 \cos(\omega t - \alpha)$$

Substituting these in (6-1) and setting $f(l,t)=0$ yields

$$EI\frac{d^4\phi(l)}{dl^4}c_0\cos(\omega t-\alpha) - \rho A c_0 \omega^2 \phi(l)\cos(\omega t-\alpha) = 0$$

or by defining

$$\lambda^4 := \frac{\rho A \omega^2}{EI} \tag{6-6}$$

then

$$\frac{d^4\phi(l)}{dl^4} - \lambda^4\phi(l) = 0 \tag{6-7}$$

A general solution to (6-7) is well known to be

$$\phi(l) = c_1 \sinh(\lambda l) + c_2 \cosh(\lambda l) + c_3 \sin(\lambda l) + c_4 \cos(\lambda l) \tag{6-8}$$

where we have 5 unknowns (the 4 amplitude coefficients and the eigenvalue λ). The next two subsections use different sets of boundary conditions for two configurations of the beam: the hinged-free beam and the fixed-free beam.

6.2.1 Hinged-Free Beam: Modal Shapes and Frequencies

Assume the beam is hinged at $l = 0$ and free at $l = L$. Now apply the 4 known boundary conditions. For a beam hinged at $l = 0$ boundary conditions (6-4) imply

$$\begin{aligned} \phi(0) = 0 &\Rightarrow c_2 + c_4 = 0 \\ \left.\frac{d^2\phi}{dl^2}\right]_{l=0} = 0 &\Rightarrow \lambda^2(c_2 - c_4) = 0 \end{aligned} \tag{6-9}$$

and the free boundary conditions at $l = L$ imply, from (6-3),

$$\left.\frac{d^2\phi}{dl^2}\right]_{l=L} = 0 \Rightarrow \lambda^2 (c_1 \sinh\lambda L + c_2 \cosh\lambda L - c_3 \sin\lambda L - c_4 \cos\lambda L) = 0$$
$$\left.\frac{d^3\phi}{dl^3}\right]_{l=L} = 0 \Rightarrow \lambda^3 (c_1 \cosh\lambda L + c_2 \sinh\lambda L - c_3 \cos\lambda L + c_4 \sin\lambda L) = 0 \qquad (6\text{-}10)$$

To get a nontrivial ($\lambda \neq 0$) solution to (6-9) we see that

$$c_2 = c_4 = 0$$

Substituting this result in (6-10) will result in

$$\lambda^2 (c_1 \sinh\lambda L - c_3 \sin\lambda L) = 0$$
$$\lambda^3 (c_1 \cosh\lambda L - c_3 \cos\lambda L) = 0 \qquad (6\text{-}11)$$

which can be written in matrix form as:

$$\begin{bmatrix} \lambda^2 \sinh\lambda L & -\lambda^2 \sin\lambda L \\ \lambda^3 \cosh\lambda L & -\lambda^3 \cos\lambda L \end{bmatrix} \begin{bmatrix} c_1 \\ c_3 \end{bmatrix} = \begin{bmatrix} 0 \\ 0 \end{bmatrix}$$

Again for this to have a non-trivial solution, we can set the determinant of this matrix to 0 and solve for λL:

$$\begin{vmatrix} \lambda^2 \sinh\lambda L & -\lambda^2 \sin\lambda L \\ \lambda^3 \cosh\lambda L & -\lambda^3 \cos\lambda L \end{vmatrix} = 0$$

$$\Rightarrow \sinh\lambda L \cos\lambda L - \cosh\lambda L \sin\lambda L = 0$$

This equation has many solutions, a few of which were found numerically and are listed here:

$$\begin{aligned} \lambda_1 L &= 3.9266 \\ \lambda_2 L &= 7.0686 \\ \lambda_3 L &= 10.2102 \\ \lambda_4 L &= 13.3518 \end{aligned} \tag{6-12}$$

Now from the definition of λ in (6-6), we can get the modal frequencies

$$\omega^2 = \frac{\lambda^4 L^4 EI}{\rho A L^4}$$

$$\Rightarrow \omega_i = (\lambda_i L)^2 \sqrt{\frac{EI}{\rho A L^4}} \tag{6-13}$$

Table 6-1: Approximate physical parameters of a 105mm gun barrel

L	= Length of barrel = 5 m
d_o	= Outer diameter = 0.125 m
d_i	= Inner diameter = 0.105 m
A	= Cross-sectional area = $(\pi/4)(d_o^2 - d_i^2)$ = 0.00361 m^2
I	= Cross-sectional moment of inertia = $(\pi/64)(d_o^4 - d_i^4) = 6.02\times10^{-6}$ m^4
E	= Elastic modulus of steel = 2.068×10^{11} N/m^2
ρ	= Density of steel = 8000 kg/m^3

For a generic 105mm tank gun barrel, the approximate physical parameters in Table 6-1 can be used. Combining these numerical values with the values of $\lambda_i L$ from (6-12) and substituting in (6-13) yields the modal frequencies for the hinged-free hollow gun tube:

$$\begin{aligned} \omega_1 &= (3.9266^2)\ (8.3) = 128 \text{ rad/s} = 20.4 \text{ Hz} \\ \omega_2 &= (7.0686^2)\ (8.3) = 415 \text{ rad/s} = 66 \text{ Hz} \\ \omega_3 &= (10.2102^2)\ (8.3) = 865 \text{ rad/s} = 138 \text{ Hz} \\ \omega_4 &= (13.3518^2)\ (8.3) = 1480 \text{ rad/s} = 235 \text{ Hz} \end{aligned} \tag{6-14}$$

To obtain the corresponding modal shape functions, we return to finding the amplitude

coefficients c_i. From the first equation of (6-11) we can express

$$c_1 = \frac{\sin\lambda L}{\sinh\lambda L} c_3$$

and since we previously established that $c_2 = c_4 = 0$ then we get from (6-8) the modal shape functions for the hinged-free tube:

$$\phi_i(l) = c_3\left[\sin\lambda_i L\frac{l}{L} + \left(\frac{\sin\lambda_i L}{\sinh\lambda_i L}\right)\sinh\lambda_i L\frac{l}{L}\right] \tag{6-15}$$

These modal shape functions (with c_3 arbitrarily set to 1) are plotted in Fig. 6-2.

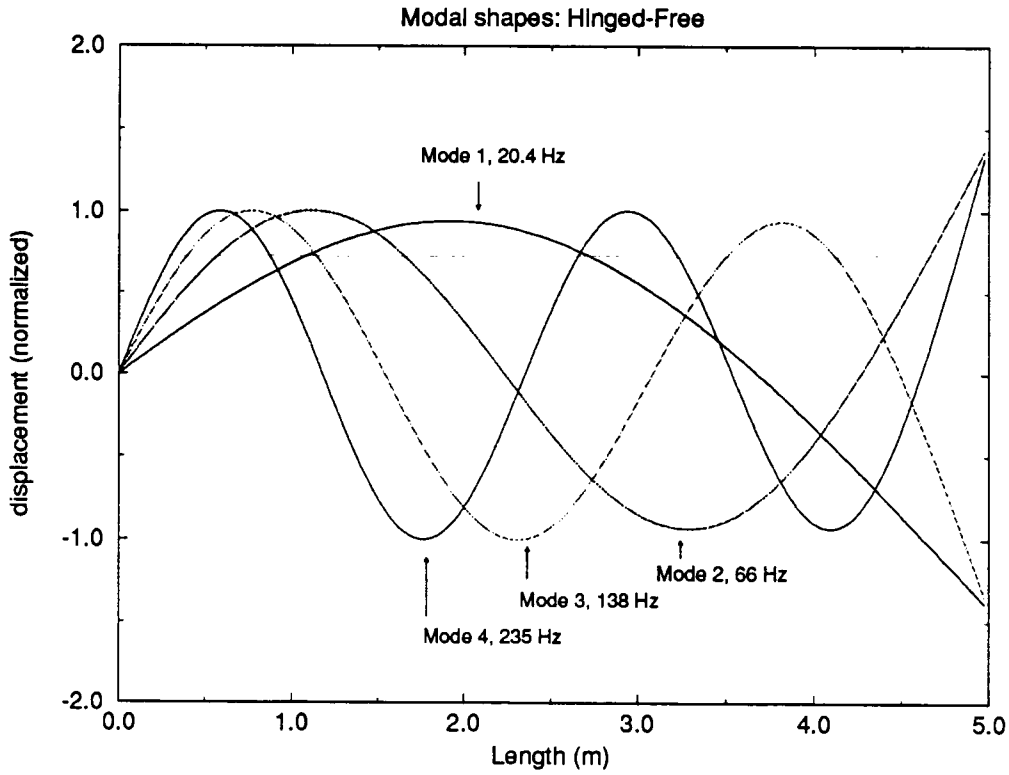

Fig. 6-2: Modal Shape Functions of Hinged-Free Hollow Tube

6.2.2 Fixed-Free Beam: Modal Shapes and Frequencies

In the second situation, we assume the beam is fixed at $l = 0$ and free at $l = L$. For this case the boundary conditions at $l = 0$ come from (6-2):

$$\phi(0) = 0 \Rightarrow c_2 + c_4 = 0$$

$$\left.\frac{d\phi}{dl}\right]_{l=0} = 0 \Rightarrow \lambda(c_1 + c_3) = 0$$

and, as before, the free boundary conditions at $l = L$ imply from (6-3)

$$\left.\frac{d^2\phi}{dl^2}\right]_{l=L} = 0 \Rightarrow \lambda^2(c_1\sinh\lambda L + c_2\cosh\lambda L - c_3\sin\lambda L - c_4\cos\lambda L) = 0$$

$$\left.\frac{d^3\phi}{dl^3}\right]_{l=L} = 0 \Rightarrow \lambda^3(c_1\cosh\lambda L + c_2\sinh\lambda L - c_3\cos\lambda L + c_4\sin\lambda L) = 0$$

These 4 equations can be written in matrix form as:

$$\begin{bmatrix} 0 & 1 & 0 & 1 \\ \lambda & 0 & \lambda & 0 \\ \lambda^2\sinh\lambda L & \lambda^2\cosh\lambda L & -\lambda^2\sin\lambda L & -\lambda^2\cos\lambda L \\ \lambda^3\cosh\lambda L & \lambda^3\sinh\lambda L & -\lambda^3\cos\lambda L & -\lambda^3\sin\lambda L \end{bmatrix} \begin{bmatrix} c_1 \\ c_2 \\ c_3 \\ c_4 \end{bmatrix} = \begin{bmatrix} 0 \\ 0 \\ 0 \\ 0 \end{bmatrix} \qquad (6\text{-}16)$$

As before, a nontrivial set of solutions to this set of equations is obtained if the determinant of the matrix is set to zero:

$$\begin{vmatrix} 0 & 1 & 0 & 1 \\ \lambda & 0 & \lambda & 0 \\ \lambda^2\sinh\lambda L & \lambda^2\cosh\lambda L & -\lambda^2\sin\lambda L & -\lambda^2\cos\lambda L \\ \lambda^3\cosh\lambda L & \lambda^3\sinh\lambda L & -\lambda^3\cos\lambda L & -\lambda^3\sin\lambda L \end{vmatrix} = 0$$

$$\Rightarrow \quad \cos\lambda L\cosh\lambda L + 1 = 0$$

Numerical solution of this equation leads us again to several solutions, one for each mode:

$$\lambda_1 L = 1.8751$$
$$\lambda_2 L = 4.6941$$
$$\lambda_3 L = 7.8548$$
$$\lambda_4 L = 10.996$$

so substituting these (6-13) yields the modal frequencies for the fixed-free hollow gun tube:

$$\begin{aligned}\omega_1 &= (1.875^2)\ (8.3) = 29 \text{ rad/s} = 4.6 \text{ Hz}\\ \omega_2 &= (4.694^2)\ (8.3) = 183 \text{ rad/s} = 29 \text{ Hz}\\ \omega_3 &= (7.855^2)\ (8.3) = 512 \text{ rad/s} = 82 \text{ Hz}\\ \omega_4 &= (10.996^2)\ (8.3) = 1004 \text{ rad/s} = 160 \text{ Hz}\end{aligned} \tag{6-17}$$

To obtain the corresponding modal shape functions of the fixed-free beam, we need the amplitude coefficients c_i. It is straightforward to show from (6-16) that

$$c_4 = -c_2$$
$$c_3 = -c_1$$
$$c_1 = -c_2\left[\frac{\cosh\lambda_i L + \cos\lambda_i L}{\sinh\lambda_i L + \sin\lambda_i L}\right]$$

so that by leaving c_2 arbitrary and substituting these coefficients in the general modal shape equation (6-8), then the mode shapes for the fixed-free beam are (and as plotted in Fig. 6-3):

$$\phi_i(l) = c_2\left[\cosh\lambda_i L\frac{l}{L} - \cos\lambda_i L\frac{l}{L} - r_i\left(\sinh\lambda_i L\frac{l}{L} - \sin\lambda_i L\frac{l}{L}\right)\right] \tag{6-18}$$

$$\text{where}\quad r_i := \frac{\cosh\lambda_i L + \cosh\lambda_i L}{\sinh\lambda_i L + \sin\lambda_i L}$$

6.3 FORMULATION OF STATE EQUATIONS

With the assumed form of the solution of the main differential equation (6-1) describing the dynamics of a transversely vibrating beam having been established in the previous section as a product of the modal shape functions, (6-15) or (6-18), with time-varying simple harmonic functions, it is possible to derive a set of state equations that describe the relative contributions of these mode shapes at any point along the beam, at any time and given any forcing function and/or initial conditions. These state equations then form the basis of the prediction filter.

6.3.1 Development of the State Equations

The method described in Sasiadek and Srinivasan (1989) was used to derive the state equations and is summarized here. The beam is considered to be of the fixed-free configuration of Section 6.2.2 so the modal shape functions of (6-18) are used, but an additional degree of

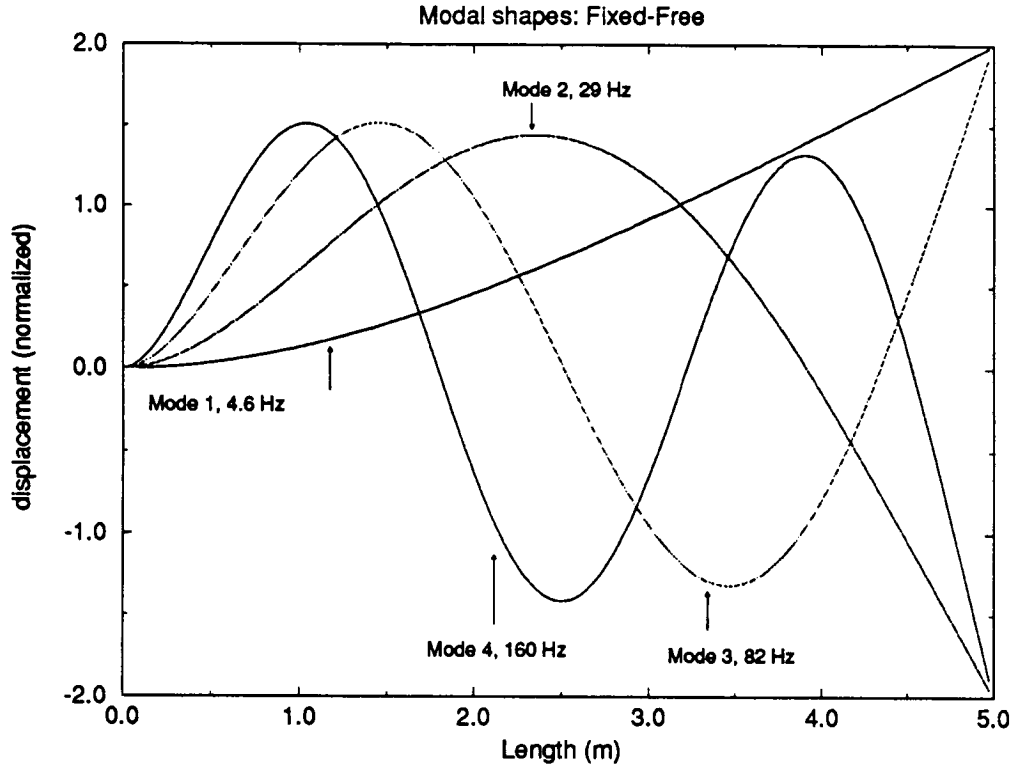

Fig. 6-3: Modal Shape Functions of Fixed-Free Hollow Tube

freedom is introduced at the "fixed" end by allowing that end to rotate by an angle θ (see Fig. 6-1). In this way we could introduce a control action at the fixed end to drive the beam to any desired pointing angle. In essence this is a reasonable representation of the gun barrel attached to the gun control system.

The assumed mode solution describes the deflection of any point of the beam as the product of the modal shape functions, $\phi_i(l)$ from (6-18), with arbitrary temporal functions, $e_i(t)$, which in vector form is denoted by

$$\eta(l,t) = \boldsymbol{e}(t)^T \, \boldsymbol{\Phi}(l) = \sum_{i=1}^{n} \left(e_i(t) \; \phi_i(l) \right) \tag{6-19}$$

If we choose our state vector x_c as

$$\boldsymbol{x}_c(t) := \left[\; \theta(t) \quad e_1(t) \quad e_2(t) \quad \cdots \quad e_n(t) \; \right]^T$$

then Sasiadek and Srinivasan (1989) show that the dynamic equation representing the undamped transverse vibrations of the beam pictured in Fig. 6-1 is

$$M\,\ddot{x}_c + K\,x_c = f \tag{6-20}$$

where

$$M := \begin{bmatrix} m_\theta & m_{\theta\phi}^T \\ m_{\theta_\phi} & [M_\phi] \end{bmatrix}, \qquad K := \begin{bmatrix} 0 & \mathbf{0}^T \\ \mathbf{0} & [K_\phi] \end{bmatrix}, \qquad f := \begin{bmatrix} \tau \\ 0 \\ \vdots \\ 0 \end{bmatrix}$$

and where

$$m_\theta := \rho A L^3/3$$

$$m_{\theta\phi} := \rho A \int_0^L l\vec{\phi}(l)dl$$

$$M_\phi := \rho A \int_0^L \vec{\phi}(l)\vec{\phi}^T(l)dl$$

$$K_\phi := EI \int_0^L \frac{\partial^2 \vec{\phi}(l)}{\partial l^2} \frac{\partial^2 \vec{\phi}(l)}{\partial l^2}^T dl$$

τ := applied torque at the hinged end

Note that the second derivatives of the modal shape functions are obtained from (6-18) as

$$\frac{\partial^2 \phi_i(l)}{\partial l^2} = c_2 \frac{(\lambda_i L)^2}{L^2}\left[\cosh\lambda_i L\frac{l}{L} + \cos\lambda_i L\frac{l}{L} - r_i\left(\sinh\lambda_i L\frac{l}{L} + \sin\lambda_i L\frac{l}{L}\right)\right]$$

Since, in reality, the oscillations are not undamped, we introduce a damping matrix into (6-20) denoted by D := diag [$d_\theta\ d_1\ d_2\ \ldots\ d_n$] so that the damped dynamic equation becomes

$$M\,\ddot{x}_c + D\,\dot{x}_c + K\,x_c = f$$

or in more convenient state space form:

$$\begin{bmatrix} \ddot{x}_c \\ \dot{x}_c \end{bmatrix} = \begin{bmatrix} -M^{-1}D & -M^{-1}K \\ [I] & [0] \end{bmatrix} \begin{bmatrix} \dot{x}_c \\ x_c \end{bmatrix} + \begin{bmatrix} M^{-1} \\ [0] \end{bmatrix} f \tag{6-21}$$

where $[I]$ represents the $(n+1)$ by $(n+1)$ identity matrix and $[0]$ is the similarly dimensioned zero matrix. The gun barrel dynamics as specified in this last equation are now of the form $\dot{x} = Fx + Gu$ that can readily be modelled in a Kalman filter.

6.3.2 Numerical Calculations and Simulations

To make the state equation, (6-21), more concrete, we can compute some numerical values. Commercial numerical software was used to compute the various integrals for terms of the state dynamics matrices and the inverse and products of the various matrices. The physical gun parameters of Table 6-1 were used to calculate the first 4 modes. The integrals evaluated to

$$m_\theta = 1204.28$$

$$m_{\theta\phi} = \begin{bmatrix} 410.98 \\ 65.62 \\ 23.47 \\ 11.89 \end{bmatrix}, \quad M_\phi = \begin{bmatrix} 144.5 & 0 & 0 & 0 \\ 0 & 144.5 & 0 & 0 \\ 0 & 0 & 144.5 & 0 \\ 0 & 0 & 0 & 144.5 \end{bmatrix}$$

$$K_\phi = \begin{bmatrix} 123054 & -18.22 & 42.66 & -47.93 \\ -18.22 & 4.833\times10^6 & -1114.5 & 1223.54 \\ 42.66 & -1114.5 & 3.79\times10^7 & -2230.7 \\ -47.93 & 1223.54 & -2230.7 & 1.455\times10^8 \end{bmatrix}$$

and when the damping matrix was chosen as

$$D = \text{diag}\begin{bmatrix} 2000 & 0.1 & 0.1 & 0.1 & 0.1 \end{bmatrix}$$

then the continuous time state equations, (6-21), with an abbreviation of notation, are

$$\dot{x} = Fx + Gf$$

$$x := \begin{bmatrix} \dot{x}_c \\ x_c \end{bmatrix} = \begin{bmatrix} \dot{\theta} & \dot{e}_1 & \dot{e}_2 & \dot{e}_3 & \dot{e}_4 & \theta & e_1 & e_2 & e_3 & e_4 \end{bmatrix}^T$$

where the coefficient matrices are

F matrix:

-2782	0.39	5	6.316e-02	2.258e-02	1.144e-02	0	4.87e+05	3.052e+06	8.558e+06	1.665e+07
7913	-1.12		-0.179	-6.424e-02	-3.255e-02	0	-1.38e+06	-8.682e+06	-2.434e+07	-4.737e+07
1263.2	-0.179		-2.93e-02	-1.025e-02	-5.196e-03	0	-2.21e+05	-1.419e+06	-3.886e+06	-7.563e+06
451.7	-6.424e-02		-1.025e-02	-4.358e-03	-1.858e-03	0	-79049	-4.956e+05	-1.651e+06	-2.704e+06
228.9	-3.255e-02		-5.196e-03	-1.858e-03	-1.633e-03	0	-40057	-2.511e+05	-7.041e+05	-2.377e+06
1	0		0	0	0	0	0	0	0	0
0	1		0	0	0	0	0	0	0	0
0	0		1	0	0	0	0	0	0	0
0	0		0	1	0	0	0	0	0	0
0	0		0	0	1	0	0	0	0	0

G matrix:

1.391	-3.95651	-0.631614	-0.225851	-0.114447
-3.95651	11.2607	1.79654	0.642401	0.325529
-0.631614	1.79654	0.293719	0.102552	5.196719e-02
-0.225851	0.642401	0.102552	4.358950e-02	1.858225e-02
-0.114447	0.325529	5.196719e-02	1.858225e-02	1.633524e-02
0	0	0	0	0
0	0	0	0	0
0	0	0	0	0
0	0	0	0	0
0	0	0	0	0

The time-varying magnitudes of the various states are dependent on the initial conditions and input forcing function *f*. Computer simulations were conducted on the above barrel model with a relatively large (2 cm) initial amplitude on mode 1 (state e_1) and no input forces, f=0. The output, $y(t)$, was chosen as the displacement at the free end of the beam:

$$y(t) := \eta(L,t) = \sum_{i=1}^{4} \left(e_i(t)\phi_i(L) \right)$$

$$= 2e_1(t) - 2e_2(t) + 2e_3(t) - 2e_4(t)$$

$$= \begin{bmatrix} 0 & 0 & 0 & 0 & 0 & 0 & 2 & -2 & 2 & -2 \end{bmatrix} \boldsymbol{x}(t)$$

where the values for $\phi_i(L)$ are obtained from (6-18) with $l = L$.

The resulting time history of the output is shown below in Fig. 6-4. Note that the motion is primarily a damped sinusoid, with an apparently clean harmonic content. The power spectral density (PSD) function of the tip displacement is shown in Fig. 6-5. A sampling frequency of 600 Hz was used in the simulation so the response of all modes could be observed. Note that the modal frequencies now match those of a hinged-free beam because of the introduction of the extra degree of freedom at the "fixed" end, *i.e.* the angle θ. Mode 1 is by far dominant, being at least 40 db higher than mode 2. Higher modes are even less significant. This observation will be exploited in the design of the Kalman filter - only the first two modes will be modelled.

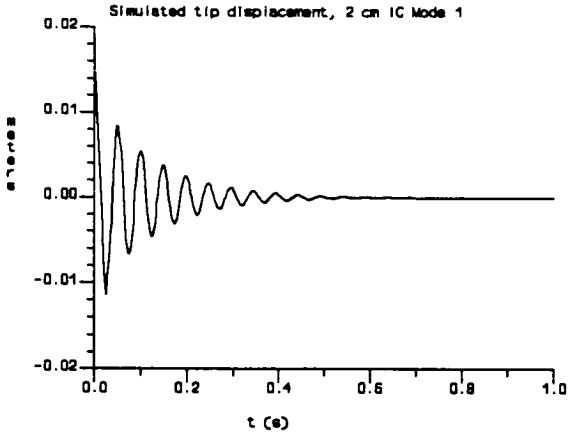

Fig. 6-4: Simulated tip motion

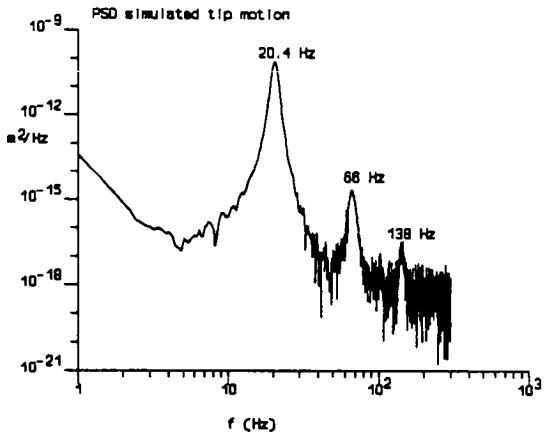

Fig. 6-5: PSD of simulated tip motion

6.3.3 Experimental Corroboration

The model of the tank gun barrel was partly validated by a series of field trials conducted on a Leopard C1 tank with a 105mm gun as described in Bird (1990). Briefly, the barrel was instrumented with a number of accelerometers and gyroscopes and the tank was driven over various types of natural and artificial terrain. Gyros mounted in the elevation plane at the mantlet and the muzzle of the gun provided angular rate signals that were sampled at 60 Hz and numerically integrated to give the mantlet and muzzle elevation angles such as those shown in Fig. 6-6 below. An estimate of the elevation flex of the barrel was obtained by subtracting the mantlet angle from the muzzle angle resulting in the "derived flex" shown in Fig. 6-7. The power spectral density of this is shown in Fig. 6-8. Unfortunately, the signals were sampled at only 60 Hz so PSD information is only valid up to 30 Hz. The dominant mode at about 20 Hz appears as expected but higher modes are cut off by anti-aliasing filters at 30 Hz. As well, the broadband power seen in the 1 Hz to 5 Hz region is that of the tank moving over the ground at moderate speeds and was not included in the simulations of the last section. Nonetheless, it is encouraging to see at least general agreement between simulated and experimental results. In future experiments it would be valuable to conduct more controlled tests with the tank stationary with barrel motion induced by initial displacements and with high speed data recording to better validate the model.

In any event, it will be assumed that the model is a reasonable approximation of the dynamics. Of course, a number of assumptions have already been made to arrive at the linear state equations, not the least of which is that the barrel has a uniform cross-section along its length. If this assumption is not made, there is no closed-form solution available and the dynamics must be simulated by complex numerical techniques such as finite element methods and a Kalman filter would not be a candidate for muzzle pointing prediction algorithms. The state space model lends itself immediately to such techniques.

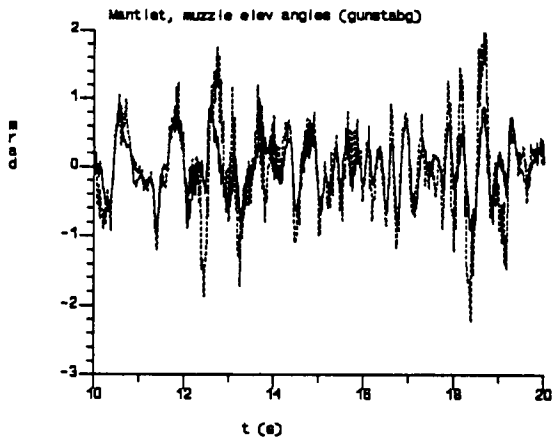

Fig. 6-6: Measured barrel angles

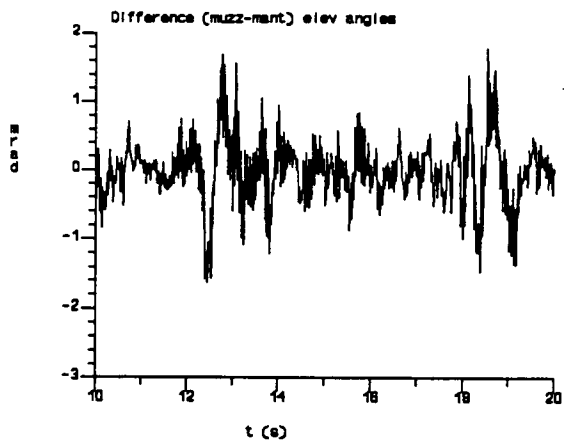

Fig. 6-7: Derived barrel flex

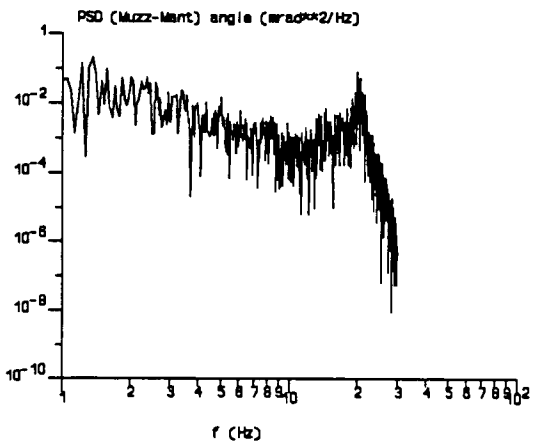

Fig. 6-8: PSD of flex

6.4 A KALMAN FILTER FOR THE DMRS

6.4.1 Filter Design

This section describes the design of a Kalman filter based on the previously developed state equations. The filter is tested on its ability to predict the muzzle pointing angle of the real data in the next section.

From the observations of the last section, only the first two modes of vibration are considered, so our state equation is

$$\dot{x} = Fx + Gf$$

where

$$x := \begin{bmatrix} \dot{\theta} \\ \dot{e}_1 \\ \dot{e}_2 \\ \theta \\ e_1 \\ e_2 \end{bmatrix}, \qquad f := \begin{bmatrix} \tau \\ 0 \\ 0 \end{bmatrix}$$

and where the coefficient matrices (for the 2 mode case) work out to be, from (6-21),

F matrix:

-363.15	5.16462e-02	8.24476e-03	0	63551	3.98487e+05
1032.9	-0.14759	-2.34511e-02	0	-1.81614e+05	-1.13344e+06
164.9	-2.34511e-02	-4.43573e-03	0	-28857	-2.14389e+05
1	0	0	0	0	0
0	1	0	0	0	0
0	0	1	0	0	0

G matrix:

0.181574	-0.516462	-8.244756e-02
-0.516462	1.47592	0.234511
-8.244756e-02	0.234511	4.435732e-02
0	0	0
0	0	0
0	0	0

Define the product Gf as

$$w := Gf = \begin{bmatrix} 0.1816\ \tau \\ -0.5165\ \tau \\ -0.08244\ \tau \\ 0 \\ 0 \\ 0 \end{bmatrix} \tag{6-22}$$

The forcing function, τ, is modelled as a Gaussian white noise stochastic process with zero mean ($E[\tau] = 0$) and power spectral density (see Appendix B for a justification of this):

$$E[\tau(t_a)\tau(t_b)] = 5.0\ \delta(t_a - t_b)$$

Thus the power spectral density of the input forcing vector, w, is

$$E[w(t_a)w^T(t_b)] = \begin{bmatrix} 0.1816 \\ -0.5165 \\ -0.08245 \\ 0 \\ 0 \\ 0 \end{bmatrix} E[\tau(t_a)\tau(t_b)] \begin{bmatrix} 0.1816 \\ -0.5165 \\ -0.08245 \\ 0 \\ 0 \\ 0 \end{bmatrix}^T$$

$$= \begin{bmatrix} 0.16 & 0 & 0 & 0 & 0 & 0 \\ 0 & 1.3 & 0 & 0 & 0 & 0 \\ 0 & 0 & 0.03 & 0 & 0 & 0 \\ 0 & 0 & 0 & 0 & 0 & 0 \\ 0 & 0 & 0 & 0 & 0 & 0 \\ 0 & 0 & 0 & 0 & 0 & 0 \end{bmatrix} \delta(t_a - t_b) := Q\ \delta(t_a - t_b)$$

So in summary, the state model so far is

$$\dot{x}(t) = F\ x(t) + w(t)$$
$$E[w(t_a)w^T(t_b)] = Q\ \delta(t_a - t_b) \qquad (6\text{-}23)$$

This is exactly the form of the continuous time stochastic system of (2-2) which can readily be converted to the discrete time system

$$x_{k+1} = \Phi x_k + w_k$$

$$E[w_k w_j^T] = Q_k \delta_{kj}$$

according to the discretization procedure (2-3).

The measurement for the filter will be the angle, ψ, of the muzzle with respect to the mantlet (see Fig. 6-9) which can be related to the vertical displacement of the muzzle from the centreline of the barrel, $\eta(L,t)$, and the length of the gun, L:

$$\psi(t) = \sin^{-1} \frac{\eta(L,t)}{L}$$

$$\approx \frac{\eta(L,t)}{L}$$

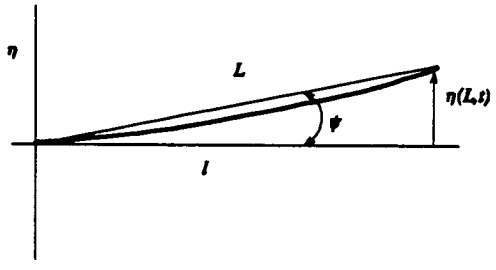

Fig. 6-9: Measured angle from muzzle reference system

The mantlet-mounted laser transceiver of the muzzle reference system measures the angular flex of the barrel using a reflecting mirror mounted on the muzzle. This measurement consists of the angle, ψ, plus a random noise component, v_k:

$$z_k := \psi(t_k) + v_k$$

$$\approx \frac{\eta(L,t_k)}{L} + v_k$$

$$= \frac{1}{L} \sum_{i=1}^{2} \phi_i(L) e_i(t_k) + v_k$$

$$= \frac{1}{L} \begin{bmatrix} 0 & 0 & 0 & 0 & 2 & -2 \end{bmatrix} x_k + v_k$$

$$=: H\, x_k + v_k$$

Finally we take the measurement noise to be zero mean and covariance

$$E[v_k v_j] = (0.2 \text{ mrad})^2 \, \delta_{kj}$$

$$= (0.0002 \text{ rad})^2 \, \delta_{kj}$$

$$:= R_k \, \delta_{kj}$$

This noise level was chosen based on expected MRS performance and also happens to describe the extent of the noise seen in the field data of the next section quite well.

6.4.2 Filter Execution on Real Data

Now that the specification of the filter is complete, the derived barrel flex from the measured field trial data, Fig. 6-7, was used as the data sequence, z_k, to drive the filter of the previous section. It is difficult to evaluate the performance of the filter because there is no truth data available that would definitively indicate how well the filter is predicting the future muzzle pointing angle. All we have is the sequence of noisy measurement data. However it is possible to qualitatively evaluate the filter by looking at the predicted muzzle angle relative to the measured angle as a function of time. The filter was used to predict what the measured flex would be 3 steps (or 50 ms, since the measurement rate is 60 Hz) ahead, $\hat{z}_{k+3|k} = H_k \, \Phi_k^3 \, \hat{x}_{k|k}$. (The notation here is the same as in Chapter 2.)

Shown in Fig. 6-10 below is a short section of the measured barrel flex as derived from the difference of the two gyros at opposite ends of the gun. The solid line is the actual measurement sequence, z_k, fed to the filter and the dotted line is the what the filter predicted the measurement would be at that point based only on data received up to 3 steps (50 ms) before that point, *i.e.*, $\hat{z}_{k|k-3} = H_{k-3} \, \Phi_{k-3}^3 \, \hat{x}_{k-3|k-3}$. It is fairly evident from Fig. 6-10 that the filter is predicting the gun flex quite well. Given that the filter was told that the standard deviation of the measurement noise was 0.2 mrad, the differences between measured and predicted muzzle angles all appear to be of that order, as could be expected, in that section of the data sequence.

However, there are other portions of the measured barrel flex data sequence that were not as satisfactorily predicted by the filter. One of these is shown in Fig. 6-11. What is different about this portion is that the 20 Hz vibratory mode is not dominant from about t=12.2 to t=13.2. During that time that tank likely experienced a fairly long (1/2) second upward acceleration followed by a similar downward acceleration that essentially biased the shape of the gun barrel slightly while the accelerations were occurring. This effect was not included in the barrel model used by the Kalman filter and hence the predicted measurements during these times are not particularly good. In fact they tend to lag behind by 3 or 4 samples. After the acceleration transients die away at about 13.2 sec, the filter returns to fairly good prediction performance.

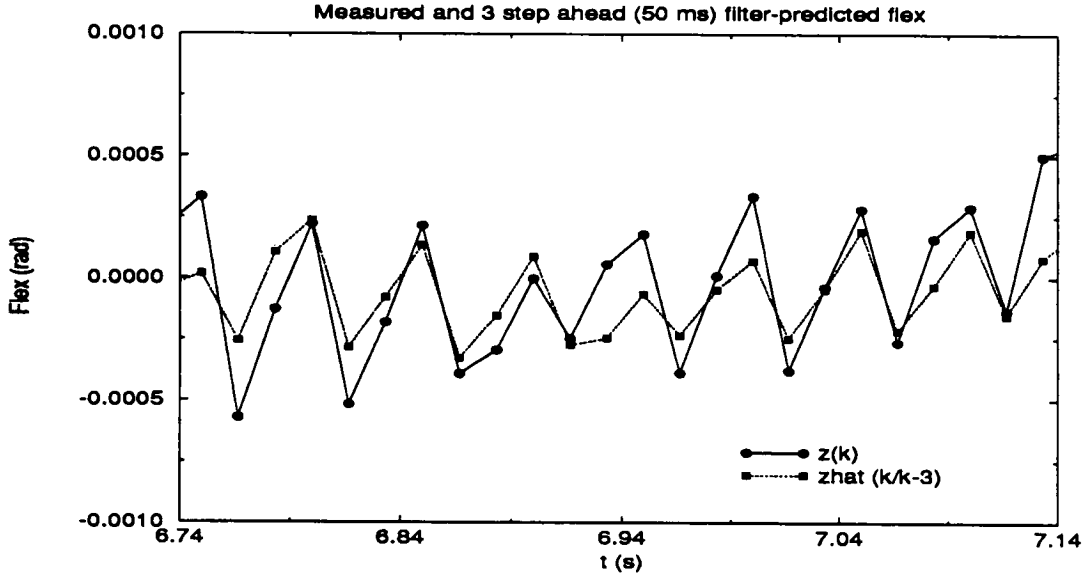

Fig. 6-10: Real barrel flex measurements and 3-step ahead Kalman filter prediction. This shows fairly good muzzle angle prediction when the 20 Hz mode is the dominant.

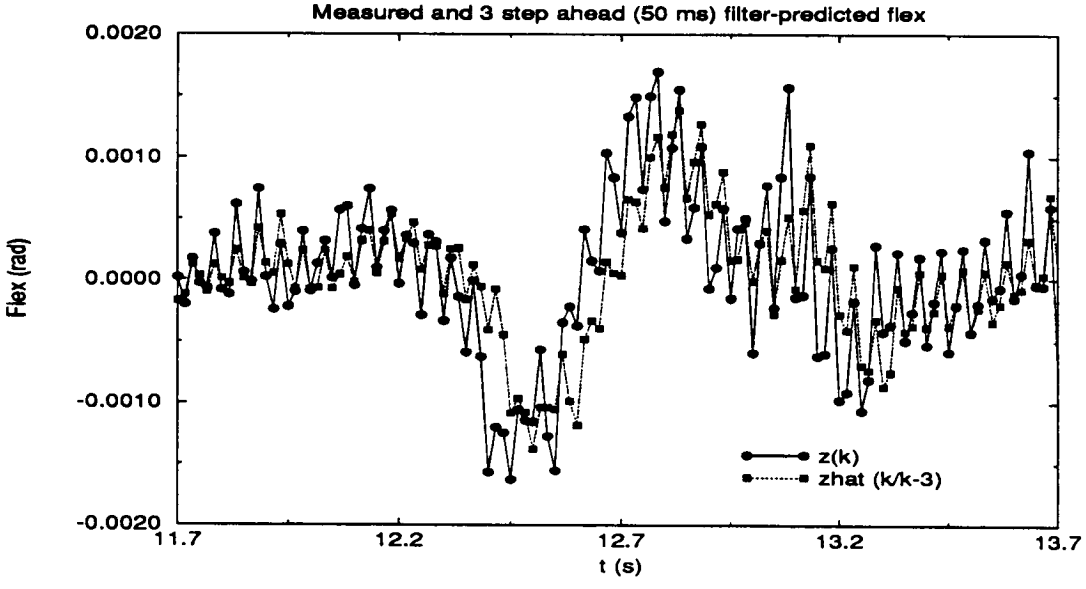

Fig. 6-11: Real barrel flex measurements and 3-step ahead Kalman filter prediction. This shows poorer muzzle angle prediction when unmodelled accelerations dominate.

6.4.3 Discussion of Filter Results

The Kalman filter design, as presented, is not yet of sufficient fidelity to include in a real-time predictive DMRS since it does not accurately model the low frequency effects caused by sustained accelerations as manifested in Fig. 6-11. This is not an insurmountable problem. Relatively modest changes to the state equations, process noise models, and software simulator and careful tuning of the noise parameters would yield a filter that could predict the muzzle angle through these sustained accelerations as accurately as the current model can predict the higher frequency vibrations. This has not yet been done since the filter so far has been designed around the angular flex data derived from gyroscopes, while the DMRS system that will be installed on the tank will be laser and mirror based. This is such a sufficient difference that fine-tuning the model on the existing data may not yield a suitable filter for data from the laser system. In any event, the results so far have been quite encouraging and the modelling efforts in this chapter should be a good launching point for further studies on predictive muzzle referencing systems.

7.0 A POTENTIAL ADM ARCHITECTURE

This chapter presents a preliminary proposal for an overall architecture of an Advanced Development Model for a highly advanced, fire-on-the-move fire control system for future direct-fire support vehicles. The previous chapters have dealt in detail with some of the more pressing problems such as trajectory prediction and dynamic muzzle referencing. However it may be useful to briefly step back and look at the overall system as a whole.

Fig. 7-1 is an attempt at showing both the major system components and the sequence of events that would occur as the data travels through the system from the time of initial target detection until the weapon is fired.

First, we assume that there will be two operators of the system. In current generations of vehicles, they are called Commander and Gunner but we shall use the more generic terms Observer and Engager. The diagram has a top portion for the equipment associated with the observer's duties and a bottom portion for equipment associated with the engager's. Each operator has his own imaging sensor(s) that can be aimed independently of the weapon and each other. Associated with each operator station, is a high-speed, dedicated image processing computer that can be configured by the operator to aid in image enhancement (by contrast stretching, motion highlighting, etc.) image stabilization (jitter removal by registering the image against a stationary background), target extraction (by highlighting potential targets and extracting the more promising ones) and target tracking (by running Kalman filters similar to those in Chapter 4) to assist in finding the target in the next scan.

A sensor control computer will be used to control the functions of each image processor and act as the human interface to the system. This control computer can be used to suggest a prioritization of the targets to the observer, possibly assist in their identification, accept all operator hand or voice inputs, and cue the imaging sensor to follow a specific target or the operator's hand control. The control computers of the two stations would be in constant communication so that targets could be handed off from the observer to the engager, or in emergencies could redirect the output of one image processor to the other operator's display.

When it is decided that a particular target is to be engaged, the engager's control computer would concentrate solely on that target. It would run a more sophisticated Kalman tracking filter, perhaps with more states, maneuver detectors, etc, to attempt to estimate very accurately the true state of the target. It would drive the imaging sensor to closely follow that target. An interesting possibility is that it might be able to estimate the probability of hitting the target based on its estimate of the target acceleration, for example.

Provided the engager is satisfied with his chance of success, the laser range finder (LRF), environment sensors (wind, air pressure, temperature, etc) would be activated by the control computer and the ballistic solution would be calculated based on the data from these sensors and the target velocity/acceleration available from the target state estimator. The gun control servos would slew the gun to the proper lead angles in preparation for firing. At this point, an optional interrogation of the target might take place based on an optical IFF (Identify Friend or Foe) system and the computer would inform the engager that firing can commence.

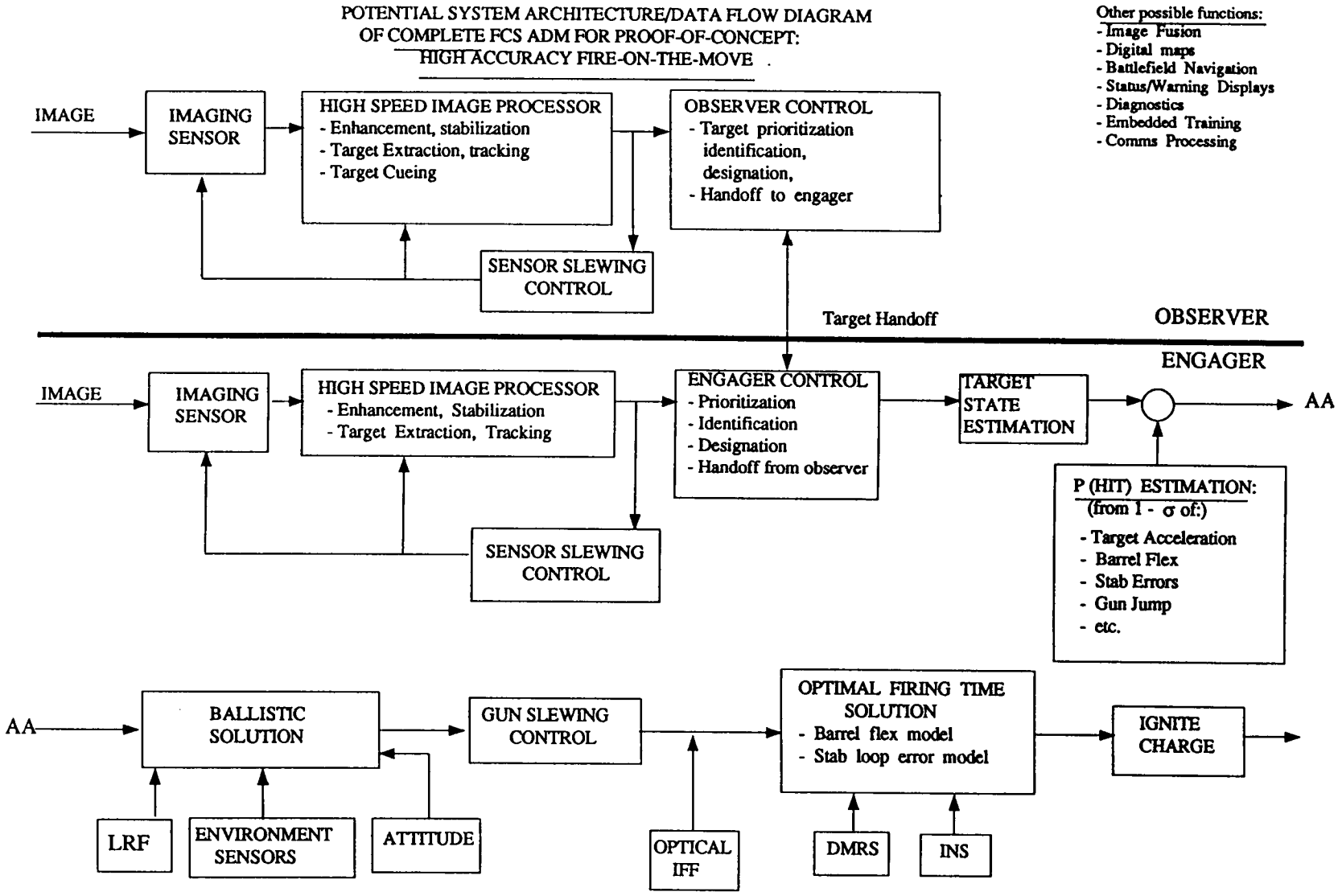

Fig. 7-1: A Potential ADM Architecture

When the engager presses the firing button, there may be a slight delay as the barrel flex data from the DMRS (Dynamic Muzzle Reference System) laser on the gun barrel (and possibly other vehicle dynamics from the onboard Inertial Navigation System (INS)) is processed through a predictive Kalman filter similar to that of Chapter 6 and a barrel zero crossing time is predicted. The charge would be ignited at a time such that the shell could be expected to exit the muzzle at a zero crossing time.

After the results of the initial shot are observed, the observer will have the next target ready for the engager. The target is handed off to the engager's control computer and the process repeats.

From this very cursory design, it can be seen that such a system is very flexible, powerful and very comprehensive. The algorithms discussed in this report make up just two of the overall components, the optimal firing time solution and the target state estimation. Much more work remains to be done before such a system is ready to be fielded.

8.0 SUMMARY

This report has summarized some applications of Kalman filters in the fire control systems of future direct-fire support vehicles, especially in the high dynamic moving-target/moving-platform scenario. Two areas were studied in some detail, target state estimation and dynamic muzzle referencing. A number of modelling studies were conducted, simulation software was written and exercised, candidate filters were designed and implemented and, where possible, real data was used to test the resulting filters. The results show sufficient potential to conclude that such techniques can be extremely useful in predicting the dynamics of both the target and the firing platform. An overall architecture of an advanced development model was proposed to establish the context in which the filters of this report can play a vital role.

REFERENCES

Baran, R., *et al.*, "Stochastic Modeling for Improved Weapon Performance," Proc. *Fifth U.S. Army Symposium on Gun Dynamics*, U.S. Army Research, Development and Engineering Center, Watervliet, New York, 23-25 September 1987.

Bird, J.S., "Measurement of Tank Gun Dynamics in Support of a Dynamic Muzzle Referencing System," Defence Research Establishment Ottawa Technical Report 1053, December 1990.

Blackman, S.S., *Multiple Target Tracking with Radar Applications*, Artech House, Dedham, MA, 1986.

Bogler, P.L., *Radar Principles with Applications to Tracking Systems*, Wiley & Sons, New York, 1990.

Brosseau, T.L., M.D. Kregel, and A.F. Baran," Autonomous Accuracy Enhancement System," Proc. *Sixth US Army Symposium on Gun Dynamics*, U.S. Army Research, Development and Engineering Center, Watervliet, New York, 1990.

Burke, H.H., T.R. Perkins, and J.F. Leathrum, "State Estimation of Maneuvering Vehicles via Kalman Filtering," US Army AMSAA Tech. Report No. 186, 1976.

Chang, C.B. and J.A. Tabaczynski, "Application of State Estimation to Target Tracking," *IEEE Trans. Automatic Control*, Vol. AC-29, No. 2, 1984.

Craig, R.R. Jr., *Structural Dynamics - An Introduction to Computer Methods*, Wiley & Sons, New York, 1981.

Farina, A. and F.A. Studer, *Radar Data Processing: Vol. I - Introduction and Tracking*, Wiley & Sons, New York, 1985.

Fitzgerald, R.J., "Simple Tracking Filters: Closed-Form Solutions," *IEEE Trans. Aerospace and Electronic Sys.*, Vol. AES-17, No. 6, 1981.

Gast, R.G., "Normal Modes Analysis of Gun Vibrations by the Uniform Segment Method," Proc. *Fifth U.S. Army Symposium on Gun Dynamics*, U.S. Army Research, Development and Engineering Center, Watervliet, New York, 23-25 September 1987.

Gelb, A., *Applied Optimal Estimation*, M.I.T. Press, Cambridge, Ma., 1974.

Goldstein, H., *Classical Mechanics*, Addison Wesley, Reading, Ma., 1950.

Levin, V., "Accuracy Improvement of Flexible Gun Tubes - A Kalman Filter Approach," Proc. *Second U.S. Army Symposium on Gun Dynamics*, U.S. Army Research, Development and Engineering Center, Watervliet, New York, 19-22 September 1978.

McMillan, J.C., "An Integrated System for Land Navigation," *Journal of the Institute of Navigation*, Vol. 34, No. 1, 1987.

McMillan, J.C., and Sang Seok Lim, "Data Association Algorithms for Multiple Target Tracking," Defence Research Establishment Ottawa Technical Report 1040, July 1990.

Rouhi, A. and M. Farooq, "Development of a Multiple Structure Adaptive Target Tracking Technique," Royal Military College of Canada, EE Tech. Report No. 89/9, 1989.

Roy, J.M.J, "Overview of Multisensor Tracking and Classification of Maneuvering Targets in a Cluttered Environment," Defence Research Establishment Valcartier Momorandum DREV-M-3018/90, April 1990.

Sasiadek, J.Z., and R. Srinivasan, "Dynamic Modelling and Adaptive Control of a Single-Link Flexible Manipulator," *AIAA J. Guidance, Control and Dynamics,* Vol. 12, No. 6, 1989.

Sorenson, H.W,. Editor, *Kalman Filtering: Theory and Application,* IEEE Press, New York, 1985.

TTCP-WAG10, "Tank Gun Systems Accuracy," Final Report, TTCP Sub-group W, Action Group 10, September 1989.

Woolfson, M.S., "An Evaluation of Manoeuvre Detector Algorithm," *GEC Journal of Research*, Vol. 3, No. 3, 1985.

APPENDIX A. DERIVATION OF Q VALUES FOR THE TRACKING FILTERS

The general continuous-time model of target motions, from (2-2), is

$$\dot{x}_c(t) = Fx_c(t) + w_c(t) \tag{A-1}$$

with the covariance of the driving process given by

$$E\{w_c(t)w_c(\tau)^T\} = Q_c(t)\delta(t-\tau)$$

If we look only at the velocity state in one horizontal direction, say v_{YG}, the randon walk velocity (RWV-r) continuous time velocity model is driven by white noise (from Eqn. (3-14)):

$$\dot{v}_{Y_G}(t) = w_{a_{YG}}(t) \tag{A-2}$$

We wish to estimate a value, Q_c, for the covariance of $w_{a_{YG}}$. We will approach the problem first from the discrete-time point of view and then return to continuous time. The discrete time version of (A-1) is, as shown by (2-1):

$$x_{k+1} = \Phi_k x_k + w_k \tag{A-3}$$

where, from (2-3),

$$\Phi_k = e^{F(t_{k+1}-t_k)} \tag{A-4}$$

But since F=0 for the velocity state (A-2) of the RWV model, then $\Phi = 1$. The discrete-time velocity model is thus

$$v_{Y_G}(t_{k+1}) = v_{Y_G}(t_k) + w_k \tag{A-5}$$

where we have simplified notation by redefining w_k as the scalar noise process driving the v_{YG} velocity state. The covariance of this discrete driving noise is also given by (2-3):

$$E\{w_k^2\} = Q_k = \int_{t_k}^{t_{k+1}} e^{F(t_{k+1}-\tau)} Q_c(\tau) e^{F^T(t_{k+1}-\tau)} d\tau \tag{A-6}$$

but since F=0, this simplifies to

$$Q_k = \int_{t_k}^{t_{k+1}} Q_c(\tau) d\tau \tag{A-7}$$

which, for sufficiently small time steps ($t_{k+1} - t_k \rightarrow 0$), can be approximated by

$$Q_k \approx Q_c(t_k)\ (t_{k+1} - t_k) \tag{A-8}$$

Thus by estimating a value for $Q_k = E\{w_k^2\}$, we can obtain the Q_c we are looking for.

Let us assume that a reasonably maneuverable ground target is to be tracked, say one that can accelerate from 0 to 100 km/hr in 5 seconds, or equivalently, can execute a 90 degree turn at 100 km/hr in 5 seconds (both of which are quite realistic for modern fighting vehicles). This is equivalent to an acceleration of 5.55 m/s^2. With a discretization time step of $t_{k+1} - t_k = 0.1$s, this corresponds to a velocity change of 0.555 m/s in 0.1s. Thus we will model the noise driving the discrete velocity state as an uncorrelated Gaussian sequence with zero mean and covariance

$$\begin{aligned} Q_k &= (0.555 \text{ m/s})^2 \\ &= 0.3 \text{ m}^2/\text{s}^2 \end{aligned} \tag{A-9}$$

so that from (A-8),

$$\begin{aligned} Q_c &\approx Q_k / (t_{k+1} - t_k) \\ &= 0.3 / 0.1 \\ &= 3 \text{ m}^2/\text{s}^3 \end{aligned} \tag{A-10}$$

In the vertical direction, we assume the vehicle is only a tenth as maneuverable as it is horizontally. Thus Q_k in the vertical is (0.0555 m/s)^2 so the corresponding Q_c is 0.03 m^2/s^3. These are the values used in the Q_c matrix in the RWV(r) simulations of Chapters 4 and 5.

For the angular rate model, RWV(s), a similar derivation is used. Since the range to the target is unknown, however, a nominal range of about 2000m is used to derive the Q values. (This is not atypical for land engagements.) A cross-range linear velocity change of 0.555 m/s over 0.1s at a range of 2000m results in an angular velocity change of about 0.25 mrad/s. Thus the discrete noise driving the horizontal angular velocity state will be assumed to have a covariance of

$$\begin{aligned} Q_k &= (0.00025 \text{ rad/s})^2 \\ &= 6.25 \times 10^{-8} \text{ rad}^2/\text{s}^2 \end{aligned} \tag{A-11}$$

so that again from (A-8),

$$
\begin{aligned}
Q_c &= Q_k \,/\, (t_{k+1} - t_k) \\
&= 6.25 \times 10^{-8} \,/\, 0.1 \\
&= 6.25 \times 10^{-7} \text{ rad}^2/\text{s}^3
\end{aligned}
\qquad \text{(A-12)}
$$

The corresponding vertical angular velocity covariance, assuming the similar 1/10 maneuverability, results in a Q_c of 6.25×10^{-9} rad^2/s^3.

APPENDIX B. DERIVATION OF Q VALUES FOR THE MRS FILTER

To estimate the Q matrices for the muzzle reference filter, we take a similar approach as for the tracking filters in Appendix A. First we must determine a level a "maneuverability" of the gun barrel by looking at some of the collected field data. For the same sequence of data shown in Fig. 6-6, the angular rate and acceleration of the mantlet are shown in Fig. B-1 and Fig. B-2 respectively.

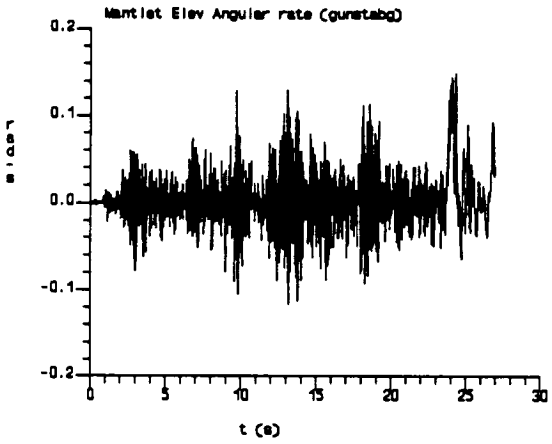

Fig. B-1: Mantlet angular rate

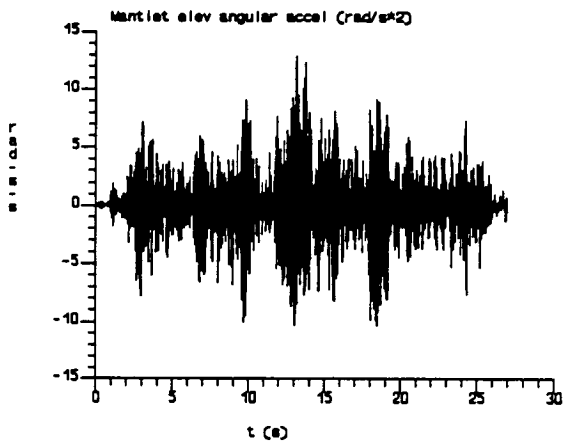

Fig. B-2: Mantlet angular acceleration

From Fig. B-2, a not unreasonable assumption for the level of maneuverability of the mantlet can be rather arbitrarily chosen as 3 rad/s^2. For the 60 Hz sampling rate of the data in question, this corresponds to an angular velocity change of about 0.051 rad/s in 1/60th of a second. Thus we will model the noise driving the discrete angular velocity state as an uncorrelated Gaussian sequence with zero mean and covariance

$$\begin{aligned} Q_k &= (0.051 \text{ rad/s})^2 \\ &= 0.0026 \text{ rad}^2/\text{s}^2 \end{aligned} \tag{B-1}$$

so that from (A-8),

$$\begin{aligned} Q_c &\approx Q_k \,/\, (t_{k+1} - t_k) \\ &= 0.0026 \,/\, 0.0166667 \\ &= 0.16 \text{ rad}^2/\text{s}^3 \end{aligned} \tag{B-2}$$

From the first element of the vector equation relating the noise driving the angular velocity state with the noise on the applied torque τ, Eqn. (6-22), we can conclude

$$E[\tau(t_a)\tau(t_b)] = 0.16 / 0.1816^2 \, \delta(t_a - t_b)$$
$$= 5 \, \delta(t_a - t_b) \qquad \text{(B-3)}$$

This value is then used to derive the remainder of the Q elements of Chapter 6.

DOCUMENT CONTROL DATA

(Security classification of title, body of abstract and indexing annotation must be entered when the overall document is classified)

1. ORIGINATOR (the name and address of the organization preparing the document. Organizations for whom the document was prepared, e.g. Establishment sponsoring a contractor's report, or tasking agency, are entered in section 8.)

DEFENCE RESEARCH ESTABLISHMENT OTTAWA
Ottawa, Ontario
K1A OK2

2. SECURITY CLASSIFICATION (overall security classification of the document. including special warning terms if applicable)

UNCLASSIFIED

3. TITLE (the complete document title as indicated on the title page. Its classification should be indicated by the appropriate abbreviation (S,C or U) in parentheses after the title.)

Some Applications of Kalman Filtering in Advanced Land Fire Control Systems (U)

4. AUTHORS (Last name, first name, middle initial)

Bird, J.S.

5. DATE OF PUBLICATION (month and year of publication of document)

April 1993

6a. NO. OF PAGES (total containing information. Include Annexes, Appendices, etc.)

82

6b. NO. OF REFS (total cited in document)

22

7. DESCRIPTIVE NOTES (the category of the document, e.g. technical report, technical note or memorandum. If appropriate, enter the type of report, e.g. interim, progress, summary, annual or final. Give the inclusive dates when a specific reporting period is covered.)

Technical Report

8. SPONSORING ACTIVITY (the name of the department project office or laboratory sponsoring the research and development. Include the address.)

Defence Research Establishment Ottawa
Ottawa, Ontario
K1A OK2

9a. PROJECT OR GRANT NO. (if appropriate, the applicable research and development project or grant number under which the document was written. Please specify whether project or grant)

0318E

9b. CONTRACT NO. (if appropriate, the applicable number under which the document was written)

N/A

10a. ORIGINATOR'S DOCUMENT NUMBER (the official document number by which the document is identified by the originating activity. This number must be unique to this document.)

DREO REPORT 1172

10b. OTHER DOCUMENT NOS. (Any other numbers which may be assigned this document either by the originator or by the sponsor)

11. DOCUMENT AVAILABILITY (any limitations on further dissemination of the document, other than those imposed by security classification)

(X) Unlimited distribution
( ) Distribution limited to defence departments and defence contractors; further distribution only as approved
( ) Distribution limited to defence departments and Canadian defence contractors; further distribution only as approved
( ) Distribution limited to government departments and agencies; further distribution only as approved
( ) Distribution limited to defence departments; further distribution only as approved
( ) Other (please specify):

12. DOCUMENT ANNOUNCEMENT (any limitation to the bibliographic announcement of this document. This will normally correspond to the Document Availabilty (11). However, where further distribution (beyond the audience specified in 11) is possible, a wider announcement audience may be selected.)

Unlimited

UNCLASSIFIED

SECURITY CLASSIFICATION OF FORM

13. ABSTRACT (a brief and factual summary of the document. It may also appear elsewhere in the body of the document itself. It is highly desirable that the abstract of classified documents be unclassified. Each paragraph of the abstract shall begin with an indication of the security classification of the information in the paragraph (unless the document itself is unclassified) represented as (S), (C), or (U). It is not necessary to include here abstracts in both offical languages unless the text is bilingual).

The report describes several potential applications of Kalman filters for advanced land fire control systems. Two areas that are especially important in the moving-target/moving-platform scenario are addressed in some detail: the tracking and trajectory prediction of multiple maneuvering targets and the prediction of gun pointing angles in the instant before firing. This is particularly important in the design of a dynamic muzzle reference system. The equations for the filters are developed, simulations are described, and some real data is processed through the muzzle angle prediction filter. An architecture for a complete advanced land fire control system is proposed.

14. KEYWORDS, DESCRIPTORS or IDENTIFIERS (technically meaningful terms or short phrases that characterize a document and could be helpful in cataloguing the document. They should be selected so that no security classification is required. Identifiers, such as equipment model designation, trade name, military project code name, geographic location may also be included. If possible keywords should be selected from a published thesaurus. e.g. Thesaurus of Engineering and Scientific Terms (TEST) and that thesaurus-identified. If it is not possible to select indexing terms which are Unclassified, the classification of each should be indicated as with the title.)

Kalman Filtering
Fire Control
Target Tracking
Gun Dynamics
Muzzle Reference